



Title	Synthesis of Sumanene Derivatives Using Aromatic Electrophilic Substitution Reactions
Author(s)	中澤, 廣宣
Citation	大阪大学, 2023, 博士論文
Version Type	VoR
URL	https://doi.org/10.18910/91912
rights	
Note	

The University of Osaka Institutional Knowledge Archive : OUKA

<https://ir.library.osaka-u.ac.jp/>

The University of Osaka

Doctoral Dissertation

**Synthesis of Sumanene Derivatives Using
Aromatic Electrophilic Substitution Reactions**

(芳香族求電子置換反応を用いた
スマネン誘導体の合成)

Hironobu Nakazawa

January 2023

Department of Applied Chemistry
Graduate School of Engineering
Osaka University

Table of contents

Chapter 1	General introduction	
	Section 1. Curved π -conjugated molecule; sumanene	1
	Section 2. Chemical modification of sumanene	4
	Section 3. This work	6
	References	8
Chapter 2	Sumanene-fused acene	
	Section 1. Introduction of sumanene-fused acene	10
	Section 2. Synthesis of sumanene-fused quinones and their properties	11
	Section 3. Synthesis of sumanene-fused acenes and their properties	15
	Section 4. Summary	20
	Experimental section	21
	References	34
Chapter 3	Fully substituted sumanenes at the aromatic periphery through hexabromomethylation	
	Section 1. Introduction of fully substituted buckybowl at the aromatic periphery	37
	Section 2. Synthesis of hexahalomethyl sumanene	40
	Section 3. Transformation of bromomethylsumanene by nucleophilic substitution reaction	44
	Section 4. Summary	47
	Experimental section	48
	References	66
Chapter 4	Pentagon-fused sumanenes on the aromatic peripheries en route to the bottom-up synthesis of fullerenes	
	Section 1. Introduction of C_{60} synthesis	68
	Section 2. Synthesis of azafullerene $C_{54}N_6$ and fullerene C_{60} fragments	70
	Section 3. Properties of azafullerene $C_{54}N_6$ and fullerene C_{60} fragments	75
	Section 4. Summary	76
	Experimental section	77
	References	87
Conclusions		89
List of Publications		90
Copyright		91
Acknowledgments		92

Chapter 1. General introduction

Section 1. Curved π -conjugated molecule; sumanene

Synthetic organic chemistry is a field that has been growing since the late 1800s. It involves the creation of complex molecules through various reactions, including cross-coupling reactions.¹ This has led to the production of many valuable molecules. In particular, the study of π -conjugated molecules, which have applications in optoelectronic materials, has been an active area of research around the world.² Despite being a relatively new area in the field of synthetic organic chemistry, π -conjugated molecules continue to be a focus of many researchers as they hold significant potential and promise.

Research on the curved π -conjugated molecule, the buckybowl, has been active in recent years. Buckybowls such as corannulene,³ sumanene,⁴ circumtrindene,⁵ and so on, have a partial structure of fullerene (C_{60}). Mainly, corannulene (C_{5v}) and sumanene (C_{3v}) are actively studied, and their derivatives have been well synthesized, and their structural features and properties have been compared (Figure 1).

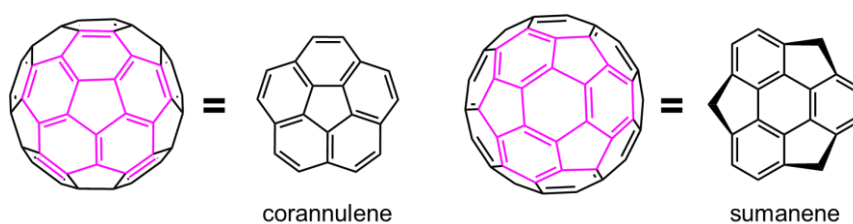
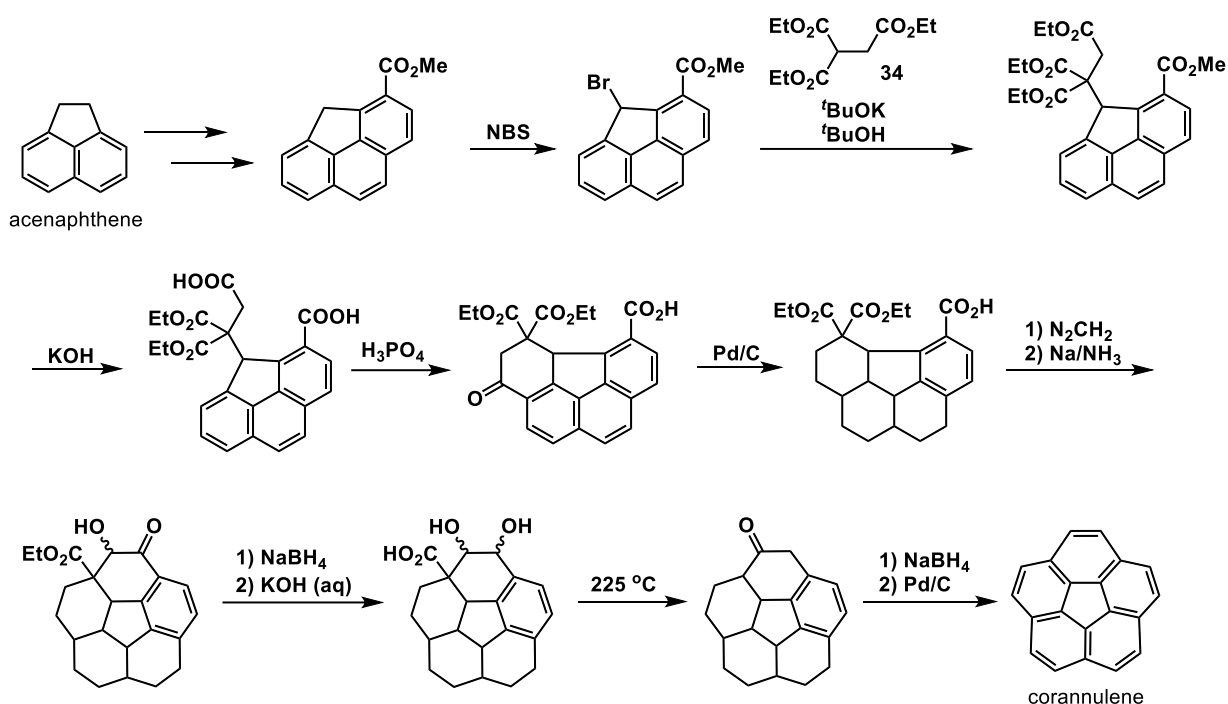


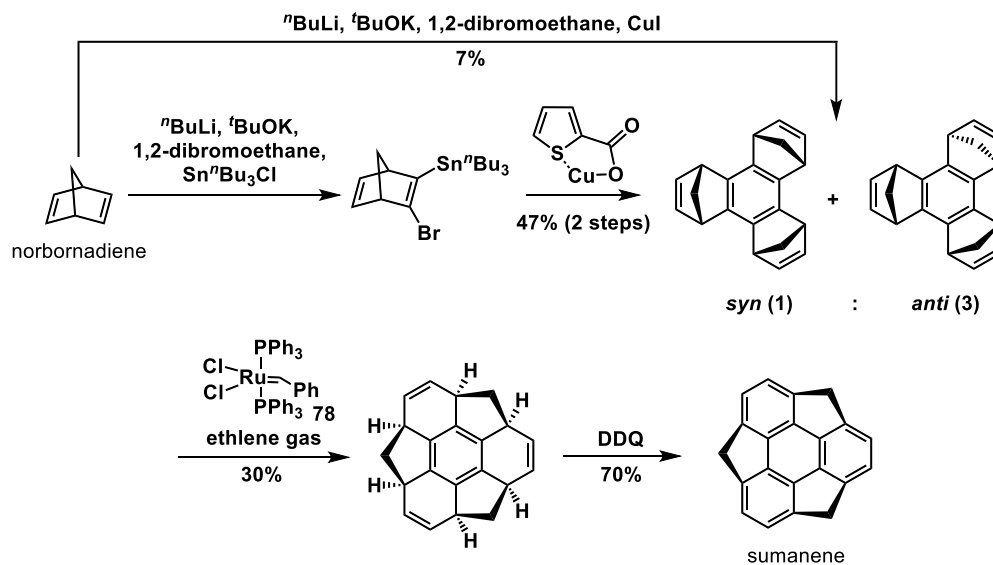
Figure 1. Buckybowls

The study of corannulene, a molecule with a C_{60} substructure consisting of a central five-membered ring and five fused six-membered rings, began before the discovery of C_{60} itself. In 1966, Barth and Lawton first synthesized corannulene from acenaphthene in a process that took 17 steps (Scheme 1).³ The synthesis of corannulene was motivated by the desire to extend the chemistry of radialene and circulene. In contrast, it was not until 2003 that Sakurai and Hirao successfully synthesized sumanene, a molecule with a similar bowl-shaped structure named by Mehta,⁶ from norbornadiene in just three steps (Scheme 2).⁴ Although the naming of sumanene and the attempt of the synthesis by the flash vacuum pyrolysis (FVP) method were reported by Mehta et al. in 1993,⁶ Both corannulene and sumanene have unique properties due to their curved structures, including bowl inversion, host-guest interaction, and metal coordination. In the 20 years since its synthesis, sumanene has been found to have many exciting features not found in corannulene.⁷

Scheme 1. Synthesis of corannulene by Barth and Lawton.



Scheme 2. Synthesis of sumanene by Sakurai and Hirao.



The first of its characteristics is its deep bowl structure. Sumanene has a triphenylene skeleton bridged by three methylenes, and its bowl depth (the distance between the bottom six-membered ring plane of the sumanene skeleton and the surrounding aromatic carbon) is 1.11 Å (Figure 2).⁸ This value is larger than 0.87 Å for corannulene (Figure 2).⁹ This results in a slower bowl inversion in solution, as the inversion energy is higher.¹⁰

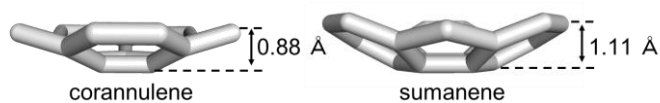


Figure 2. The bowl depths of buckybowls

Another distinctive feature of sumanene is that it forms one-dimensional (1D) columnar structures when crystallized, due to its C_{3v} symmetry and curved shape, which allow for strong intermolecular interactions between curved surfaces (Figure 3A). The crystals also have an eclipsed stacking structure in which the molecules are stacked in a 60° twisted configuration (Figure 3B), maximizing the overlap of their HOMO and LUMO, and resulting in a high charge transport capacity with anisotropy in the columnar direction.¹¹

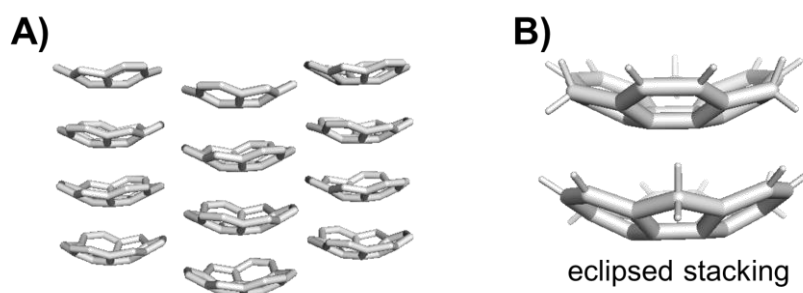


Figure 3. Crystal structures of sumanene (1). A) 1D columnar structure. B) Intermolecular interactions within the columns.

Additionally, sumanene has a benzyl-positioned carbon in its structure, which allows for the introduction of different substituents on the concave and convex planes¹² through endo- or exo-selective chemical modification, creating molecules with unique properties and intramolecular bifacial nature (Figure 4).¹³

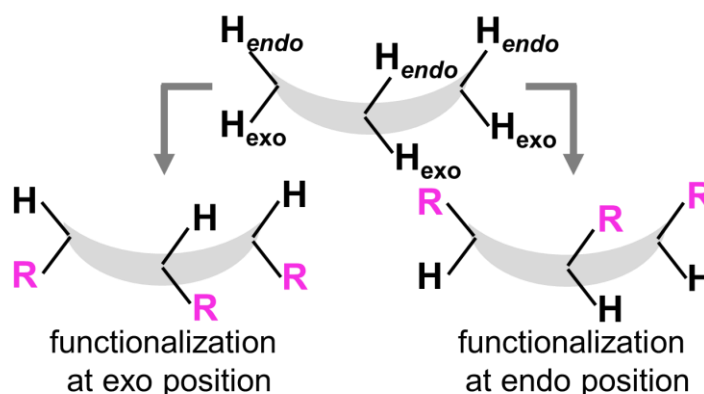


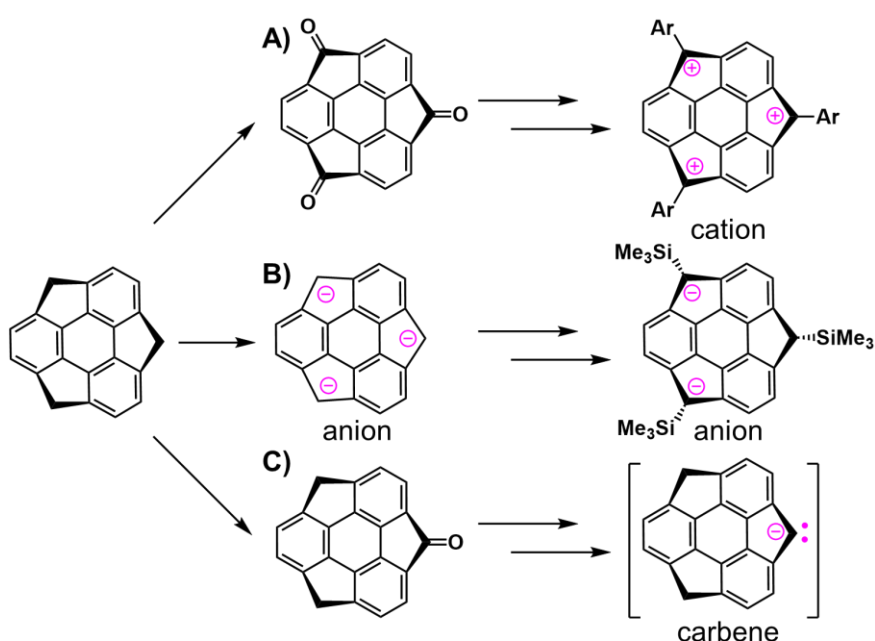
Figure 4. Conceptual figure of functionalization at exo or endo position of sumanene.

As a result of its deep bowl structure, symmetry, and combination of benzyl and aromatic moieties, sumanene is expected to exhibit features not seen in corannulene and to be modified through chemical reactions.

Section 2. Chemical modification of sumanene

Sumanene has both aromatic and benzyl moieties on its periphery, and its unique benzyl moiety has been the focus of many chemical modification studies. For example, trioxosumanene,¹⁴ obtained through oxidation of the benzyl moiety, can be converted into a cationic species through the addition of Grignard reagents and dehydration with acids. (Scheme 3A).¹⁵ The generation of anions through reaction with strong bases (Scheme 3B)⁸ and carbenes¹⁶ (Scheme 3C) via monoxosumanene^{14,17} has also been reported. Thus, the benzyl position of sumanene is highly reactive and can be chemically modified in various ways.

Scheme 3. Generation of active species at the benzyl position of sumanene.



Furthermore, using their oxo-compound and active species as key intermediates, sumanene derivatives with various properties have been reported. For example, difluorosumanene with an intramolecularly biased dipole moment exhibits a dielectric response to an external electric field in a single crystal state (Figure 5A).¹⁸ Other reported examples include benzyl trisubstituted sumanenes that selectively incorporate cesium cations (Figure 5B)¹⁹ and sumanenes that exhibit a bifacial nature by introducing hydrophilic and hydrophobic substituents on the endo and exo sides, respectively (Figure 5C).²⁰ Hence, chemical modification of the benzyl position has contributed to the creation of sumanene derivatives with various properties.

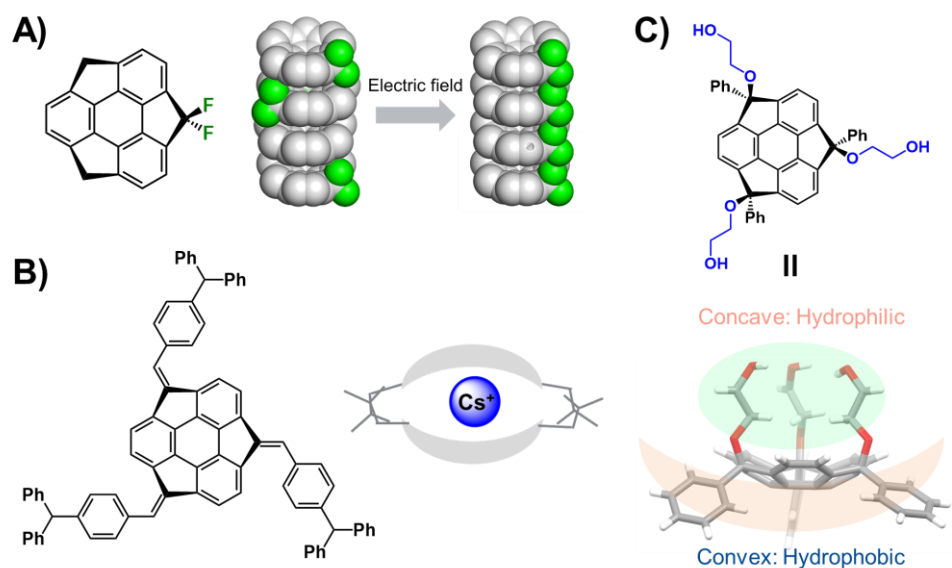
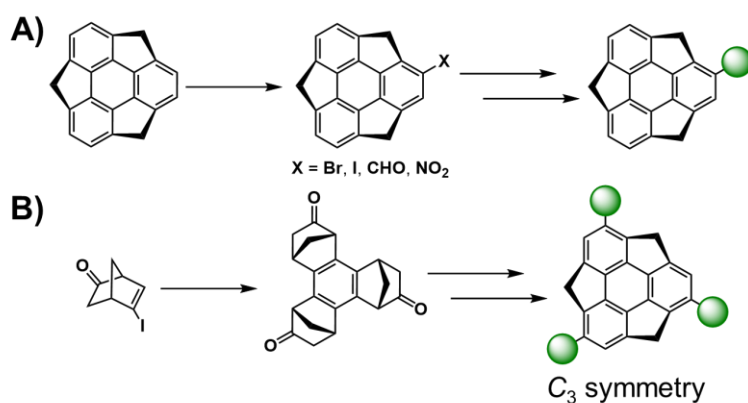


Figure 5. Various properties of benzyl-substituted sumanenes

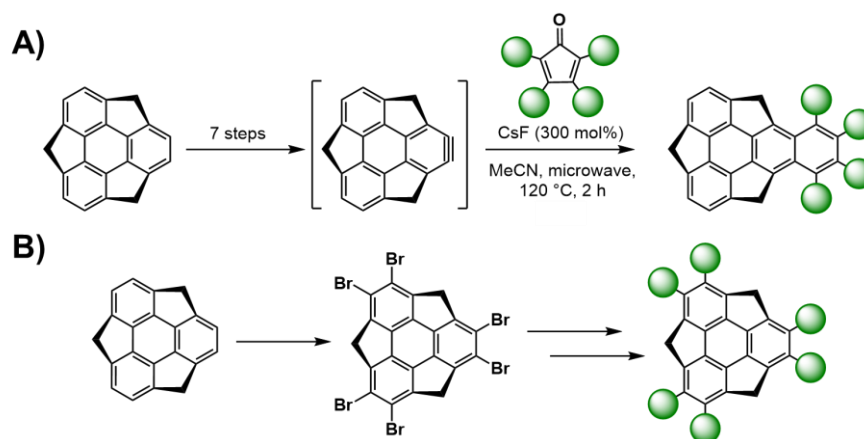
In contrast, chemical modification of the peripheral aromatic carbons of sumanene is less reactive and more difficult due to the steric hindrance of methylene substitutions at the ortho positions. However, some essential modifications have been achieved, such as the synthesis of mono-substituted sumanenes through monohalogenation²¹ or monoformylation²² which allows for the introduction of various substituents through subsequent reactions (Scheme 4A).²³ Trimethyl sumanenes with C_3 symmetry, synthesized from chiral norbornadienone trimers, have also been found to exhibit bowl chirality (Scheme 4B).²⁴

Scheme 4. Synthesis of A) mono and B) tri-substituted sumanene.



While the variety of ortho-disubstituted sumanenes and hexa-substituted sumanene derivatives is limited (Scheme 5), a benzyne intermediate called sumanyne has been shown to be promising for synthesizing various ortho-disubstituted sumanenes, though the process involves multiple steps (Scheme 5A).²⁵ Many hexa-substituted sumanenes have been synthesized since the synthesis of hexabromosumanene²⁶ by Sakurai and Fukushima et al., but the reactions applicable to these molecules are still limited to cross-coupling reactions and aromatic nucleophilic substitution reactions (Scheme 5B).²⁷

Scheme 5. The previous synthesis of A) ortho-disubstituted and B) hexa-substituted sumanenes.



Section 3. This work

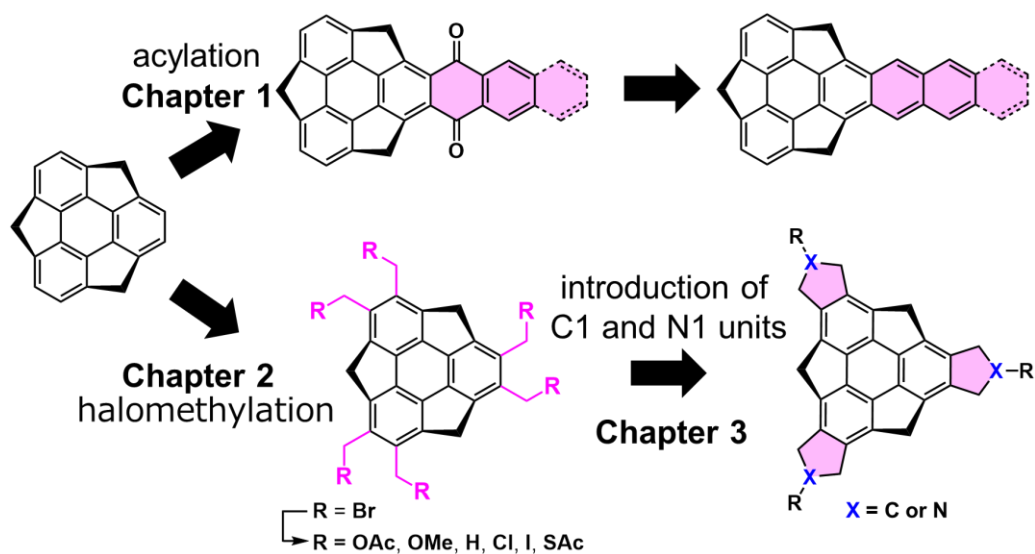
Therefore, the author focused on ortho-disubstituted sumanene and hexa-substituted sumanene derivatives, which had been considered difficult to synthesize. In this doctoral dissertation, the author aimed to synthesize ortho-disubstituted sumanene and hexa-substituted sumanene derivatives by aromatic electrophilic substitution reactions, expecting the appearance of new properties generated by introducing new functional groups into the sumanene skeleton (Scheme 6).

Chapter 2 describes the research on acenes having a bowl structure, in which the acene structure is fused to the sumanene skeleton. In this chapter, the author developed a simple method for the synthesis of sumanene-fused acenes and obtained information on their packing structure in solids (crystals), and clarified their properties, such as stability and solubility.

Chapter 3 describes the synthesis of new hexa-substituted sumanenes as alternatives to hexabromosumanenes and their derivatives' properties. In this chapter, first, the complete halomethylation of the peripheral aromatic carbon of sumanene was investigated. Subsequently, the obtained halomethyl sumanenes were transformed by reaction with various nucleophiles to synthesize new hexa-substituted sumanenes.

Chapter 4 describes the synthesis and properties of a hemispherical molecule (C₃₀) having a sumanene

Scheme 6. This work: synthesis of sumanene derivatives by aromatic electrophilic substitution reactions



skeleton, which is directed toward the bottom-up synthesis of fullerenes. In this chapter, the author focused on sumanene's partial structure of fullerenes and attempted to synthesize hemispherical molecules using halomethyl sumanene obtained in Chapter 3 as starting material.

References

- 1 A. Biffis, P. Centomo, A. del Zotto, M. Zecca, *Chem. Rev.* **2018**, *118*, 2249.
- 2 O. Ostroverkhova, *Chem. Rev.* **2016**, *116*, 13279.
- 3 W. E. Barth, R. G. Lawton, *J. Am. Chem. Soc.*, **1966**, *88*, 380.
- 4 H. Sakurai, T. Daiko, T. Hirao, *Science* **2003**, *301*, 1887.
- 5 L. T. Scott, M. S. Bratcher, S. Hagen, *J. Am. Chem. Soc.* **1996**, *118*, 8743.
- 6 G. Mehta, S. R. Shah, K. Ravikumar, *J. Chem. Soc., Chem. Commun.* **1993**, 1006.
- 7 a) S. Higashibayashi, H. Sakurai, *Chem. Lett.* **2011**, *40*, 122. b) M. Saito, H. Shinokubo, H. Sakurai, *Mater. Chem. Front.* **2018**, *2*, 635.
- 8 H. Sakurai, T. Daiko, H. Sakane, T. Amaya, T. Hirao, *J. Am. Chem. Soc.* **2005**, *127*, 11580.
- 9 J. C. Hanson, C. E. Nordman, *Acta Crystallogr.* **1976**, *B32*, 1147.
- 10 T. Amaya, H. Sakane, T. Muneishi, T. Hirao, *Chem. Commun.* **2008**, 765.
- 11 T. Amaya, S. Seki, T. Moriuchi, K. Nakamoto, T. Nakata, H. Sakane, A. Saeki, S. Tagawa, T. Hirao, *J. Am. Chem. Soc.* **2009**, *131*, 408.
- 12 M. Mebs, P. Weber, B. M. Luger, H. Schmidt, S. Sakurai, S. Higashibayashi, S. Onogi, D. Lentz *Org. Biomol. Chem.* **2012**, *10*, 2218.
- 13 S. Higashibayashi, S. Onogi, H. K. Srivastava, G. N. Sastry, Y. Wu, H. Sakurai, *Angew. Chem. Int. Ed.* **2013**, *52*, 7314.
- 14 T. Amaya, M. Hifumi, M. Okada, Y. Shimizu, T. Moriuchi, K. Segawa, K. Y. Ando, T. Hirao, *J. Org. Chem.* **2011**, *76*, 8049.
- 15 Y. Ohigashi, **2017**, Master thesis.
- 16 Y. Yakiyama, Y. Wang, S. Hatano, M. Abe, H. Sakurai, *Chem. Asian J.* **2019**, *14*, 1844.
- 17 M. Nishimoto, Y. Uetake, Y. Yakiyama, F. Ishiwari, A. Saeki, H. Sakurai, *J. Org. Chem.* **2022**, *87*, 2508.
- 18 M. Li, J.-Y. Wu, K. Sambe, Y. Yakiyama, T. Akutagawa, T. Kajitani, T. Fukushima, K. Matsuda, H. Sakurai, *Mater. Chem. Front.* **2022**, *6*, 1752.
- 19 A. Kasprzak, A. Tobolska, H. Sakurai, W. Wróblewski, *Dalton Trans.* **2022**, *51*, 468.
- 20 Y. Shi, **2020**, master thesis.
- 21 B. B. Shrestha, S. Karanjit, G. Panda, S. Higashibayashi, H. Sakurai, *Chem. Lett.* **2013**, *42*, 386.
- 22 N. Ngamsomprasert, G. Panda, S. Higashibayashi, H. Sakurai, *J. Org. Chem.* **2016**, *81*, 11978.
- 23 a) B. Topolinski, B. M. Schmidt, S. Higashibayashi, H. Sakurai, D. Lentz, *Dalton Trans.* **2013**, *42*, 13809. b) B. B. Shrestha, S. Higashibayashi, H. Sakurai, *Beilstein J. Org. Chem.* **2014**, *10*, 841. c) B. B. Shrestha, S. Karanjit, S. Higashibayashi, T. Amaya, T. Hirao, H. Sakurai, *Asian J. Org. Chem.* **2015**, *4*, 62.
- 24 a) S. Higashibayashi, H. Sakurai, *J. Am. Chem. Soc.* **2008**, *130*, 8592. b) S. Higashibayashi, Nasir Baig

- R. B., Y. Morita, H. Sakurai, *Chem. Lett.* **2012**, *41*, 84.
- 25 N. Ngamsomprasert, Y. Yakiyama, H. Sakurai, *Chem. Lett.* **2017**, *46*, 446.
- 26 H. Toda, Y. Yakiyama, Y. Shoji, F. Ishiwari, T. Fukushima, H. Sakurai, *Chem. Lett.* **2017**, *46*, 1368.
- 27 a) Y. Shoji, T. Kajitani, F. Ishiwari, Q. Ding, H. Sato, H. Anetai, T. Akutagawa, H. Sakurai, T. Fukushima, *Chem. Sci.* **2017**, *8*, 8405. b) I. Hisaki, H. Toda, H. Sato, N. Tohnai, H. Sakurai, *Angew. Chem. Int. Ed.* **2017**, *56*, 15294. c) H. Toda, Y. Uetake, Y. Yakiyama, H. Nakazawa, T. Kajitani, T. Fukushima, H. Sakurai, *Synthesis* **2019**, *51*, 4576. d) Y. Yakiyama, T. Hasegawa, H. Sakurai, *J. Am. Chem. Soc.* **2019**, *141*, 18099.

Chapter 2. Sumanene-fused acene

Section 1. introduction of sumanene-fused acene

Singlet fission (SF) is a multiple exciton generation process that produces two excitons from a single photon.¹ Singlet fission was first proposed in 1965 to explain the optical properties of anthracene.² In 1968, it was used to explain why the quantum yield of fluorescence in tetracene crystals was significantly lower, and in 1969 studies of magnetic field effects proved the correctness of this proposal.³ It has been widely studied for applications in organic solar cells in recent years.¹ In particular, acene derivatives such as pentacene are known as critical molecular units and excellent SF molecules in organic electronics.⁴ SF of pentacene proceeds within about 80 fs, giving a high quantum yield of nearly 180%.⁵ However, pentacene has problems in terms of stability and chemical modification due to its low solubility in organic solvents and easy oxygen oxidation. In addition, since SF is an orbital-to-orbital process between molecules, it is known that the molecular arrangement in the solid has a significant effect on its efficiency. The herringbone structure formed by pentacene in crystals has an insufficient overlap of π orbitals. From the above point of view, pentacene is still not the optimal solution as an SF molecule.⁶ As a means of overcoming these problems, many cases have been reported in which the intramolecular distances and angles between chromophores were adjusted by directly or indirectly covalently linking pentacene molecules to each other, and SF was observed. Therefore, many pentacene dimers and oligomers have recently been synthesized by this technique.⁷

On the other hand, sumanene derivatives tend to form 1D columnar structures based on the convex-concave type stacking pattern in the crystal state.⁸ Nakano et al. focused on this point and proposed, based on theoretical calculations, that by fusing sumanene (**1**) with acenes, it is possible to create excellent SF molecules by controlling the arrangement of molecules with the sumanene skeleton while maintaining the SF properties of the acene skeleton (Figure 6).⁹ Here, it is assumed that the sumanene-fused acenes are arranged in eclipsed stacking rather than staggered stacking; the orbits overlap significantly, so efficient SF is expected. Furthermore, the dissymmetric charge distribution between concave and convex surfaces of the sumanene skeleton is expected to promote the generation of dipole moments in the entire molecule. Thus, sumanene-fused acenes are expected to have a higher solubility than pentacenes and are more easily modified by chemical reactions.¹⁰ However, there are few examples¹¹ of studies on buckybowl-fused acenes, and the validity of the design proposed by Nakano et al. was unclear. Therefore, in this chapter, double acylation of sumanene by aromatic electrophilic substitution reaction followed by reductive aromatization was studied to synthesize sumanene-fused acenes and to elucidate their single crystal structures and properties (Scheme 7).

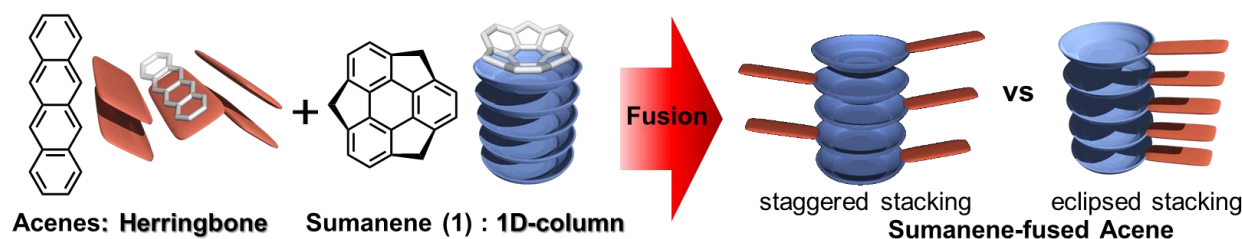
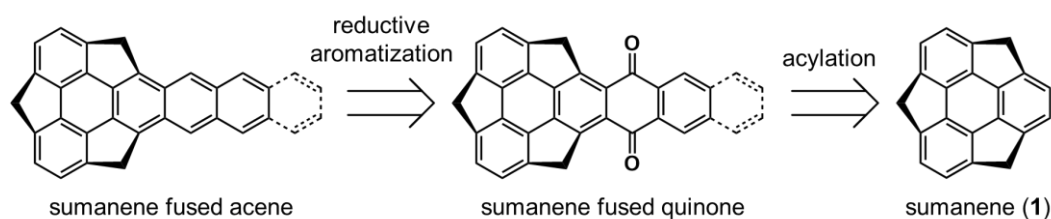


Figure 6. Conceptual figure of sumanene-fused acene system.

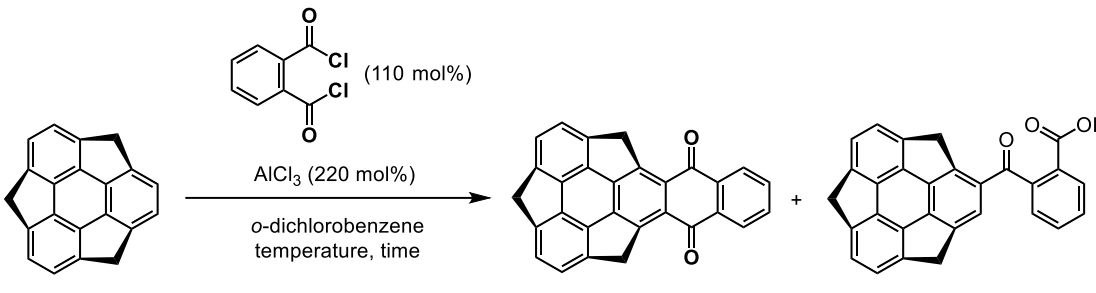
Scheme 7. Synthetic route for sumanene-fused acene



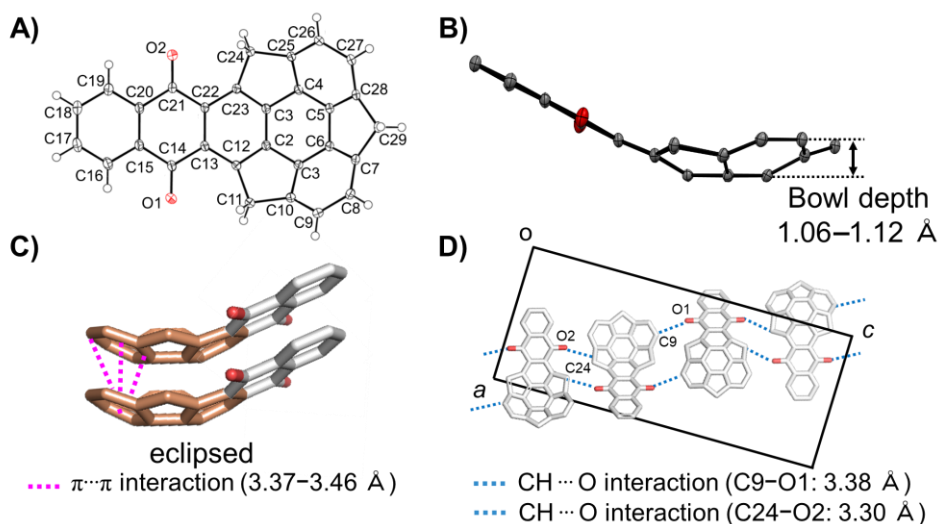
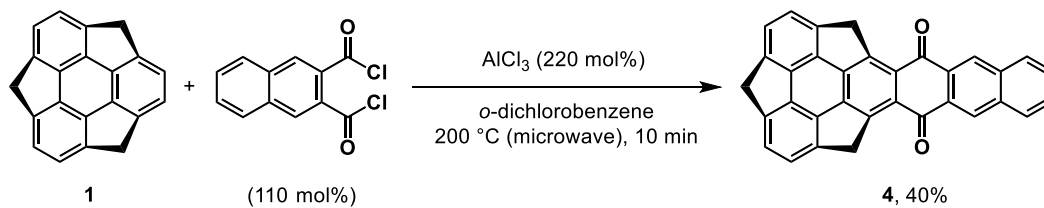
Section 2. Synthesis of sumanene-fused quinones and their properties

Initially, the author aimed to synthesize sumanene-fused naphthoquinone (**2**) by double acylation of sumanene using phthaloyl chloride as an acylating agent and aluminum chloride as Lewis acid (Table 1). In entry 1, the reaction was carried out at 40 °C for 2 h. As a result, it was found that the desired quinone **2** was obtained in 2% yield together with the monoacylated compound (**3**). The reaction temperature was then increased to 100 °C, and the yield was increased to 28% (Entry 2). Finally, quinone **2** was obtained in 54% yield under microwave irradiation at 200 °C (entry 3). This reaction did not yield a product with two phthaloyl chlorides introduced into the sumanene. The same approach was also applied to obtain sumanene-fused anthraquinone (**4**) in 40% yield by changing the acid chloride used to 2,3-naphthalenedicarbonyl dichloride (Scheme 8).

Next, a single crystal X-ray structure analysis of quinone **2** was carried out (Figure 7A). Single crystals of quinone **2** were obtained by slow evaporation from CHCl_3 solution. The bowl depth of quinone **2** was 1.06 Å-1.12 Å (Figure 7B), which is comparable to that of **1** (1.11 Å), and no change in the bowl depth due to the introduction of the quinone moiety was observed.¹² Focusing on the packing structure, **2** formed a 1D columnar structure characteristic of sumanene derivatives as expected (Figure 7C). Each molecule in the columnar structure was stacked in an eclipsed manner, and π - π interactions between the six-membered rings in the sumanene skeleton were observed (3.37-3.46 Å). Furthermore, $\text{CH}\cdots\text{O}$ interactions were formed between the carbons of the sumanene skeleton and the carbonyl oxygen of the quinone skeleton between each column, giving a 1D chain structure ($\text{C9}\cdots\text{O1}$: 3.38 Å, $\text{C24}\cdots\text{O2}$: 3.30 Å, Figure 7D). These results suggested that quinone **4** underwent the same crystallization process as trioxosumanene, and it can be

Table 1. Optimization of double acylation


entry	temperature (°C)	time	2 ^a	3
1	40	2 h	2%	28%
2	100	2 h	28%	10%
3	200 (microwave)	10 min	58% (54%) ^b	0%

^aNMR yield. ^bIsolated yield**Scheme 8.** Synthesis of sumanene-fused quinone (**4**)**Figure 7.** Crystal structures of quinone **2**. A) Displacement ellipsoid plot of **2** at 50% probability. B) Bowl depth of the sumanene skeleton of **2**. C) Intermolecular interactions within the columns. D) Intercolumnar interactions viewed from the *b* axis. The pink dotted line shows $\pi \cdots \pi$ interactions; The blue dotted line shows CH \cdots π interactions. For clarity, hydrogen atoms in (B)–(D) are omitted.

inferred that the 1D chain is first formed by the CH \cdots O interaction, followed by the formation of the columnar structure.¹³

The electronic properties of quinones **2** and **4** were evaluated by cyclic voltammetry (CV), UV-vis

absorption, and emission spectra. CV measurements showed that both molecules exhibited two redox waves on the reduction side, one originating from the quinone moiety ($E_p^{\text{red}} = -1.64$ and -2.06 V (for **2**) and -1.67 and -2.09 V (for **4**)) and one redox wave derived from the sumanene moiety ($E_p^{\text{red}} = -2.44$ V (for **2**) and -2.46 V (for **4**)) (Figure 8). The values derived from the quinone moiety were comparable to the redox waves of anthraquinone ($E_p^{\text{red}} = -1.48$ and -2.12 V), indicating that the introduction of the sumanene moiety into the quinone does not significantly affect the redox properties. The intensity of the first redox wave on the reduction side of quinone **2** is smaller than that of the second and third redox waves is probably due to the slow reduction in the first step and the instability of the intermediate formed there. In CV measurement of sumanene (**1**), an irreversible peak was observed on the reduction side. In contrast, the waves on the reducing side derived from the sumanene moiety of quinones **2** and **4** were observed as reversible peaks, probably because the introduction of the quinone moiety stabilizes them.

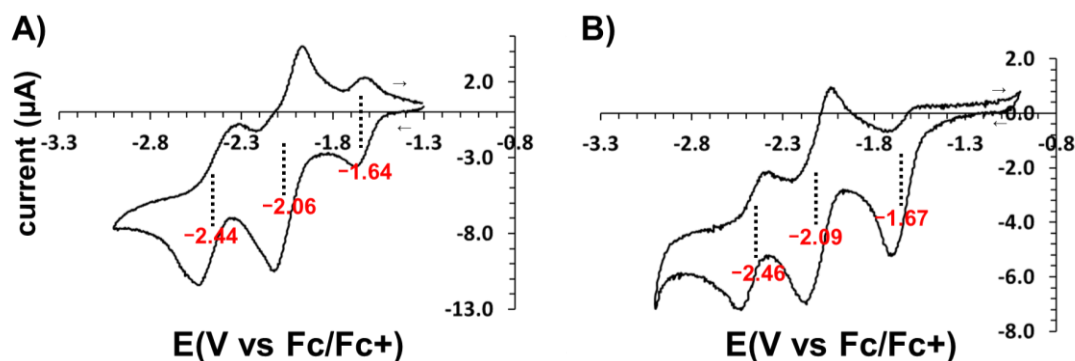


Figure 8. Cyclic voltammograms of quinones A) **2** and B) **4** (5.0×10^{-4} M in THF) measured in the presence of $[n\text{-Bu}_4\text{N}][\text{ClO}_4]$ (0.1 M) supporting electrolyte. Working electrode: GCE, counter electrode: Pt, reference electrode: Ag/AgNO_3 . Scan rate: 50 mV s^{-1} . The ferrocene/ferrocenium couple (Fc^0/Fc^+) was used as a reference. All the solutions were purged with nitrogen prior to the measurements.

UV-vis absorption spectra measurements of quinones **2** and **4** were performed along with anthraquinones and **1** for comparison (Figure 9). In the sumanene-fused quinone, the characteristic peaks derived from the $\pi \rightarrow \pi^*$ (280 nm) of sumanene and $n \rightarrow \pi^*$ (320 nm) of anthraquinone, reflecting the structure of the quinone and sumanene moieties, respectively, were observed with a bathochromic shift due to the π expansion associated with the ring fusion. DFT calculations at the B3LYP/6-31+g(d,p) level suggested that the LUMOs of **2** and **4** are localized at the quinone moiety, while the HOMOs are localized at the sumanene moiety, suggesting that they have charge transfer (CT) ability (Figure. 10). Because of the possibility of intramolecular CT in solution, the solvent dependence of the respective emission spectra was evaluated (Figure 11). As the result, the emission wavelengths of both **2** and **4** shifted to the longer wavelength side as the polarity of the solvent increased. This result indicates that the sumanene-fused quinone has a CT-like structure based on intramolecular charge transfer from the sumanene moiety to the quinone moiety in the excited state.

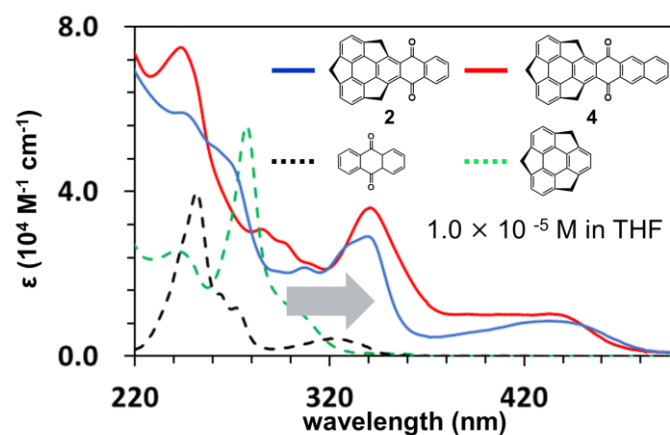


Figure 9. UV-vis absorption spectra of quinone **2**, **4**, anthraquinone, and sumanene in THF (1.0×10^{-5} mol/L).

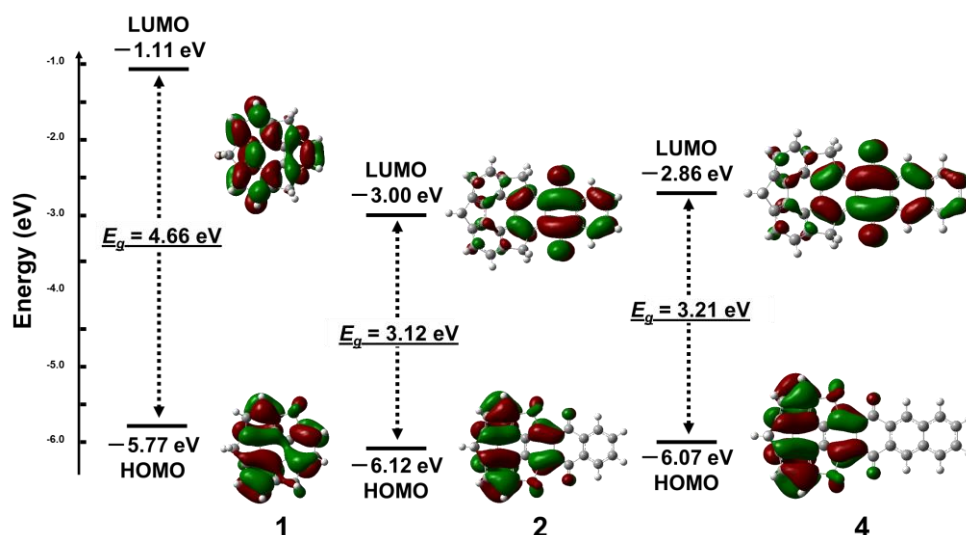


Figure 10. Frontier molecular orbitals of **1**, **2** and **4** and their energy diagrams calculated at B3LYP/6-31G+(d,p) level of theory (isovalue = 0.02).

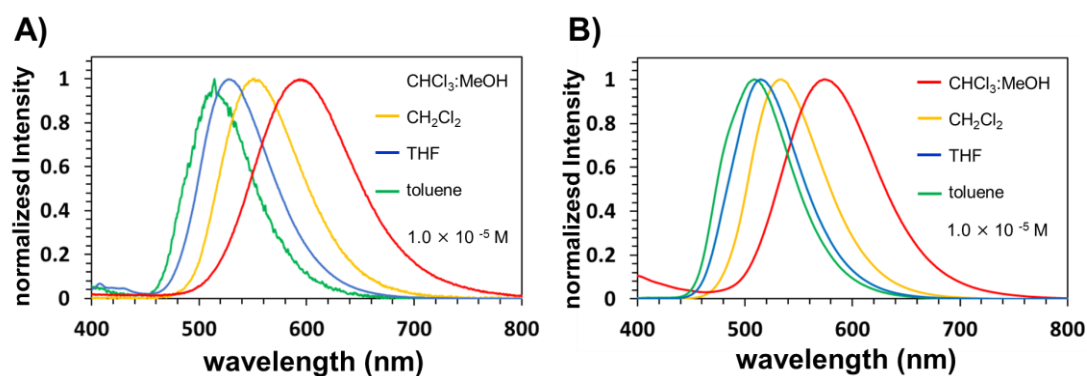
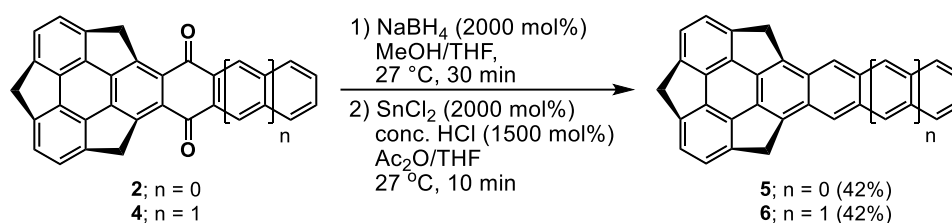


Figure 11. Emission spectra of quinone A) **2** and B) **4** in various solvents (1.0×10^{-5} mol/L). Excitation wavelength: 278 nm for **2**, 342 nm for **4**.

Section 3. Synthesis of sumanene-fused acenes and their properties

The next step is the conversion of sumanene-fused quinones to acenes. The author considered the conditions for the reduction of sumanene-fused quinone with sodium borohydride, followed by aromatization with hydrochloric acid and tin chloride (Scheme 9). In this condition, acetic anhydride was used as the solvent because there was concern that the cationic intermediates generated in situ during the aromatization step would be converted to alcohol by adding H₂O. As a result, the corresponding sumanene-fused acenes were obtained as the major products in 42% yield, respectively.

Scheme 9. Synthesis of sumanene-fused acenes.



Single crystals of acene **5** were obtained by slow evaporation from CH₂Cl₂ solution (Figure 12A). Single crystal X-ray structure analysis revealed that its bowl depth is 0.97-1.09 Å, indicating that it had a shallower bowl structure than **1** and quinone **2** (Figure 12B). A possible reason for this is that the sumanene moiety's bowl depth was made shallow to form a large orbital overlap between the sumanene and acene moiety and stabilize the structure.¹⁴ In the packing arrangement of the crystal, as aimed, acene **5** was found to form a 1D columnar structure unique to the sumanene derivative like quinone **2** (Figures 12C and 12D). This result is characteristic of the sumanene-fused acenes since the recently reported corannulene-fused acenes do not have a columnar structure,^{11f} but rather a slip-stack packing structure due to CH interactions. However, unlike the case of quinone **2**, acene **5** formed a staggered stacking (Figure 12C). This may be due to the strong CH $\cdots\pi$ interaction (3.70-3.76 Å) between the benzene ring of the acene moiety and the benzyl carbon on the five-membered ring of sumanene. Another noteworthy is that the bending in the acene skeleton was also observed in the crystal structure (Figure 13A). In the optimized structure calculated at the B3LYP/6-31G+(d,p) level (Figure 13B), no recognizable distortion was observed in the acene skeleton, which is considered to be due to the CH $\cdots\pi$ interaction described above, in addition to the packing requirement.

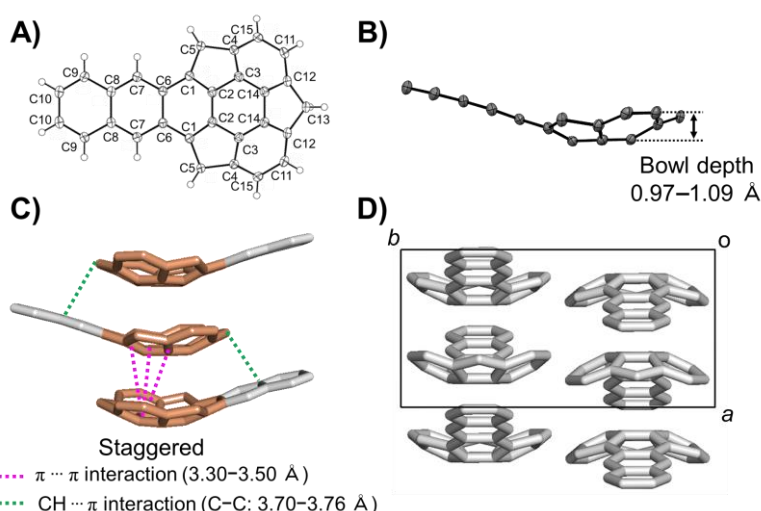


Figure 12. Crystal structure of acene **5**. A) Displacement ellipsoid plot of **5** at 50% probability. B) Bowl depth of the sumanene skeleton of **5**. C) Intermolecular interactions within the columns. The green dotted line denotes CH $\cdots\pi$ interactions; The pink dotted line shows $\pi\cdots\pi$ interactions. D) Packing structure viewed from the *c* axis. For clarity, hydrogen atoms in (B)–(D) are omitted.

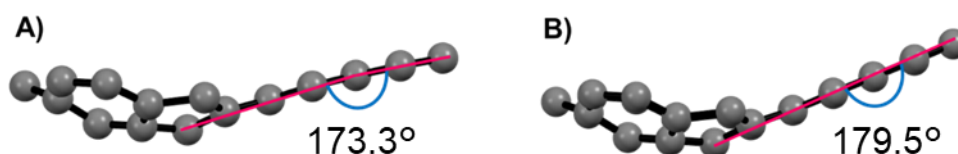


Figure 13. The comparison of curved acene's angle between A) crystal structure and B) optimized structure of **5** calculated at B3LYP/6-31G+(d,p) level of theory.

Both acenes **5** and **6** exhibited oxidation peaks derived from the acene moiety ($E_p^{\text{ox}} = +0.58$ V (for **5**), $+0.36$ V, $+0.63$ V (for **6**)) and broad oxidation peaks derived from the sumanene moiety in CV measurements, as well as reduction peaks derived from both the acene and sumanene moieties (Figure 14). However, no reversible peaks were obtained on either the oxidation or reduction side, possibly due to the species' instability. The respective HOMO-LUMO gaps ΔE_c (3.25 eV (for **5**) and 2.68 eV (for **6**)) estimated from the onset of the oxidation and reduction peaks in CV measurements are in good agreement with the calculated ΔE_{calc} for the B3LYP/6-31G+(d,p) levels (3.00 eV (for **5**) and 2.45 eV (for **6**)) (Table 2 and Figure 15).

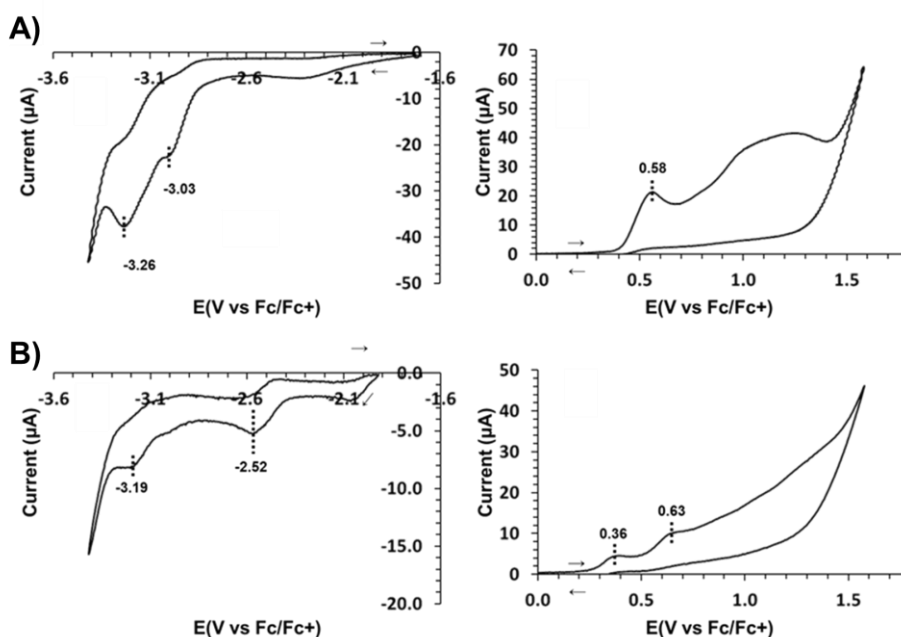


Figure 14. Cyclic voltammograms of quinones A) **5** and B) **6** (5.0×10^{-4} M in THF) measured in the presence of $[n\text{-Bu}_4\text{N}][\text{ClO}_4]$ (0.1 M) supporting electrolyte. Working electrode: GCE, counter electrode: Pt, reference electrode: Ag/AgNO₃. Scan rate: 50 mV s⁻¹. The ferrocene/ferrocenium couple (Fc⁰/Fc⁺) was used as a reference. All the solutions were purged with nitrogen prior to the measurements.

Table 2. Electrochemical parameters of acenes **5** and **6**. $E_{\text{on}}^{\text{red}}$ and $E_{\text{on}}^{\text{ox}}$: Oxidation and reduction potentials (vs. Fc/ Fc⁺) obtained from CV. Calculated HOMO and LUMO potentials (in eV), the HOMO–LUMO gaps (ΔE_{calc}) (B3LYP/6-31G+(d,p) level of theory) of **5** and **6** are also shown.

compound	cyclic voltammetry			calculation		
	$E_{\text{on}}^{\text{red}} / \text{V}^{\text{a}}$	$E_{\text{on}}^{\text{ox}} / \text{V}^{\text{a}}$	$\Delta E_{\text{cv}} / \text{eV}^{\text{b}}$	LUMO /eV	HOMO /eV	$\Delta E_{\text{calc}} / \text{eV}$
5	-2.83	0.42	3.25	-2.21	-5.21	3.00
6	-2.41	0.27	2.68	-2.54	-4.99	2.45

^aThe onset potential. ^bCalculated from the onset potential.

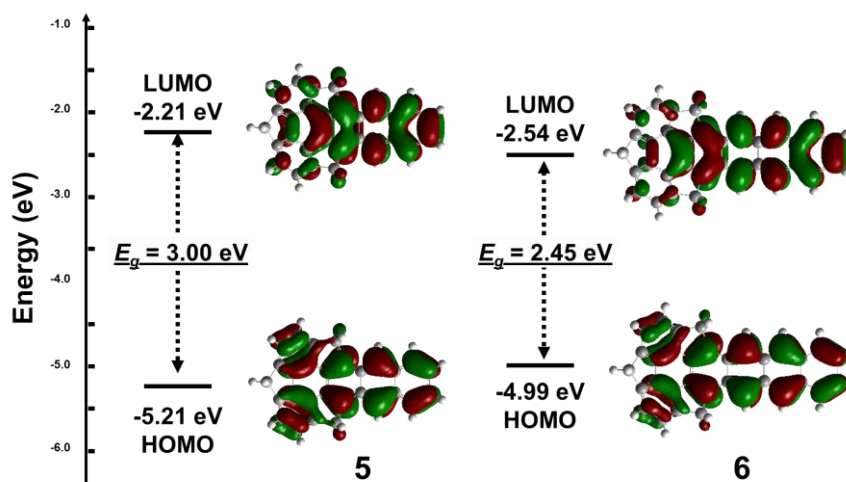


Figure 15. Frontier molecular orbitals of **1**, **5** and **6** and their energy diagram calculated at B3LYP/6-31G+(d,p) level of theory (isovalue = 0.02).

In the UV-vis absorption spectra of acenes **5** and **6**, a strong absorption attributed to the sumanene skeleton at 331 nm and 346 nm, respectively (Figure 16A), and characteristic vibrational bands derived from acenes around 390-470 nm and 460-550 nm (Figure 16B) were observed. The absorption wavelengths of **5** and **6** were intermediate between anthracene and tetracene and between tetracene and pentacene, respectively. This result was consistent with the calculated NICS(0) value, which is used to evaluate aromaticity and indicates that the more negative the value is on each ring, the more strongly aromatic it is (Figure 17). The positive NICS(0) values for the benzene ring at the center of the sumanene skeleton for acenes **5** and **6** indicated that the conjugation lengths of the corresponding tetracene and pentacene skeletons were shorter than those of the pristine acenes, resulting in absorption peaks on the shorter wavelength side. A similar trend was observed in the emission spectra (Figure 18). In addition, the fluorescence quantum yield and fluorescence lifetime of the acene derivatives were compared. The fluorescence quantum yield decreased as the number of aromatic rings increased, but the fluorescence lifetime was not affected by the number of aromatic rings or the introduction of the sumanene structure (Table 3).

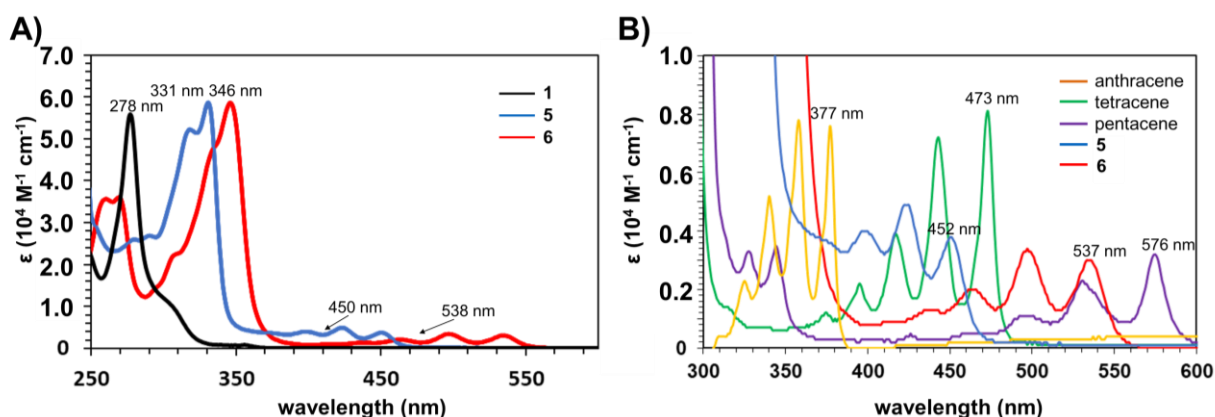


Figure 16. UV-vis absorption spectra of A) **1**, **5** and **6** and B) acenes in THF (1.0×10^{-5} mol/L).

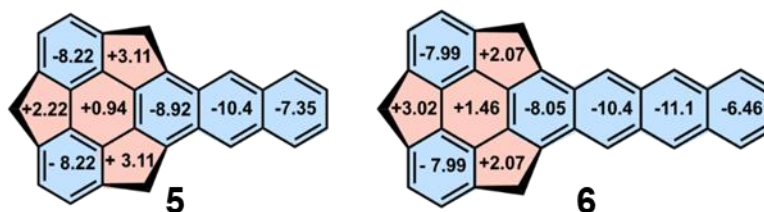


Figure 17. NICS(0) calculation results of acenes **5** and **6** at B3LYP/6-311G+(d,p) level of theory.

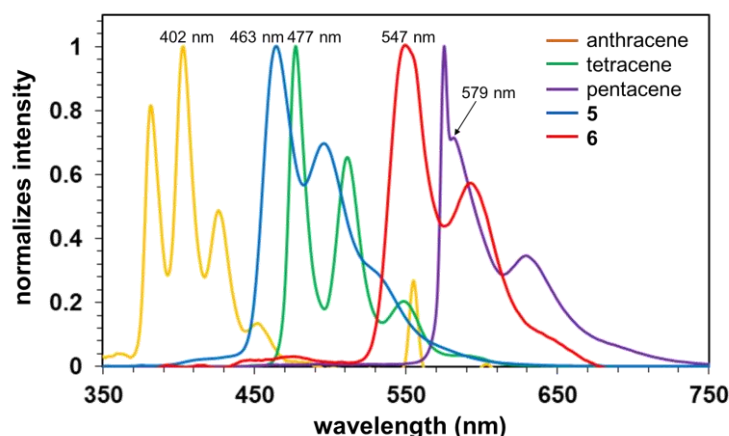


Figure 18. Emission spectra of acenes in THF (solid line, 1.0×10^{-5} mol/L). Excitation wavelength: 278 nm for anthracene, tetracene, and **6**, 337 nm for **5**, and 574 nm for pentacene.

Table 3. Fluorescence quantum yield and fluorescence lifetime of acenes in CH_2Cl_2 (1.0×10^{-6} mol/L under argon).

	5	6	tetracene	pentacene
Fluorescence quantum yield (Φ)	0.1	0.07	0.09	0.05
Fluorescence lifetime	$\tau = 4.46$ ns CHI = 1.04103	$\tau = 4.36$ ns CHI = 1.02005	$\tau = 3.30$ ns CHI = 1.13116	$\tau = 9.04$ ns CHI = 1.13347

The stability of the synthesized acene derivatives was evaluated (Figure 19). In general, the stability of acene compounds is low because they readily react with light and oxygen under the air. In this study, the stability of each acene was evaluated in THF by monitoring the decay of UV-vis absorption intensity at the maximum absorption wavelength I_{max} of **5** (331 nm), **6** (346 nm), tetracene (276 nm), and pentacene (299 nm) under fluorescent light irradiation. As a result, acene **5** showed higher stability than tetracene with the same number of fused benzene rings. Acene **6** was also more stable than pentacene. This result indicates the effect of the curved structure in the sumanene-fused acenes. The curved sumanene moiety reduces the overlap of orbitals across the acene moiety, resulting in a reduced conjugated system. Hence, the sumanene-fused acenes may have exhibited higher stability than the corresponding acenes. Then, attempts were made to identify the decomposed products of acenes **5** and **6** that reacted with light and oxygen by ^1H NMR, but only broad peaks were observed, and no dimer and oxidation products such as quinones were observed.

Regarding the solubility of acenes, pentacene is almost insoluble in CH_2Cl_2 , while acene **6** shows good solubility (Table 4). One possible reason for this is the contribution of the increased dipole moment (2.3 Debye) due to the introduction of the sumanene moiety.

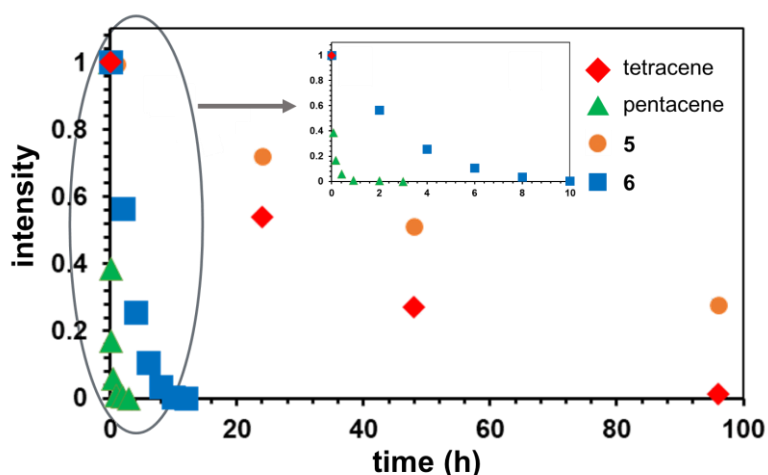


Figure 19. Time-course plots of the decay of UV absorption at I_{\max} in THF (1.0×10^{-5} mol/L, under the room light irradiation). The time (h) is when the absorption peak at I_{\max} disappeared utterly. I_{\max} : 276 nm for tetracene, 299 nm for pentacene, 331 nm for **5**, 346 nm for **6**.

Table 4. Solubility for CH_2Cl_2 and dipole moment of acenes .

	tetracene	pentacene	6
solubility for CH_2Cl_2 (mmol/L)	< 1.0	< 0.1	> 10
dipole moment (Debye)	0.0	0.0	2.3

Section 4. Summary

The author synthesized two sumanene-fused quinones via double acylation to sumanene, followed by subsequent reductive aromatization to sumanene-fused acenes **5** and **6**. Single crystal X-ray analysis of quinone **2** and acene **5** showed that both compounds form a 1D columnar structure based on the stacking ability of the sumanene skeleton, as expected. These results clearly indicate that introducing the sumanene skeleton into acenes helps control the arrangement of the acene moiety. Furthermore, CV and spectroscopic measurements also revealed that the introduction of the sumanene skeleton into acenes has no significant effect on the electronic properties but contributes to the solubility of the molecules. Thus, introducing the sumanene skeleton into acenes may be a promising strategy for creating novel SF molecules.

Experimental section

Instrumentations and chemicals

All manipulations of moisture or air-sensitive compounds were performed by standard Schlenk techniques in anhydrous solvents under a nitrogen atmosphere using flame-dried glasswares. Reactions were conducted in an EYELA PPS-2511 personal organic synthesizer. Analytical thin-layer chromatography (TLC) was performed on pre-coated silica-gel aluminum sheets (Merck silica gel 60 F254, Cat. No. 1.05554.0001). Column chromatography was conducted on a YAMAZEN automated flash chromatography system that consists of an AI-580S and a Parallel Frac FR-360 using silica-gel (Kanto Chemical Co., Inc. Silica Gel 60 N (spherical, neutral)). Preparative thin-layer chromatography (PTLC) was prepared using Wako Wakogel B-5F. Recycling preparative high-performance liquid chromatography (HPLC) was performed by LC-908W (Japan Analytical Industry Co., Ltd.) with high-resolution gel permeation chromatography (GPC) column (Japan Analytical Industry Co., Ltd., JAIGEL-1H and 2H) with CHCl_3 as an eluent. ^1H NMR (400 MHz) and ^{13}C NMR (100 MHz) spectra were measured on a JEOL JNM-ECZS400 spectrometer at room temperature. Chloroform- d_1 (CDCl_3) was used as a solvent for NMR measurements. Chemical shifts (δ) are given in parts per million (ppm) downfield from the solvent signal (for ^1H NMR: CHCl_3 δ 7.26 ppm; for ^{13}C NMR: CDCl_3 δ 77.2 ppm) as an internal standard with coupling constants (J) in hertz (Hz). The abbreviations s and d signify singlet, and doublet, respectively. Melting points were determined on an Optimelt MPA100 automated melting point apparatus (Stanford Research Systems, Inc.) and expressed without correction. High resolution mass spectra (HRMS) were measured on JEOL-JMS-T100LP (DART) and JEOL-JMS-700EI (EI). Infrared (IR) absorption spectra were measured by the attenuated total reflection (ATR) method on a JASCO FT/IR-4100 Fourier transform IR spectrometer equipped with a JASCO ATR PRO ONE single reflection ATR optical attachment and a diamond crystal plate. The absorption bands were given in wavenumber (cm^{-1}). The absorption bands were given in wavenumber (cm^{-1}). Ultraviolet-visible (UV-vis) absorption spectroscopy was measured on a JASCO V-670 spectrophotometer by transmission method. Ultraviolet-visible (UV-vis) absorption spectroscopy was measured on a JASCO V-670 spectrophotometer by transmission method. The absorption bands were given in wavelength (nm). A quartz cell (optical path length; 10 mm) was used. Fluorescence spectra were recorded on a JASCO FP6500 spectrofluorometer and expressed after normalization. A quartz cell (optical path length; 10 mm) was used. Absolute emission quantum yields were measured on a Quantaurus-QY Plus UV-NIR absolute PL quantum yield spectrometer C13534-21 (Hamamatsu Photonics K.K.). The electrochemical analyses were performed on a BAS ALS Model 650DKMP electrochemical analyzer. The theoretical calculations were performed using Research Center for Computational Science, Okazaki, Japan.

6,13-Dihydro-3H-benzo[*l*]cyclopenta[*pqr*]-as-indaceno[2,1,8,7-*defgh*]tetraphene-7,12-dione (2)

The mixture of sublimated AlCl₃ (16.5 mg, 0.124 mmol) and sumanene (**1**) (15.0 mg, 0.0568 mmol) in *o*-dichlorobenzene (2.0 mL) was stirred at room temperature for 15 s vigorously. Then, to the mixture was added phthaloyl chloride (8.2 μ L, 0.057 mmol), and the mixture was stirred for 15 s vigorously. The mixture was heated at 200 °C under irradiation of microwave for 10 min. After cooling to room temperature, to the mixture was added aqueous hydrogen chloride solution (10%) and the mixture was extracted with CH₂Cl₂. The combined organic extract was dried over Na₂SO₄ and concentrated under reduced pressure. The residue was purified by silica-gel column chromatography (CH₂Cl₂). After that, the crude was washed with aqueous KOH solution (50 wt%, 3 times) and then with *n*-hexane/CH₂Cl₂ (95:5) to give **2** (12.1 mg, 30.7 μ mol, 54%). Yellow solid; mp: 327 °C (dec); TLC: R_f = 0.61 (*n*-hexane/ AcOEt = 3:1); ¹H NMR (400 MHz, CDCl₃): δ 3.47 (d, *J* = 19.7 Hz, 1H), 4.05 (d, *J* = 21.0 Hz, 2H), 4.75 (d, *J* = 19.7 Hz, 1H), 5.13 (d, *J* = 21.0 Hz, 2H), 7.21 (d, *J* = 7.78 Hz, 2H), 7.25 (d, *J* = 7.78 Hz, 2H), 7.73–7.75 (m, 2H), 8.25–8.27 (m, 2H); ¹³C NMR (100 MHz, CDCl₃): δ 42.1 (2C), 44.9 (1C), 123.9 (2C), 125.7 (2C), 127.3 (2C), 131.6 (2C), 133.9 (2C), 134.0 (2C), 147.3 (2C), 149.3 (2C), 150.0 (2C), 150.8 (2C), 151.3 (2C), 152.4 (2C), 184.3 (2C); IR (ATR): ν = 2916, 2850, 1662, 1373, 1275, 1012 cm⁻¹; HRMS (EI): *m/z* calcd for C₂₉H₁₄O₂ [M]⁺: 394.0994, found: 394.0991; elemental analysis calcd (%) for C₂₉H₁₄O₂: C 88.31, H 3.58; found: C 87.98, H 3.50.

6,13-Dihydro-3H-benzo[*l*]cyclopenta[*pqr*]-as-indaceno[2,1,8,7-*defgh*]tetraphene-7,12-dione (3)

The mixture of sublimated AlCl₃ (22.2 mg, 0.167 mmol), phthalic anhydride (11.2 mg, 0.0758 mmol) and sumanene (**1**) (20.0 mg, 0.0758 mmol) in *o*-dichlorobenzene (2.0 mL) was stirred at 50 °C for 2 h. After cooling to room temperature, to the mixture was added H₂O, and the mixture was extracted with CH₂Cl₂. The combined organic extract was dried over Na₂SO₄ and concentrated under reduced pressure. The residue was purified by PTLC (AcOEt) to give **3** (28.1 mg, 68.2 μ mol, 90%).

Yellow solid; mp: 235 °C (dec); TLC: R_f = 0.55 (AcOEt); ¹H NMR (400 MHz, CDCl₃): δ 3.43 (d, *J* = 19.9 Hz, 1H), 3.44 (d, *J* = 20.4 Hz, 1H), 3.51 (d, *J* = 20.8 Hz, 1H), 4.54 (d, *J* = 19.9 Hz, 1H), 4.67 (d, *J* = 20.4 Hz, 1H), 4.72 (d, *J* = 20.8 Hz, 1H), 7.07 (d, *J* = 7.78 Hz, 1H), 7.12 (t, *J* = 7.78 Hz, 1H), 7.14 (t, *J* = 7.78 Hz, 1H), 7.19 (d, *J* = 7.78 Hz, 1H), 7.40 (d, *J* = 7.78 Hz, 1H), 7.45 (s, 1H), 7.57 (d, *J* = 7.78 Hz, 1H), 7.65 (d, *J* = 7.67 Hz, 1H), 8.07 (d, *J* = 7.67 Hz, 1H); ¹³C NMR (CDCl₃) δ 42.1 (1C), 42.9 (1C), 43.8 (1C), 123.6 (1C), 123.7 (1C), 124.3 (1C), 125.0 (1C), 126.5 (1C), 127.9 (1C), 128.1 (1C), 129.6 (1C), 131.2 (1C), 133.2 (1C), 133.5 (1C), 144.2 (1C), 147.6 (1C), 147.7 (1C), 148.3 (1C), 148.5 (1C), 148.7 (1C), 149.1 (2C), 149.2 (1C), 149.9 (1C), 150.0 (1C), 152.1 (1C), 152.2 (1C), 169.7 (1C), 196.8 (1C); IR (ATR): ν = 3748, 3649, 1716, 1541, 1260 cm⁻¹; HRMS (DART): *m/z* calcd for C₂₉H₁₇O₃ ([M+H]⁺): 313.1172, found 413.1174.

6,15-Dihydro-3H-fluoreno[3',4',5',6':3,4,5,6]-as-indaceno[1,8-*abc*]tetracene-7,14-dione (**4**)

The mixture of sublimated AlCl₃ (16.5 mg, 0.124 mmol) and sumanene (**1**) (15.0 mg, 0.0568 mmol) in *o*-dichlorobenzene (2.0 mL) was stirred at room temperature for 15 s vigorously. To the mixture was added 2,3-naphthalenedicarbonyl dichloride (14.4 mg, 0.0568 mmol), and the mixture was stirred for 15 s vigorously. The mixture was heated at 200 °C under microwave irradiation for 10 min. After cooling to room temperature, to the mixture was added aqueous hydrogen chloride solution (10%) and was extracted with CH₂Cl₂. The combined organic extract was dried over Na₂SO₄ and concentrated under reduced pressure. The residue was purified by silica-gel column chromatography (CH₂Cl₂). The crude was washed with aqueous KOH solution (50 wt%, 3 times) and then with *n*-hexane/CH₂Cl₂ (95:5) to give **4** (10.1 mg, 22.7 μmol, 40%). Yellow solid; mp: 333 °C (dec); TLC: R_f = 0.63 (*n*-hexane/ AcOEt = 3:1); ¹H NMR (400 MHz, CDCl₃): δ 3.48 (d, *J* = 19.7 Hz, 1H), 4.12 (d, *J* = 21.4 Hz, 2H), 4.77 (d, *J* = 19.7 Hz, 1H), 5.20 (d, *J* = 21.4 Hz, 2H), 7.24 (d, *J* = 7.78 Hz, 2H), 7.26 (d, *J* = 7.78 Hz, 2H), 7.66 (m, 2H), 8.07 (m, 2H), 8.80 (s, 2H); ¹³C NMR (100 MHz, CDCl₃): δ 42.1 (1C), 45.1 (2C), 124.0 (2C), 125.7 (2C), 129.4 (4C), 130.2 (2C), 130.4 (2C), 132.7 (2C), 135.4 (2C), 147.3 (2C), 149.3 (2C), 150.0 (2C), 150.9 (2C), 151.3 (2C), 152.5 (2C), 184.2 (2C); IR (ATR): ν = 2955, 2292, 2851, 1729, 1662, 1273, 1072 cm⁻¹; HRMS (EI): *m/z* calcd for C₃₃H₁₆O₂ [M]⁺: 444.1150, found: 444.1151.

6,13-Dihydro-3H-benzo[*l*]cyclopenta[*pqr*]-as-indaceno[2,1,8,7-*defgh*]tetraphene (**5**)

Quinone (**2**) (15.0 mg, 0.0363 mmol) was stirred vigorously in THF (6.0 mL) at 27 °C for 5 min, and then to this was added NaBH₄ (28.8 mg, 0.758 mmol) in MeOH (6.0 mL). After stirring for 30 min at 27 °C, the solvent was removed under the reduced pressure, and the residue was purified with silica gel column chromatography (AcOEt/CH₂Cl₂ = 1:1) to remove excess amount of NaBH₄. Then to the residue in THF (0.2 mL) was added SnCl₂ (144.1 mg, 0.760 mmol) and conc. aqueous hydrogen chloride solution (50.4 μL, 0.570 mmol) in Ac₂O (0.2 mL)/THF (1 mL) and stirred at 27 °C. After 10 min, to the mixture was added brine and was extracted with CH₂Cl₂. The combined organic extract was dried over Na₂SO₄ and concentrated under reduced pressure. The residue was immediately purified with silica gel column chromatography (CH₂Cl₂) and PTLC (*n*-hexane/CH₂Cl₂ = 4:1) in the dark to give **5** (5.8 mg, 16 μmol, 42%). Yellow solid; mp: 255 °C (dec); TLC: R_f = 0.35 (*n*-hexane/ CH₂Cl₂ = 5:1); ¹H NMR (400 MHz, CDCl₃): δ 3.36 (d, *J* = 19.2 Hz, 1H), 3.70 (d, *J* = 20.1 Hz, 2H), 4.65 (d, *J* = 19.2 Hz, 1H), 5.05 (d, *J* = 20.1 Hz, 2H), 7.09 (d, *J* = 7.78 Hz, 2H), 7.18 (d, *J* = 7.78 Hz, 2H), 7.43–7.47 (m, 2H), 7.98–8.00 (m, 2H), 8.53 (s, 2H); ¹³C NMR (100 MHz, CDCl₃): δ 42.4 (2C), 42.8 (1C), 123.8 (2C), 124.2 (2C), 125.0 (2C), 125.5 (2C), 131.2 (2C), 132.1 (2C), 145.2 (2C), 145.7 (2C), 147.1 (2C), 148.3 (2C), 148.5 (2C), 150.5 (2C); IR (ATR): ν = 3735, 2920, 2850, 1716, 1277 cm⁻¹; HRMS (EI): *m/z* calcd for C₂₉H₁₆ [M]⁺: 364.1252, found: 364.1248.

6,15-Dihydro-3H-fluoreno[3',4',5',6':3,4,5,6]-as-indaceno[1,8-*abc*]tetracene (6)

Quinone (**4**) (15.0 mg, 0.0338 mmol) was stirred vigorously in THF (6.0 mL) at 27 °C for 5 min, and then to the mixture was added NaBH₄ (25.7 mg, 0.676 mmol) in MeOH (6.0 mL). After stirring for 30 min at 27 °C, the solvent was removed under reduced pressure, and the residue was purified with silica gel column chromatography (AcOEt/CH₂Cl₂ = 1:1) to remove excess amount of NaBH₄. Then to the residue in THF (0.2 mL) was added SnCl₂ (128.2 mg, 0.676 mmol) and conc. aqueous hydrogen chloride solution (44.8 μL, 0.507 mmol) in Ac₂O (0.2 mL)/THF (1 mL) and stirred at 27 °C. After 10 min, to the mixture was added brine, and the mixture was extracted with CH₂Cl₂. The combined organic extract was dried over Na₂SO₄ and concentrated under reduced pressure. The residue was immediately purified with silica gel column chromatography (CH₂Cl₂) in dark and GPC (CHCl₃) to give **6** (5.9 mg, 0.014 mmol, 42%).

Purple solid; mp: 245 °C (dec); TLC: R_f = 0.33 (*n*-hexane/ CH₂Cl₂ = 5:1); ¹H NMR (400 MHz, CDCl₃): δ 3.36 (d, *J* = 19.2 Hz, 1H), 3.72 (d, *J* = 19.7 Hz, 2H), 4.64 (d, *J* = 19.2 Hz, 1H), 5.06 (d, *J* = 19.7 Hz, 2H), 7.10 (d, *J* = 7.78 Hz, 2H), 7.18 (d, *J* = 7.78 Hz, 2H), 7.39–7.42 (m, 2H), 7.99–8.02 (m, 2H), 8.64 (s, 2H), 8.76 (s, 2H); ¹³C NMR (100 MHz, CDCl₃): δ 41.7 (1C), 42.5 (2C), 124.0 (2C), 124.4 (2C), 125.1 (2C), 125.4 (2C), 126.4 (2C), 128.5 (2C), 129.8 (2C), 131.7 (2C), 132.4 (2C), 144.8 (2C), 145.4 (2C), 146.6 (2C), 148.1 (2C), 148.4 (2C) 150.4 (2C); IR (ATR): ν = 2921, 1261, 1093, 1019 cm⁻¹; HRMS (EI): *m/z* calcd for C₃₃H₁₈ [M]⁺: 414.1409, found: 414.1402.

Quantum chemical calculation

All theoretical calculations were conducted by Gaussian09.¹⁵ The ground state structure optimization were performed at the B3LYP/6-31G+(d,p)¹⁶ level of theory. GIAO (NICS (0) values) were also obtained at the B3LYP/6-311G+(d,p).

X-ray Crystallographic Data for **2** and **5**

The diffraction data for **2** was recorded on an ADSC Q210 CCD area detector with a synchrotron radiation ($\lambda=0.70000$ Å) at 2D beamline in Pohang Accelerator Laboratory (PAL). The diffraction images were processed by using HKL3000.¹⁷

The diffraction data for **5** was recorded on a XtaLAB Synergy with a Mo-target ($\lambda = 0.71073$ Å) equipped with a Rigaku HyPix-6000HE as the detector at 150 K in house. The diffraction images were processed by using CrysAlisPro.¹⁸

All the structures were solved by direct methods (SHELXT-2015, 2018/2)¹⁹ and refined by full-matrix least squares calculations on *F*² (SHELXL-2018/3)²⁰ using the Olex2²¹ program package.

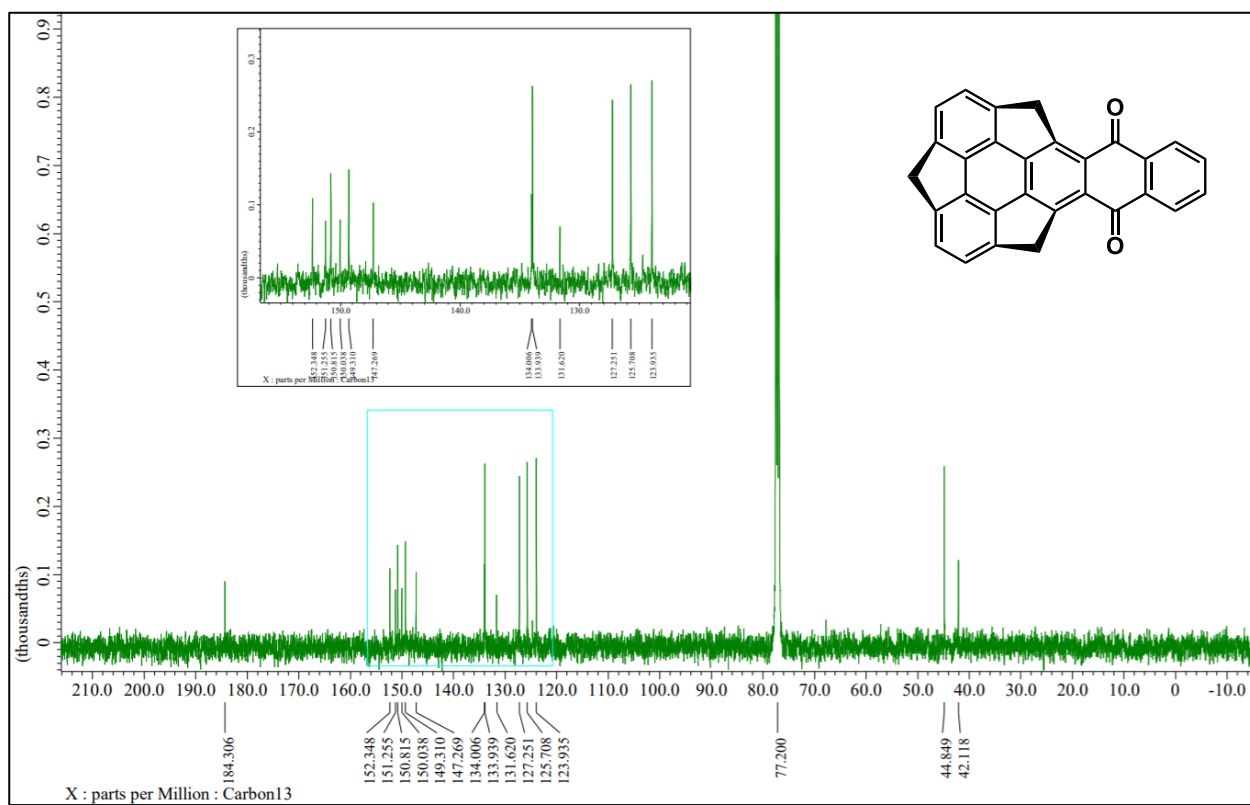
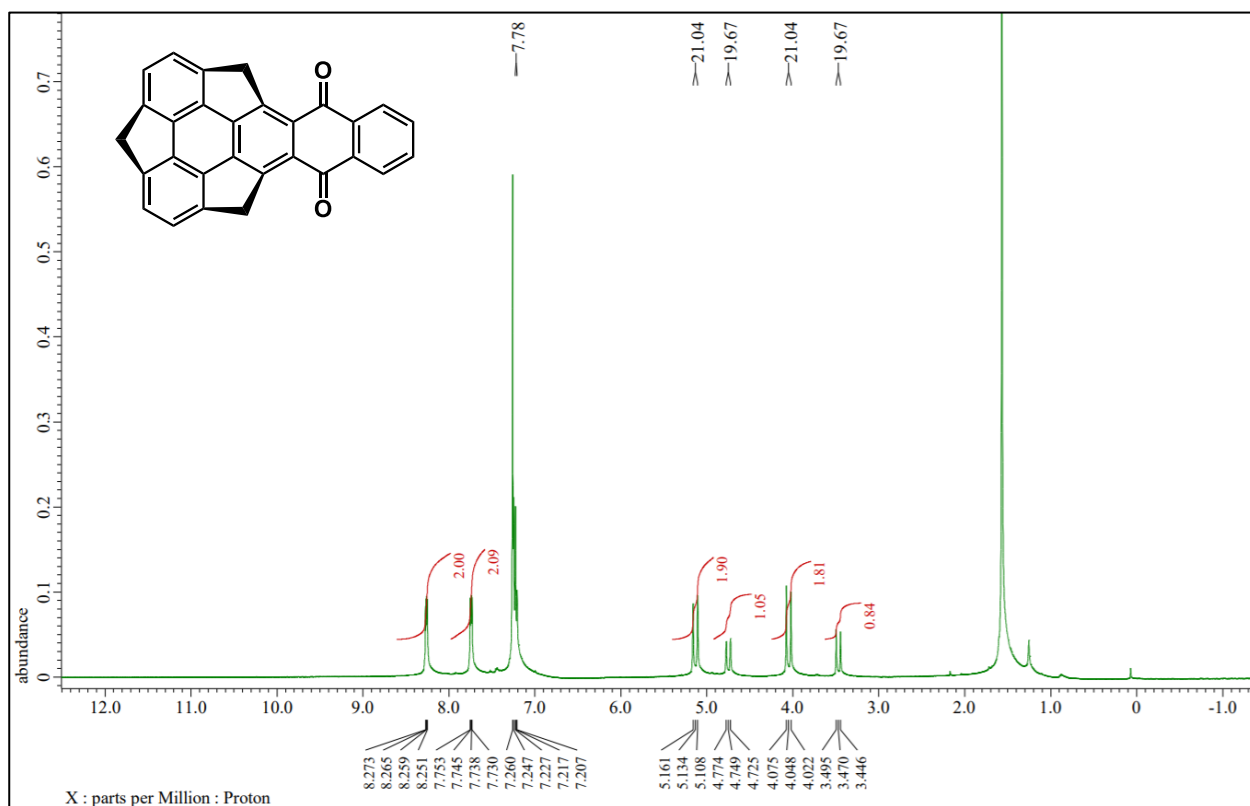
2: C₂₉H₁₄O₂, monoclinic, space group *P*2₁/*n* (No. 14), *a* = 13.718(3) Å, *b* = 3.8422(8) Å, *c* = 32.275(7) Å, β = 91.29(3)°, *V* = 1700.7(6) Å³, ρ_{calcd} = 1.540 g/cm³, *Z* = 4, 4585 unique reflections out of 4938 with *I* > 2 σ (*I*), 280 parameters, 2.433° < θ < 30.025°, *R*₁ = 0.0532, *wR*₂ = 0.1523, GOF = 1.117.

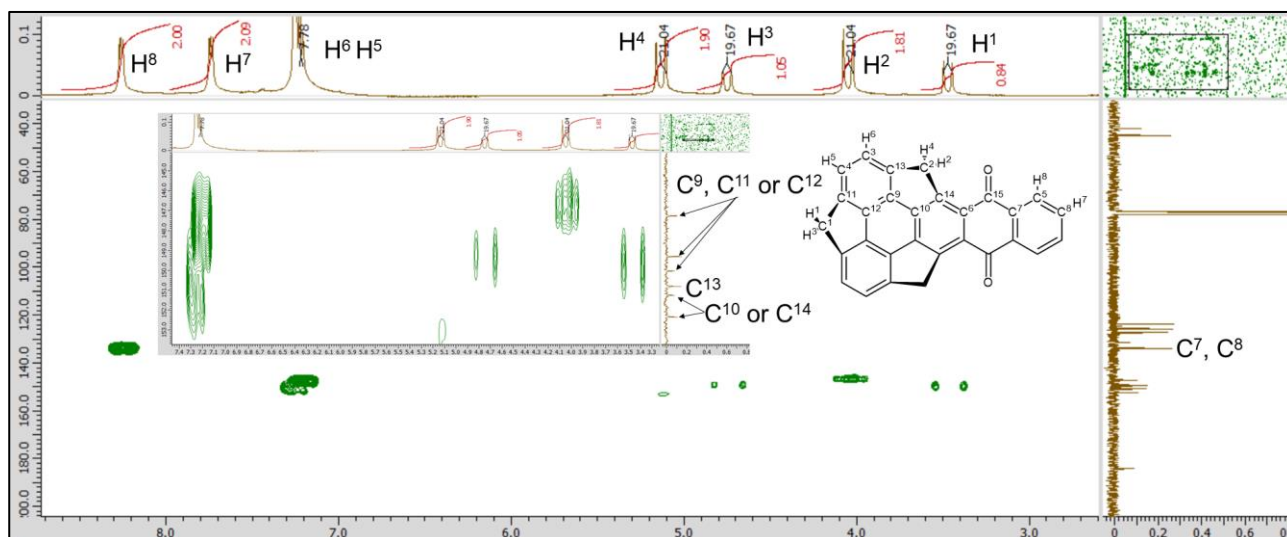
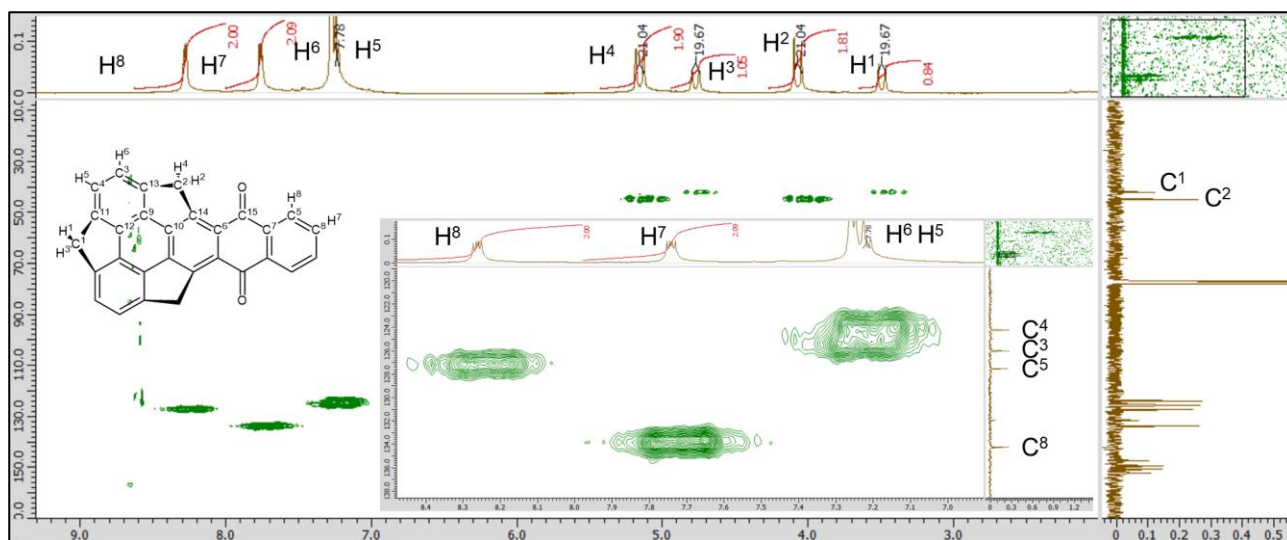
5: C₂₉H₁₆, orthorhombic, space group *Pnma* (No. 62), *a* = 7.5998(4) Å, *b* = 15.2531(7) Å, *c* = 14.7570(7) Å, *V* = 1710.6(1) Å³, ρ_{calcd} = 1.415 g/cm³, *Z* = 4, 1864 unique reflections out of 2341 with *I* > 2 σ (*I*), 133 parameters, 2.761° < θ < 30.979°, *R*₁ = 0.0581, *wR*₂ = 0.1583, GOF = 1.055.

CCDC 2117403 (**5**) and 2117404 (**2**) contain the crystallographic data for this paper. These data can be obtained free of charge from The Cambridge Crystallographic Data Centre (<https://www.ccdc.cam.ac.uk/>).

¹H and ¹³C NMR spectra

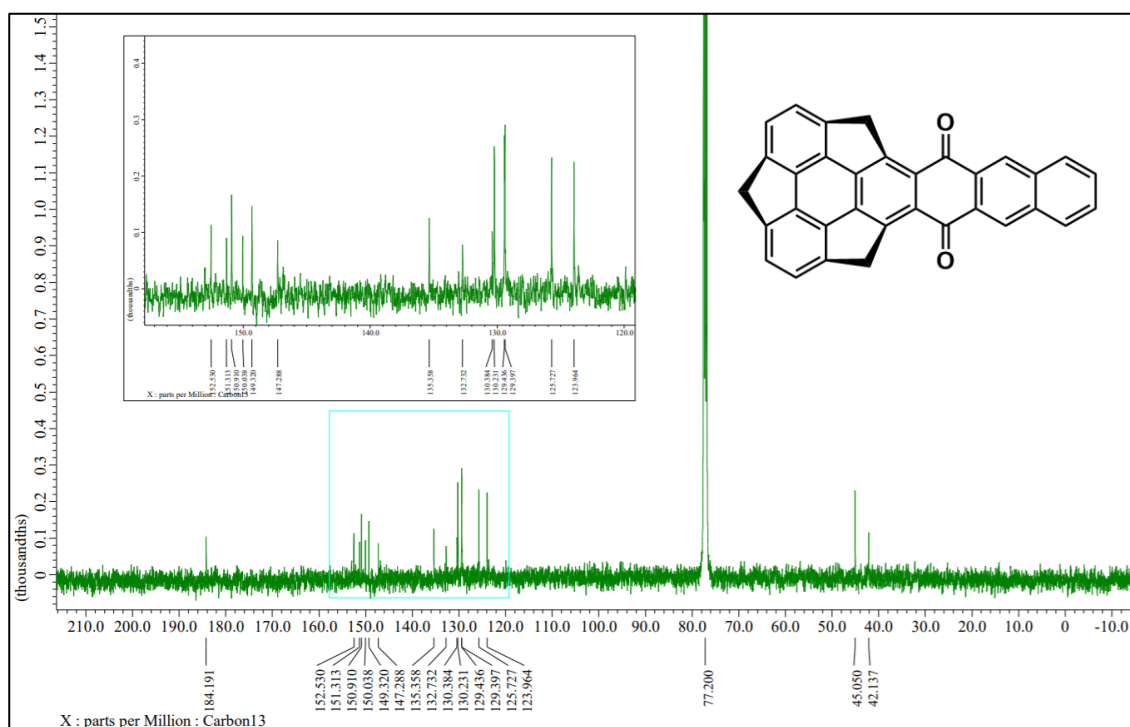
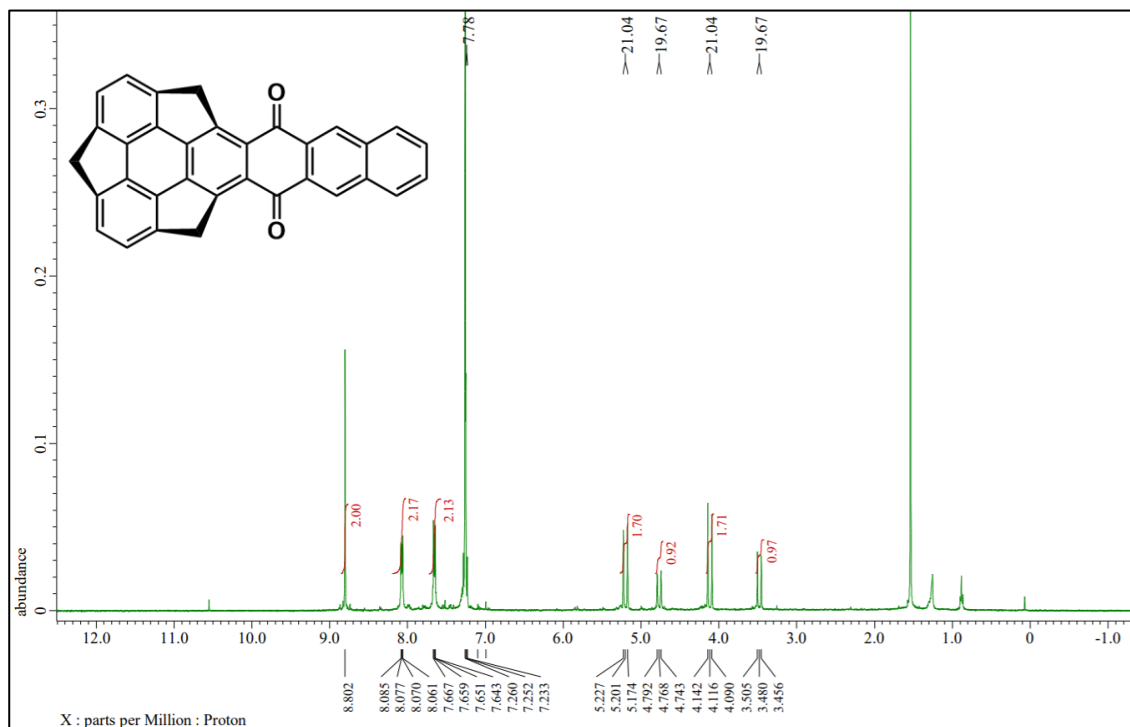
¹H NMR (400 MHz), ¹³C NMR (100 MHz), HMQC and HMBC spectra of **2** (CDCl₃)

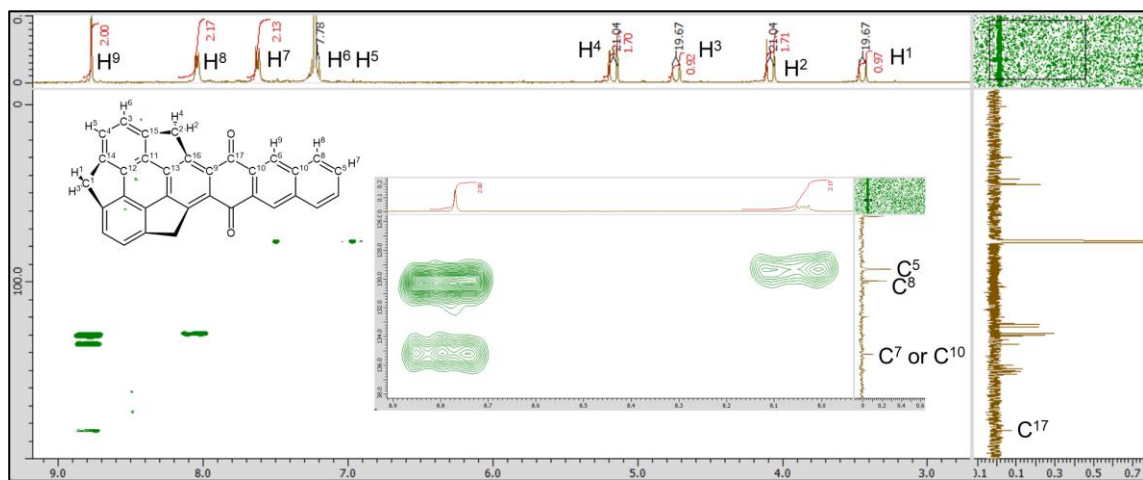
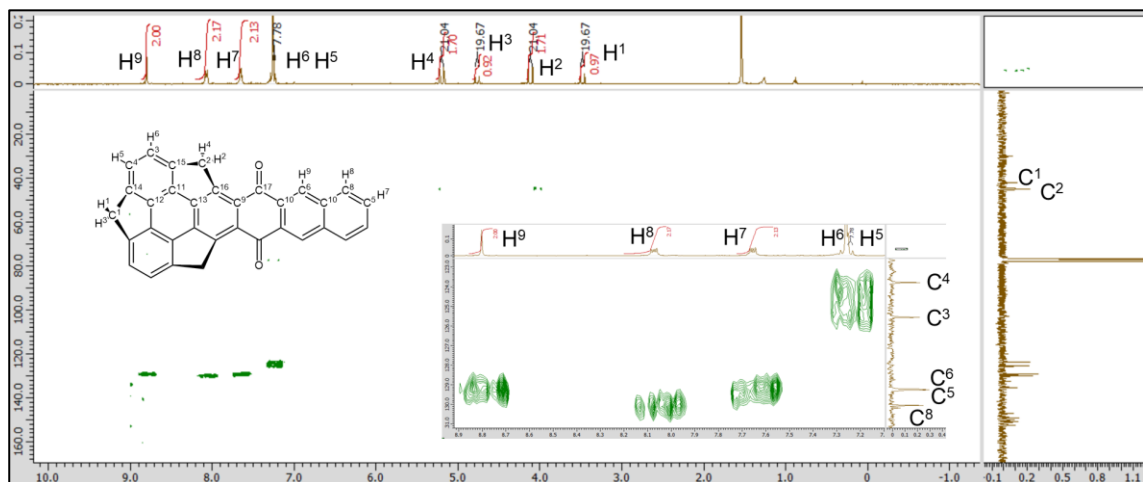




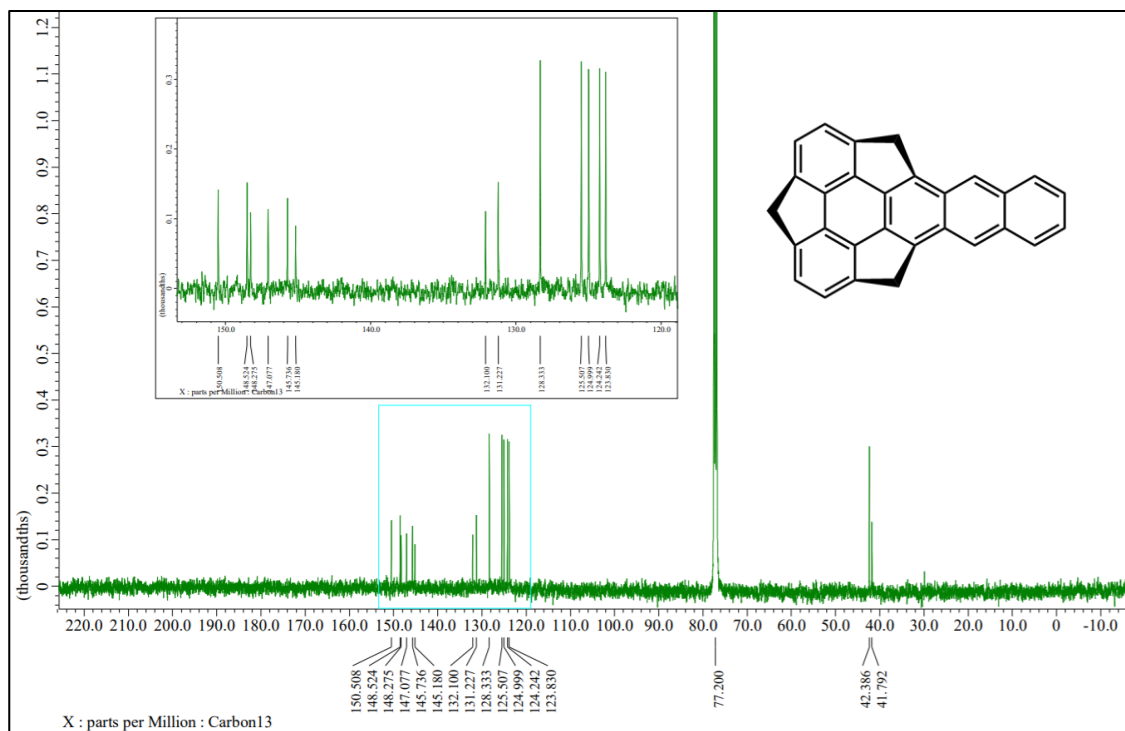
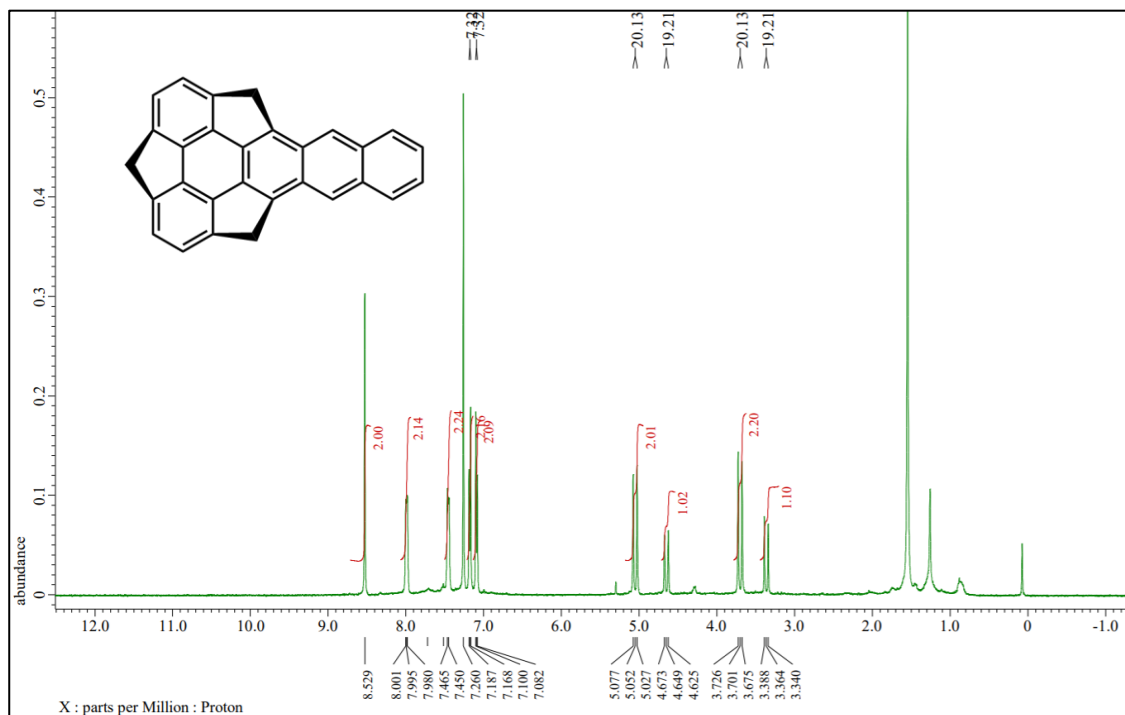
[illegible]

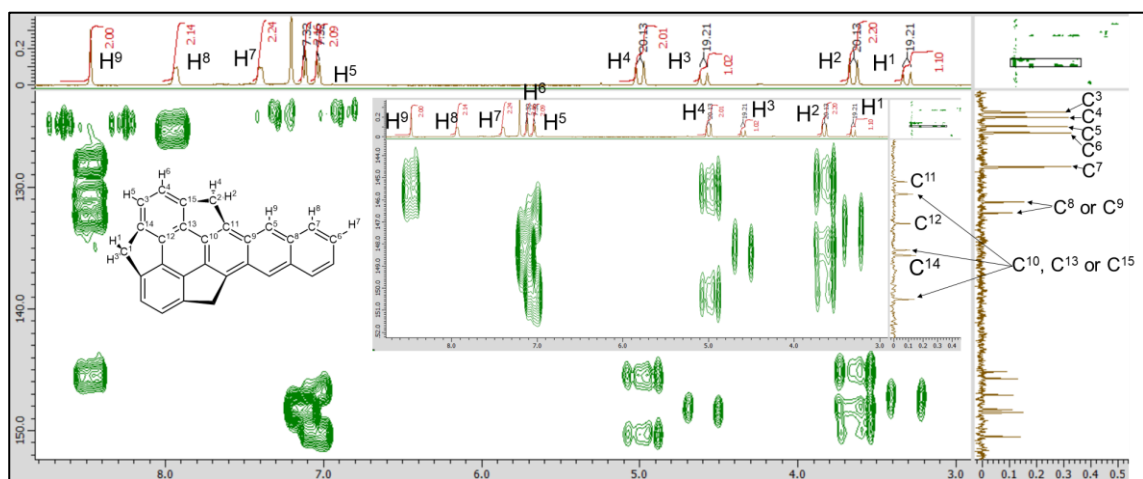
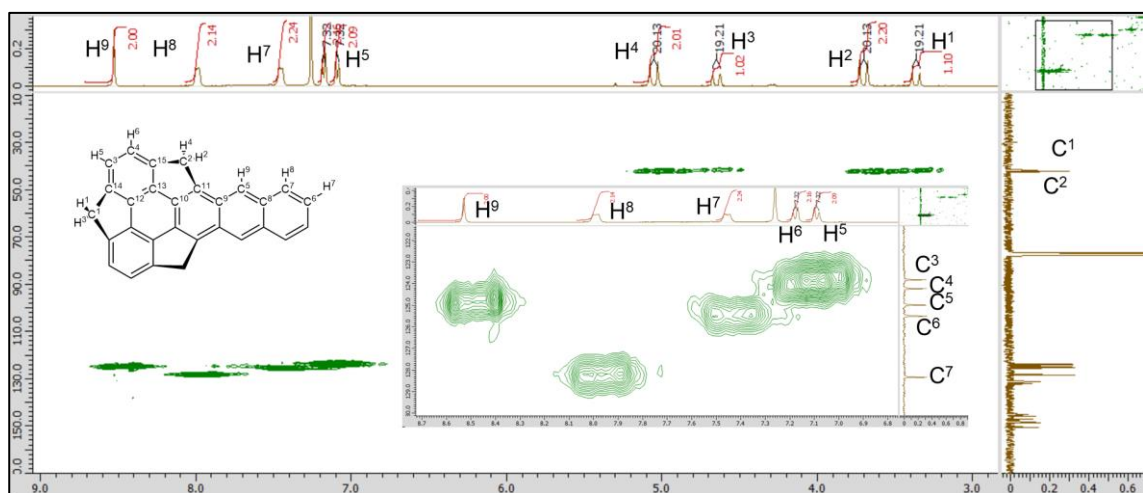
^1H NMR (400 MHz), ^{13}C NMR (100 MHz), HMQC, and HMBC spectra of **4** (CDCl_3)



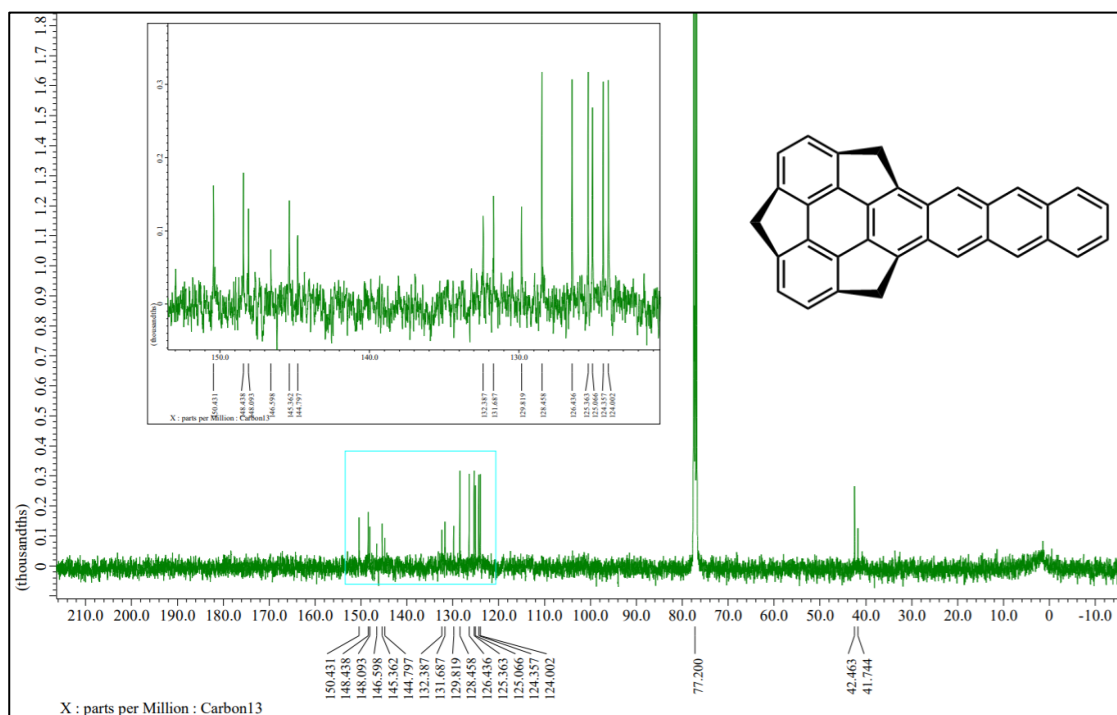
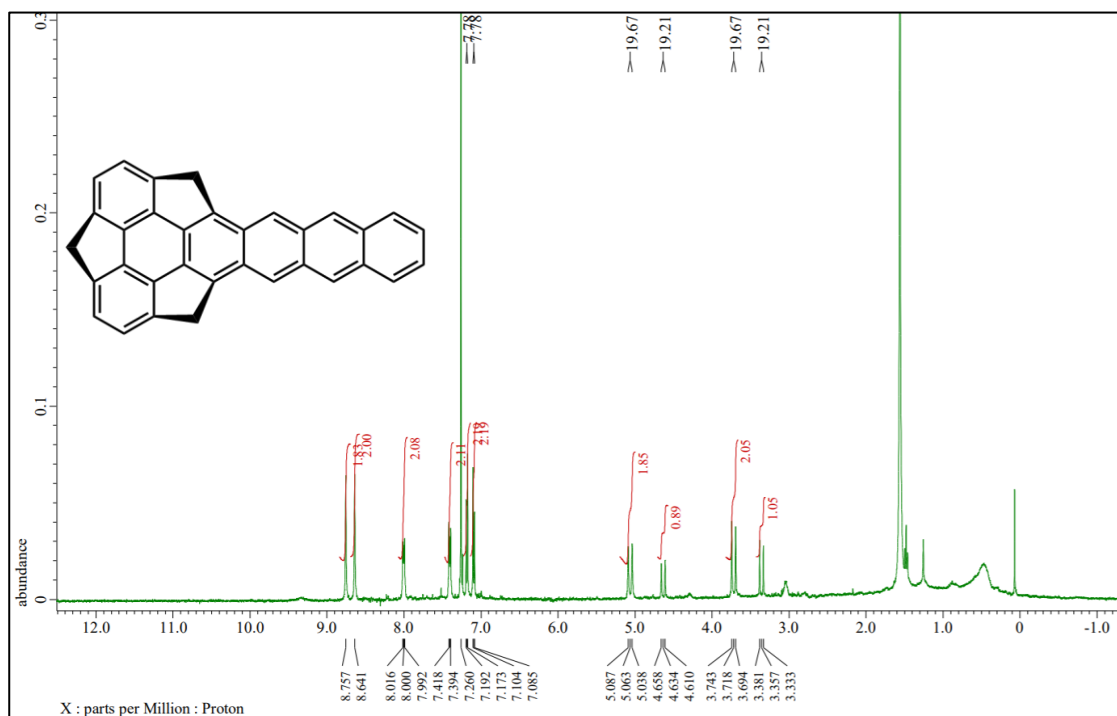


^1H NMR (400 MHz), ^{13}C NMR (100 MHz), HMQC and HMBC spectra of **5** (CDCl_3)





^1H NMR (400 MHz) and ^{13}C NMR (100 MHz) spectra of **6** (CDCl_3)



References

- 1 a) M. B. Smith, J. Michl, *Chem. Rev.* **2010**, *110*, 6891. b) D. Casanova, *Chem. Rev.* **2018**, *118*, 7164.
- 2 S. Singh, W. J. Jones, W. Siebrand, B. P. Stoicheff, W. G. Schneider, *J. Chem. Phys.* **1965**, *42*, 330.
- 3 a) N. Geacintov, M. Pope, F. E. Vogel, *Phys. Rev. Lett.* **1969**, *22*, 593. b) R. E. Merrifield, P. Avakian, R. P. Groff, *Chem. Phys. Lett.* **1969**, *3*, 386.
- 4 a) D. N. Congreve, J. Lee, N. J. Thompson, E. Hontz, S. R. Yost, P. D. Reusswig, M. E. Bahlke, S. Reineke, T. V. Voorhis, M. A. Baldo, *Science* **2013**, *340*, 334. b) X. Wang, X. Liu, R. Tom, C. Cook, B. Schatschneider, N. Marom, *J. Phys. Chem. C* **2019**, *123*, 5890.
- 5 a) M. Tabachnyk, B. Ehrler, S. Bayliss, R. H. Friend, N. C. Greenham, *Appl. Phys. Lett.* **2013**, *103*, 153302. b) J. Herz, T. Buckup, F. Paulus, J. Engelhart, U. H. F. Bunz, M. Motzkus, *J. Phys. Chem. Lett.* **2014**, *5*, 2425.
- 6 a) P. M. Zimmerman, F. Bell, D. Casanova, M. Head-Gordon, *J. Am. Chem. Soc.* **2011**, *133*, 19944. b) P. P. Lin, G. Y. Qin, N. X. Zhang, J. X. Fan, X. L. Hao, L. Y. Zou, A. M. Ren, *Org. Electron.* **2020**, *78*, 105606. c) H. Seiler, M. Krynski, D. Zahn, S. Hammer, Y. W. Windsor, T. Vasileiadis, J. Pflaum, R. Ernstorfer, M. Rossi, H. Schwörer, *Sci. Adv.* **2021**, *7*, eabg0869.
- 7 a) S. N. Sanders, E. Kumarasamy, A. B. Pun, M. Tuan Trinh, B. Choi, J. Xia, E. J. Taffet, J. Z. Low, J. R. Miller, X. Roy, X.-Y. Zhu, M. L. Steigerwald, M. Y. Sfeir, L. M. Campos, *J. Am. Chem. Soc.* **2015**, *137*, 8965. b) J. Zirzmeier, D. Lehnerr, P. B. Coto, E. T. Chernick, R. Casillas, B. S. Basel, M. Thoss, R. R. Tykwinski, D. M. Guldi, *Proc. Natl. Acad. Sci. U. S. A.* **2015**, *112*, 5325. c) S. Lukman, A. J. Musser, K. Chen, S. Athanasopoulos, C. K. Yong, Z. Zeng, Q. Ye, C. Chi, J. M. Hodgkiss, J. Wu, R. H. Friend, N. C. Greenham, *Adv. Funct. Mater.* **2015**, *25*, 5452. d) J. R. Macdonald, J. C. Phillips, *J. Chem. Phys.* **2005**, *122*, 074510. e) M. N. Berberan-Santos, E. N. Bodunov, B. Valeur, *Chem. Phys.* **2005**, *315*, 171. f) T. Sakuma, H. Sakai, Y. Araki, T. Mori, T. Wada, N. V. Tkachenko, T. Hasobe, *J. Phys. Chem. A* **2016**, *120*, 1867. g) H. Sakai, R. Inaya, H. Nagashima, S. Nakamura, Y. Kobori, N. V. Tkachenko, T. Hasobe, *J. Phys. Chem. Lett.* **2018**, *9*, 3354. h) K. Miyata, F. S. Conrad-Burton, F. L. Geyer, X.-Y. Zhu, **2019**, *119*, 4261. i) D. Kato, H. Sakai, N. V. Tkachenko, T. Hasobe, *Angew. Chem., Int. Ed.* **2016**, *55*, 5230. j) C. Hetzer, D. M. Guldi, R. R. Tykwinski, *Chem. Eur. J.* **2018**, *24*, 8245. k) K. Kuroda, K. Yazaki, Y. Tanaka, M. Akita, H. Sakai, T. Hasobe, N. V. Tkachenko, M. Yoshizawa, *Angew. Chem., Int. Ed.* **2019**, *58*, 1115. l) L. Catti, H. Narita, Y. Tanaka, H. Sakai, T. Hasobe, N. V. Tkachenko, M. Yoshizawa, *J. Am. Chem. Soc.* **2021**, *143*, 9361.
- 8 S. Mebs, M. Weber, P. Luger, B. M. Schmidt, H. Sakurai, S. Higashibayashi, S. Onogi, D. Lentz, *Org. Biomol. Chem.* **2012**, *10*, 2218.
- 9 K. Okada, M. Nakano, H. Miyamoto, H. Nakazawa, Y. Uetake, H. Sakurai, *J. Phys. Chem. C* **2020**, *124*,

19499.

- 10 a) S. Higashibayashi, H. Sakurai, *Chem. Lett.* **2011**, 40, 122. b) M. Saito, H. Shinokubo, H. Sakurai, *Mater. Chem. Front.* **2018**, 2, 635.
- 11 a) I. Aprahamian, D. V. Preda, M. Bancu, A. P. Belanger, T. Sheradsky, L. T. Scott, M. Rabinovitz, *J. Org. Chem.* **2006**, 71, 290. b) A. Sygula, R. Sygula, P. W. Rabideau, *Org. Lett.* **2006**, 8, 5909. c) V. Rajeshkumar, M. C. Stuparu, *Chem. Commun.* **2016**, 52, 9957. d) K. G. U. R. Kumarasinghe, F. R. Fronczek, H. U. Valle, A. Sygula, *Org. Lett.* **2016**, 18, 3054. e) N. Ngamsomprasert, Y. Yakiyama, H. Sakurai, *Chem. Lett.* **2017**, 46, 446. f) Q. Xu, C. Wang, X. Chen, Y. Wang, Z. Shen, H. Jiang, *Org. Chem. Front.* **2022**, 9, 4981.
- 12 H. Sakurai, T. Daiko, T. Hirao, *Science* **2003**, 301, 1887.
- 13 T. Amaya, M. Hifumi, M. Okada, Y. Shimizu, T. Moriuchi, K. Segawa, K. Y. Ando, T. Hirao, *J. Org. Chem.* **2011**, 76, 8049.
- 14 H. Toda, Y. Uetake, Y. Yakiyama, H. Nakazawa, T. Kajitani, T. Fukushima, H. Sakurai, *Synthesis* **2019**, 51, 4576.
- 15 Gaussian 09, revision E.01, M. J. Frisch, G. W. Trucks, H. B. Schlegel, G. E. Scuseria, M. A. Robb, J. R. Cheeseman, G. Scalmani, V. Barone, G. A. Petersson, H. Nakatsuji, X. Li, M. Caricato, A. Marenich, J. Bloino, B. G. Janesko, R. Gomperts, B. Mennucci, H. P. Hratchian, J. V. Ortiz, A. F. Izmaylov, J. L. Sonnenberg, D. Williams-Young, F. Ding, F. Lipparini, F. Egidi, J. Goings, B. Peng, A. Petrone, T. Henderson, D. Ranasinghe, V. G. Zakrzewski, J. Gao, N. Rega, G. Zheng, W. Liang, M. Hada, M. Ehara, K. Toyota, R. Fukuda, J. Hasegawa, M. Ishida, T. Nakajima, Y. Honda, O. Kitao, H. Nakai, T. Vreven, K. Throssell, J. A. Montgomery, Jr., J. E. Peralta, F. Ogliaro, M. Bearpark, J. J. Heyd, E. Brothers, K. N. Kudin, V. N. Staroverov, T. Keith, R. Kobayashi, J. Normand, K. Raghavachari, A. Rendell, J. C. Burant, S. S. Iyengar, J. Tomasi, M. Cossi, J. M. Millam, M. Klene, C. Adamo, R. Cammi, J. W. Ochterski, R. L. Martin, K. Morokuma, O. Farkas, J. B. Foresman, and D. J. Fox, Gaussian, Inc., Wallingford CT, 2016.
- 16 a) R. Ditchfield, W. J. Hehre, J. A. Pople, *J. Chem. Phys.* **1971**, 54, 724. b) P. C. Hariharan, J. A. Pople, *Theor. Chim. Acta* **1973**, 28, 213. c) W. J. Hehre, R. Ditchfield, J. A. Pople, *J. Chem. Phys.* **1972**, 56, 2257. d) V. A. Rassolov, M. A. Ratner, J. A. Pople, John A., P. C. Redfern, L. A. Curtiss, *J. Comput. Chem.* **2001**, 22, 976.
- 17 W. Minor, M. Cymborowski, Z. Otwinowski, M. Chruszcz, *Acta Crystallogr., Sect. D: Biol. Crystallogr.* **2006**, 62, 859.
- 18 *CrysAlis PRO*. Rigaku Oxford Diffraction, Yarnton, **2015**.
- 19 G. M. Sheldrick, *Acta Crystallogr., Sect. A: Found. Adv.* **2015**, 71, 3.
- 20 G. M. Sheldrick, *Acta Crystallogr., Sect. C: Struct. Chem.* **2015**, 71, 3.
- 21 O. V. Dolomanov, L. J. Bourhis, R. J. Gildea, J. A. K. Howard, H. Puschmann, *J. Appl. Crystallogr.*

2009, 42, 339.

Chapter 3. Fully substituted sumanenes at the aromatic periphery through hexabromomethylation

Section 1. Introduction of fully substituted buckybowl at the aromatic periphery

Buckybowls have properties not found in planar π -conjugated molecules, which are derived from the curved structure. Introducing functional groups into them makes it possible to create molecules with curved structures and substituent functions.¹ For example, buckybowl, in which the peripheral aromatic carbon is halogenated, is an important synthetic intermediate because it can introduce a new functional group in the conversion reaction. Decachlorocorannulene,² obtained by chlorination of corannulene, is an example of such an intermediate. A corannulene derivative containing ten pyrroles obtained from decachlorocorannulene by cross-coupling reaction can suppress disorder during the crystallization of fullerene derivatives, which are generally highly symmetric and challenging to analyze in crystal structures (Figure 20).³

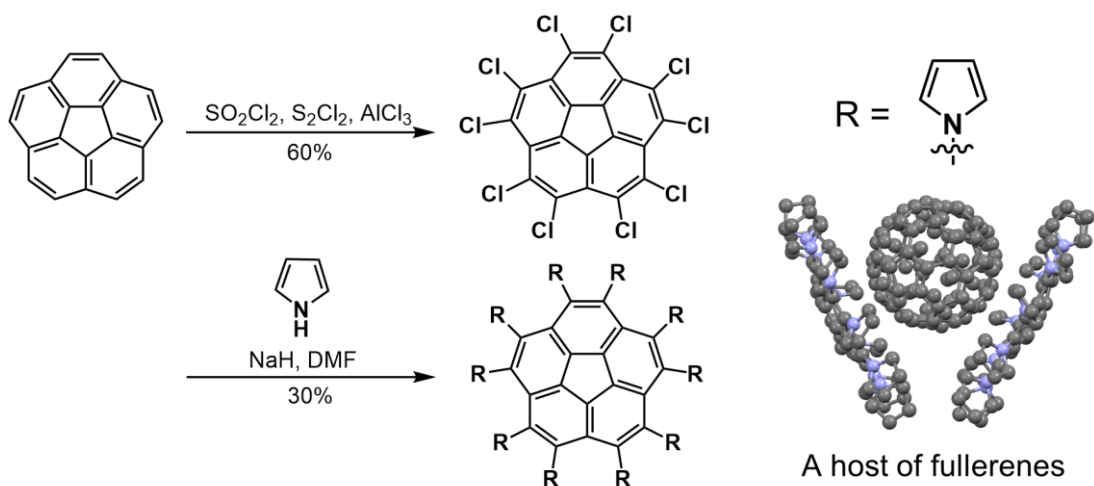


Figure 20. Synthesis of decapyrrylcorannulene host via decachlorocorannulene

On the other hand, regarding the synthesis of halogenated peripheral aromatic carbons of sumanene (**1**), the synthesis of hexabromosumanene (**7**) was reported by Sakurai and Fukushima et al. in 2017 (Scheme 10).⁴ By derivatization from **7**, many hexa-substituted sumanene derivatives have been synthesized so far and have been found to exhibit different properties depending on the substituent introduced (Figure 21).⁵

For example, the hexa-substituted sumanene obtained by introducing carboxyphenyl groups forms a two-dimensional supramolecular network due to hydrogen bonding (Figure 21A).^{5b} Hexakis(4-pyridyl)sumanene builds metal-organic structures (MOFs) with unique isolated spaces by complexation with metals (Figure 21B).^{5d} Hexathioalkylsumanene forms hexagonal columnar phases and exhibits liquid crystal properties (Figure 21C).^{5a} These previous studies strongly suggested that hexa-substituted sumanene derivatives contribute to the construction of unique supramolecular structures derived from the bowl structure and symmetry (C_{3v}) of sumanene. However, since the conversion of **7** is from $C(sp^2)$ -Br to $C(sp^2)$ -R, the reactions that could be used were limited to cross-coupling reactions and aromatic nucleophilic substitution reactions (Scheme 10).

Scheme 10. Synthesis of hexabromosumanene (**7**) and further transformation.

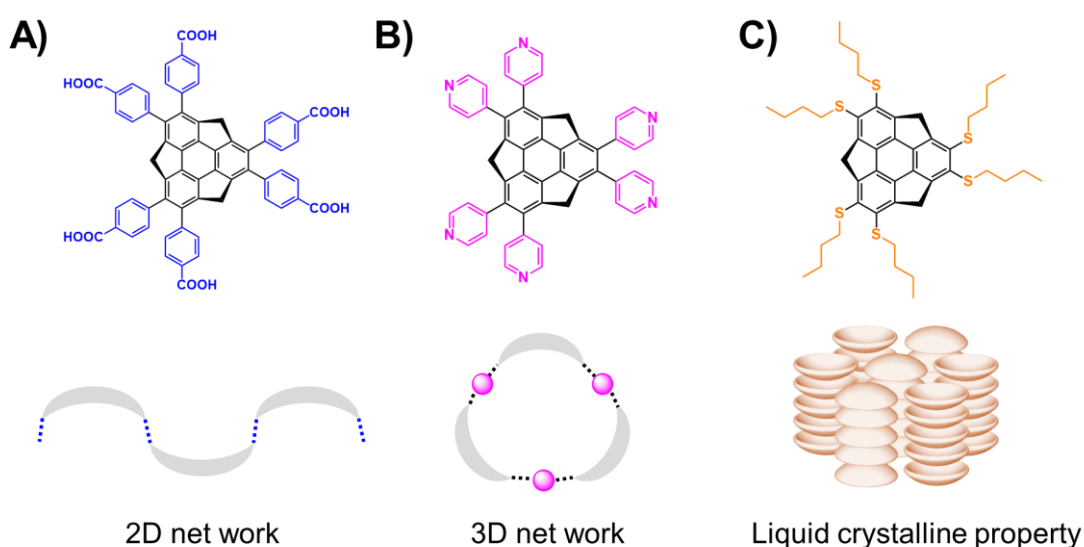
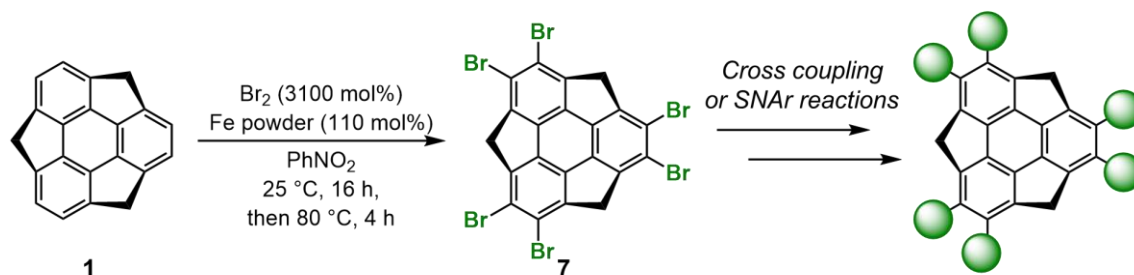
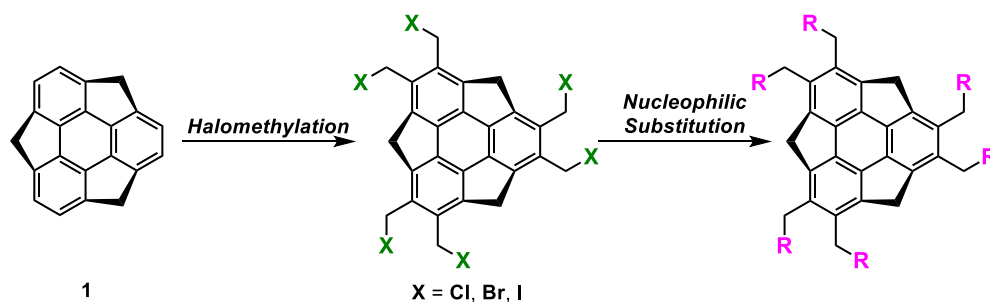


Figure 21. A) 2D-supramolecular network, B) metal-organic frameworks constructed and C) liquid crystal by hexa-substituted sumanene.

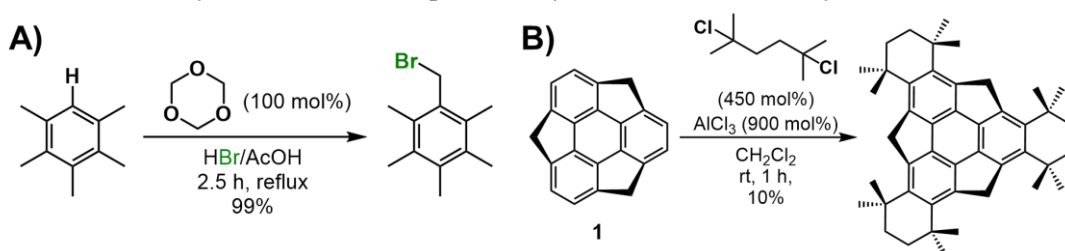
With this research background, the author thought that halomethylsumanene might be a promising new hexa-substituted sumanene precursor to replace **7** (Scheme 11). Since halomethyl groups ($C(sp^3)-X = Cl, Br, I$) can be easily substituted by nucleophilic substitution reactions, it is expected to introduce functional groups in different forms from that of **7**.⁶ The introduction of halomethyl groups into aromatic compounds has also been found to proceed at sterically crowded reaction sites. Ueda et al. reported that a bromomethylated compound was quantitatively obtained by the reaction of hydrogen bromide (in AcOH solution) and 1,3,5-trioxane on 1,2,3,4,5-pentamethylbenzene, which has a methyl group in the ortho position (Scheme 12A). Furthermore, since the hexa-alkylation of sumanene was also reported by Amaya and Hirao et al. (Scheme 12B),⁷ the author considered introducing a halomethyl group into sumanene was feasible enough.⁸

In this study, the author attempted to synthesize new hexa-substituted sumanenes by synthesizing fully substituted sumanenes with six halomethyls and subsequent transformation by nucleophilic substitution reactions.

Scheme 11. Synthesis of halomethylsumanene and further transformation.



Scheme 12. A) bromomethylation of 1,2,3,4,5-pentamethylbenzene. B) hexa-alkylation of sumanene (**1**)



Section 2. Synthesis of hexahalomethyl sumanene

First, the halomethylation reaction of sumanene (**1**) was examined (Table 5). In entry 1, chloromethyl methyl ether was used as a carbon source in the presence of zirconium tetrachloride, a Lewis acid, but the reaction did not proceed.⁹ In entry 2, chlorotrimethylsilane was reacted with 1,3,5-trioxane in an AcOH solution to generate hydrogen chloride in situ, and chloromethylation was attempted. However, the reaction did not proceed. The acid was changed to hydroiodic acid, a strong Brønsted acid, and iodomethylation was carried out. However, hexamethylsumanene is mainly obtained along with trace amounts of iodomethylsumanene (entry 3). This result suggested that iodomethylsumanene was decomposed by heat or light after formation to hexamethylsumanene. Therefore, to synthesize bromomethylsumanene, which is expected to be more stable than iodomethylsumanene, the reaction was carried out using HBr (in AcOH solution). As a result, bromomethylsumanene (**8**) was obtained in 97% yield as a stable solid in air and water (entry 4).

Table 5. Optimization of halomethylation conditions

1

conditions

X = Cl, Br or I

entry	conditions	result
1	MOMCl (3000 mol%) ZrCl ₄ (1680 mol%) (CH ₂ Cl) ₂ , 27 °C, 16 h	no reaction
2	1,3,5-trioxane (1200 mol%) TMSCl (6000 mol%) AcOH, 80 °C, 16 h	no reaction
3	1,3,5-trioxane (1200 mol%) HI (6000 mol%) AcOH, 80 °C, 10 min	X = H (21% yield) X = I (trace)
4	1,3,5-trioxane (1200 mol%) HBr (6000 mol%) AcOH, 80 °C, 16 h	X = Br (97% yield)

^aReaction conditions: **1** (38 μmol), solvent (0.5 mL). MOM: methoxymethyl.

^1H NMR spectra at 25 °C in 1,1,2,2-tetrachloroethane- d_2 in **8** showed the benzyl positioned protons of the sumanene skeleton as a doublet peak ($J = 19.0$ Hz) at 4.71 ppm (H_{exo}) and 3.80 ppm (H_{endo}), respectively (Figure 22). Similarly, the twelve methylene hydrogens of the bromomethyl group were also observed as doubled peaks ($J = 11.0$ Hz) at 4.77 and 4.81 ppm. This is likely due to the slower rate of bowl inversion than the NMR time scale. Variable temperature NMR (VT-NMR) measurements of **8** in the temperature range of 25 °C to 120 °C showed that neither broadening nor merging of the proton signal was observed for **8**, unlike for **1**, suggesting that it undergoes bowl inversion more slowly than **1** (Figure 22).¹⁰ In addition, **8** has excellent solubility in various organic solvents. (Table 6).

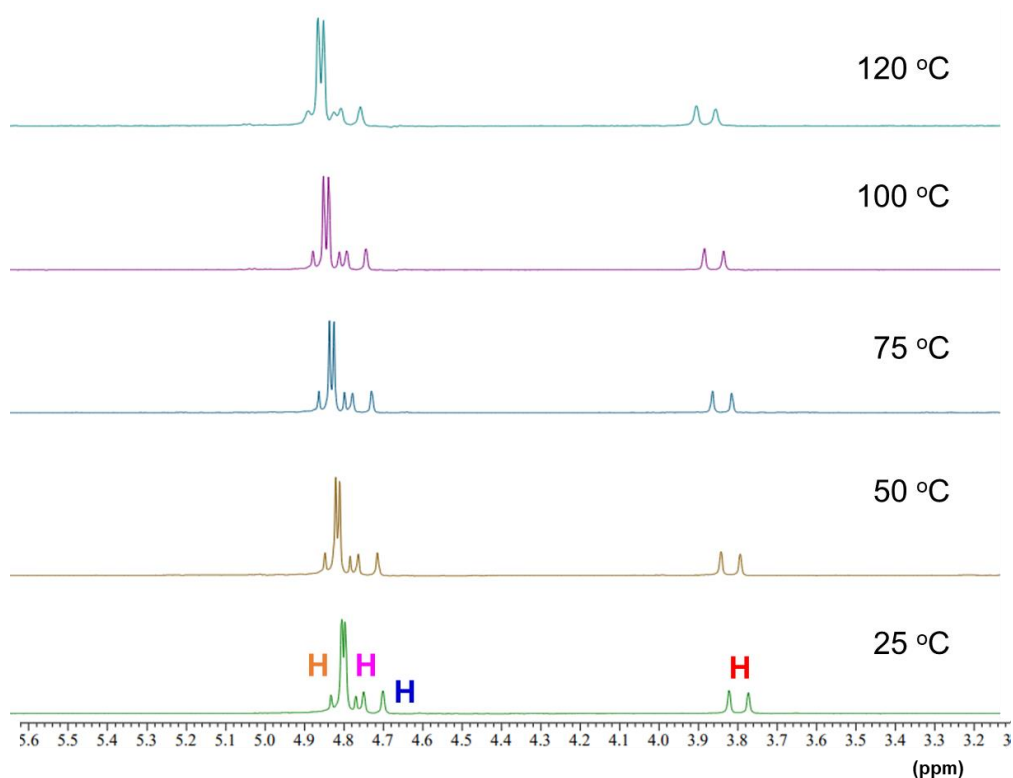


Figure 22. ^1H NMR spectra of **8** at 25, 50, 75, 100, and 120 °C.

Table 6. Solubility of **7** and **8** in various organic solvents.

	CHCl_3	<i>o</i> DCB	toluene	DMSO	THF
8 (10^{-2} mol/L)	34	34	32	16	5.1
7 (10^{-2} mol/L)	<0.10	<0.10	<0.10	<0.10	<0.10

Single crystals of **8** were obtained by vapor diffusion (CHCl_3/n -hexane) as pale yellow needle-like crystals (Figure 23A). Single crystal X-ray structure analysis of the obtained **8** was performed. The bowl depth of **8** was found to be 1.12–1.28 Å in the crystal, slightly deeper than **1** (1.11 Å) (Figure 23B).¹¹ Packing in the crystalline state was found to form a 1D columnar structure for **1**, whereas **8** forms a dimer structure (Figure 23C). Two of the six bromomethyl groups in **8** (Br2 and Br6) are oriented exo, while the remaining four (Br1, Br3, Br4, Br5) are oriented endo.

Furthermore, the close distance between the bromine atom and the central benzene ring in **8** (3.43 Å) suggested a non-negligible interaction to form the dimer. Therefore, to obtain quantitative information on the interactions in the dimer structure, a non-covalent interaction (NCI) analysis of the dimer model was performed (Figure 23D).¹² The coordinates of C and Br were obtained from the single crystal X-ray structure analysis results, and the coordinates of H were optimized by fixing the coordinates of the other elements in the $\omega\text{B97X-D/def2-SVP}$ level calculation. The electron density calculated at the $\omega\text{B97X-D/def2-TZVP}$ level was used for the optimized coordinates to account for long-range corrections. As a result, a non-covalent interaction, indicated by the green region, was observed between the central benzene ring of the facing sumanene skeleton and the bromine atom. This suggested the existence of a $\text{Br}\cdots\pi$ interaction.

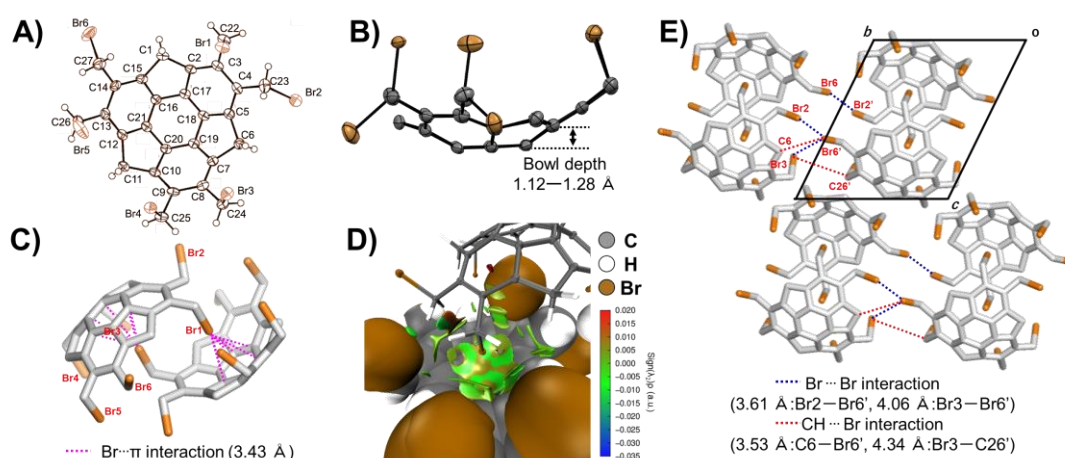


Figure 23. Crystal structures of **8**. a) Displacement ellipsoid plot of **8** at 50% probability. b) Bowl depth of the sumanene skeleton of **8**. c) Intermolecular interactions within **8**-dimer. The pink dotted line shows $\text{Br}\cdots\pi$ interactions. d) Isosurface of the non-covalent interactions of **8**-dimer (isovalue = 0.04). e) Intermolecular interactions between **8**-dimers viewed from the *a*-axis. The blue dotted line shows $\text{Br}\cdots\text{Br}$ interactions, and the red dotted line shows $\text{CH}\cdots\text{Br}$ interactions.

In addition, a quantum theory of atoms-in-molecules (QTAIM) analysis was performed to quantitatively evaluate the contribution of this interaction (Figure 24).¹³ The results showed that a bond critical point (BCP) exists between bromine (Br1) and the two internal carbons (C16' and C19'), and the electron density at the BCP [$\rho_{\text{BCP}}(r)$] was 6.98 and 8.74 ($10^{-3} e \text{ bohr}^{-3}$), respectively (Figure 24A). The $\rho_{\text{BCP}}(r)$ at the BCP between bromine atoms were 3.09, 3.95, and 3.07 ($10^{-3} e \text{ bohr}^{-3}$), respectively (Figures 24B and C). The Laplacian of

the electron density at BCP ($\nabla^2\rho_{\text{BCP}}(r)$) was all positive. These theoretical calculations suggested that the formation of the face-to-face dimer structure is due to $\text{Br}\cdots\pi$ and $\text{Br}\cdots\text{Br}$ interactions. On the other hand, $\text{Br}\cdots\text{Br}$ interactions (3.61 Å and 4.06 Å) and $\text{CH}\cdots\text{Br}$ interactions (3.53 Å and 4.34 Å) were also identified between the dimers (Figures 23E and 24D). In other words, four of the six bromine atoms in **8** contribute to forming the dimeric structure, while the remaining two contribute to the link between the dimers. Other features of the crystal structure of **8**, judging from the $\text{Br}\cdots\text{Br}$ angles (θ_1 and θ_2), can be interpreted as type II $\text{Br}\cdots\text{Br}$ interactions with electrostatic forces acting as the main factor (Figure 25).¹⁴

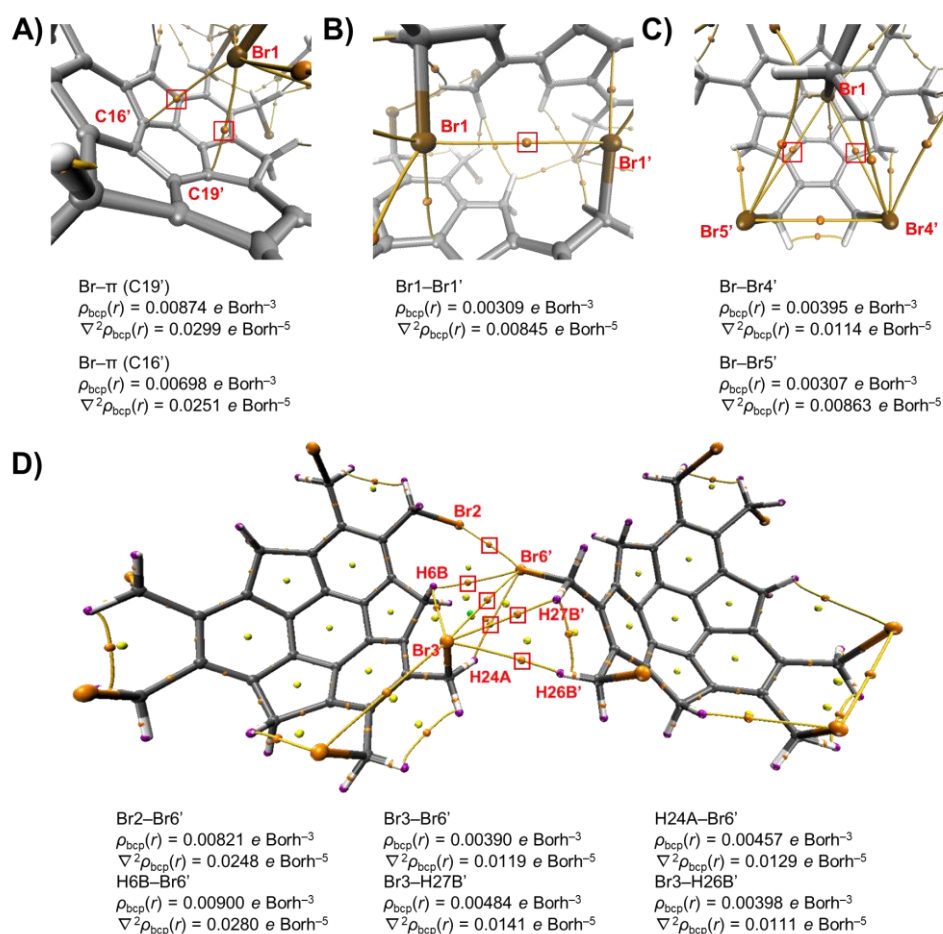


Figure 24. QTAIM analysis of **8**. A-C) Intermolecular interactions within **8**-dimer. D) Intermolecular interactions between **8**-dimers. The bond paths (yellow line), bond critical points (orange), and electron density at the bond critical points [$\rho_{\text{BCP}}(r)$ (e bohr^{-3})] are shown.

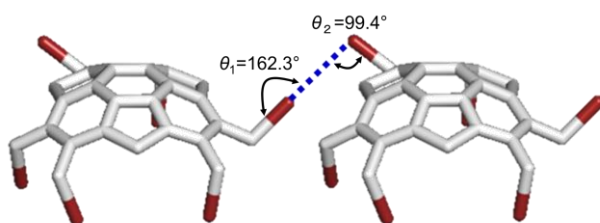
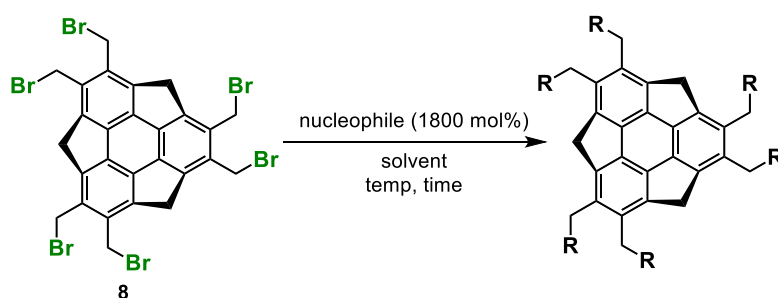


Figure 25. $\text{Br}\cdots\text{Br}$ angles (θ_1 and θ_2) of the crystal structure of **8**

Section 3. Transformation of bromomethylsumanene by nucleophilic substitution reaction

Since bromomethylsumanene (**8**) was expected to be a promising synthetic intermediate for hexa-substituted sumanene derivatives, the author performed the Williamson ether synthesis reaction, one of the most classical reactions to convert benzyl bromide (Table 7).¹⁵ When **8** was reacted with an excess amount of sodium methoxide (1800 mol%) in DMF solvent at 27 °C, no desired product was obtained, and the decomposition of **8** instantly gave a black insoluble solid (entry 1). This may be due to the presence of highly acidic benzyl hydrogens with pKa' value of about 17.1 in the **8** skeleton.¹⁶ In other words, the strong base on **8** caused deprotonation of the benzyl hydrogens of the sumanene skeleton. The generated benzyl anion reacted with the bromomethyl group to give a complex mixture. (Scheme 13). Therefore, the solvent was changed to MeCN, which has milder reactivity than DMF. As a result, the reaction did not proceed when sodium methoxide or ammonium acetate was used (entries 2 and 3). However, when potassium acetate was used, acetylation proceeded to afford **9** in low yield (19%, entry 4). Furthermore, It was assumed that the activation of the bromine atom by Ag(I) might improve the yield. So silver acetate instead of potassium salt was used in entry 5, and it was found that the yield was greatly improved, and **9** was obtained in 75% yield.

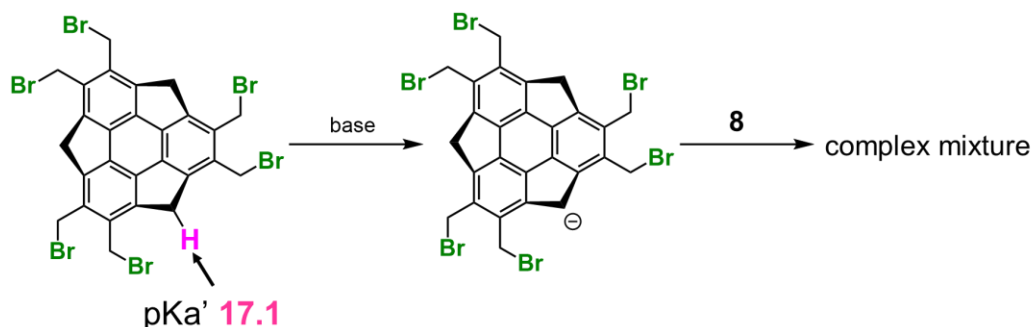
Table 7. Nucleophilic substitution of **8** with oxygen nucleophile.



entry	nucleophile	solvent	temp (°C)	time (min)	result
1	NaOMe	DMF	27	5	decomposition
2	NaOMe	MeCN	80	120	no reaction
3	NH ₄ OAc	MeCN	80	120	no reaction
4	KOAc	MeCN	80	20	19% (9)
5	AgOAc	MeCN	80	20	75% (9)

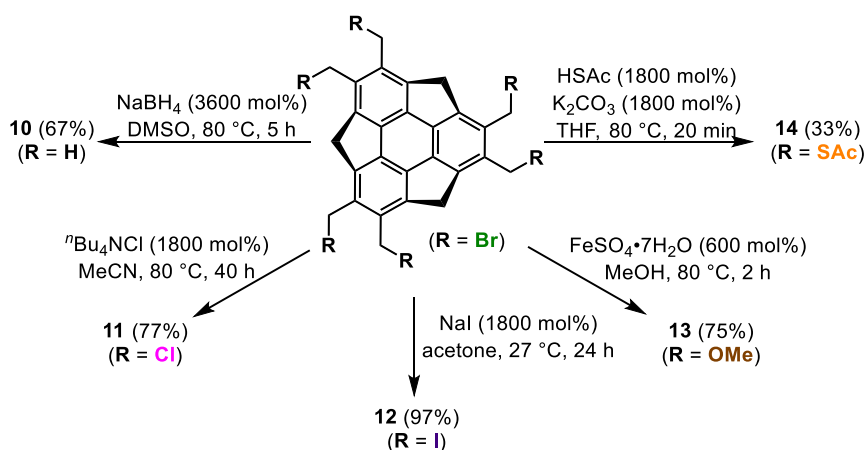
^aReaction conditions: **8** (38 μmol), solvent (0.5 mL). MOM: methoxymethyl.

Scheme 13. The reaction mechanism of generation of a complex mixture by **8** and base.



Other nucleophiles were also investigated in the same way (Scheme 14). Since **8** decomposed under strongly basic conditions, the reaction was carried out using a high nucleophilic reagent under neutral conditions. First, the reduction reaction in DMSO solvent using sodium borohydride as a nucleophile gave the corresponding reduced product (**10**) in 67% yield. Second, even when tetrabutylammonium chloride was used, the chlorinated product was obtained in 77% yield. Furthermore, when sodium iodide was reacted at 27 °C under light-shielded conditions, the iodinated product (**12**) was obtained in good yield (97%) without decomposition. When a reagent with low nucleophilicity, such as methanol was used, **13** was obtained in good yield (75%) by adding iron sulfate heptahydrate as a Lewis acid to activate the bromine atom.¹⁷ Furthermore, when thioacetic acid was used as a nucleophile, the addition of potassium carbonate as a base did not lead to the decomposition of the substrate, and the corresponding product (**14**) was obtained in 33% yield.

Scheme 14. Synthesis of hexa-substituted sumanene derivatives.



UV-vis absorption and emission spectral measurements were performed to obtain information on the electronic structure of each hexa-substituted sumanene (Figure 26). It was assumed that the HOMO-LUMO gap changes with each type of substituent, affecting the orbital distribution (Figure 27). UV-vis absorption spectra of hexa-substituted sumanenes (**8-14**) were observed in the regions 280-350 nm and 320-420 nm, and their spectral shapes were similar to those of **1** ($\lambda = 278$ nm, 308 nm) (Figure 26A). For further discussion, DFT calculations at the B3LYP/6-31G+(d,p) level showed that the HOMO and LUMO of all hexa-substituted sumanenes extend from the sumanene skeleton to the substituents (Figure 27). The HOMO-LUMO gap (ΔE) of each molecule became smaller in the order I>Br>Cl>SAc>OMe \approx OAc>H. This is thought to be due to the stabilization of the LUMO by hyperconjugation, in which the larger the introduced element, the greater the overlap between the orbital on the sumanene moiety and the orbital of the introduced element. For example, when comparing the HOMOs of the iodinated (**12**), brominated (**8**), and chlorinated (**11**) compounds, they are comparable at -6.34 eV (**12**), -6.37 eV (**8**), and -6.45 eV (**11**), but the LUMO -2.73 eV (**12**), -2.41 eV (**8**), and -2.29 eV (**11**), indicating a significant difference. The emission spectra show the same trend as the absorption spectra (Figure 26B).

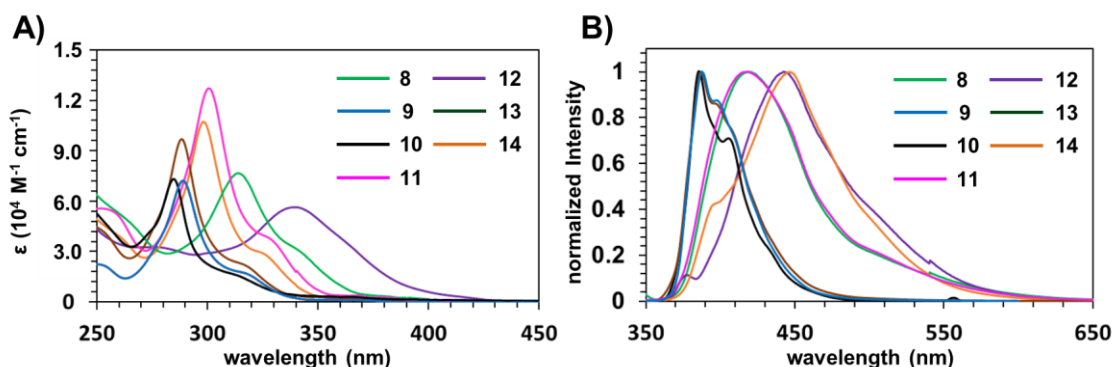


Figure 26. UV-vis absorption and emission spectra of hexa-substituted sumanene derivatives.

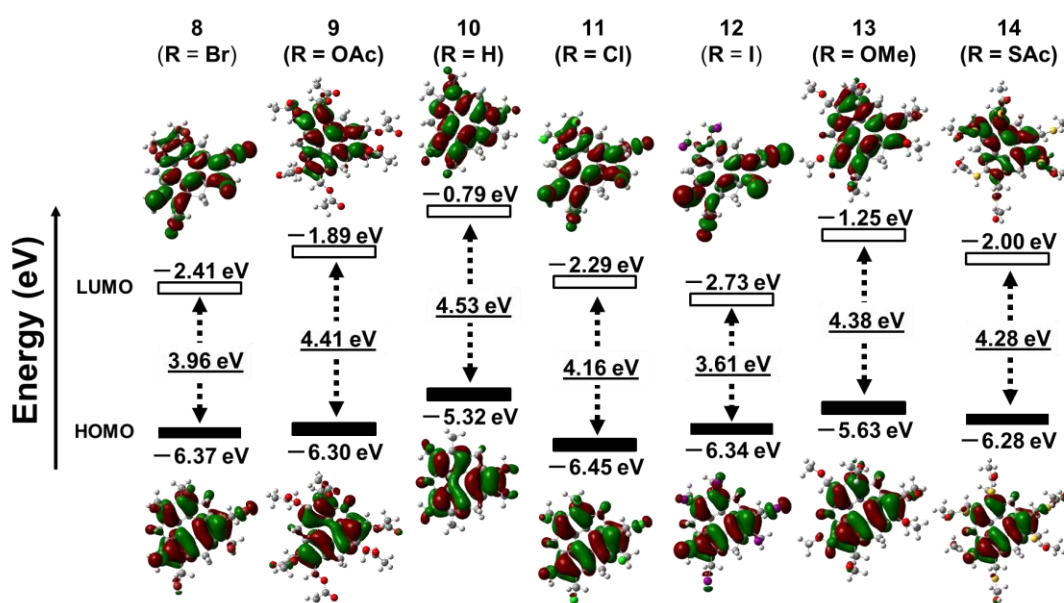


Figure 27. Frontier molecular orbitals of hexa-substituted sumanene derivatives calculated at B3LYP/6-31G+(d,p) level of theory (isovalue = 0.02).

Section 4. Summary

In this study, the author found that bromomethylsumanene can be synthesized using excess amounts of 1,3,5-trioxane and HBr (in AcOH solution). Theoretical calculations suggested that bromomethylsumanene forms dimer structures in single crystals and that the Br $\cdots\pi$ interaction is dominant. Furthermore, since bromomethylsumanene is stable in air and shows excellent solubility in various solvents, functional groups such as OAc, H, Cl, I, OMe, and SAc can be easily introduced by nucleophilic substitution reactions. And the variety of synthesizable hexa-substituted sumanene derivatives was expanded. The author believes that this achievement will be a milestone in the projects on sumanene-based nonplanar conjugated systems, including network structures such as liquid crystals and covalent bonds.

Experimental section

Instrumentations and chemicals

All manipulations of moisture or air-sensitive compounds were performed by standard Schlenk techniques in anhydrous solvents under a nitrogen atmosphere using flame-dried glassware. Reactions were conducted in an EYELA PPS-2511 personal organic synthesizer. Analytical thin-layer chromatography (TLC) was performed on precoated silica-gel aluminum sheets (Merck silica gel 60 F254, catalog no.1.05554.0001). Preparative thin-layer chromatography (PTLC) was prepared using Wako Wakogel B-5F. Recycling preparative high-performance liquid chromatography (HPLC) was performed by an LC-908W (Japan Analytical Industry Co., Ltd.) with high-resolution gel permeation chromatography (GPC) column (Japan Analytical Industry Co., Ltd., JAIGEL-1H and 2H) with CHCl_3 as an eluent. ^1H NMR (400 MHz) and ^{13}C NMR (100 MHz) spectroscopy measurements, including DEPT135, ^1H - ^{13}C HMQC, and ^1H - ^{13}C HMBC, were performed on a JEOL JNM-ECZS400 spectrometer at room temperature. Chloroform- d_1 (CDCl_3) and 1,1,2,2-tetrachloroethane- d_2 were used as solvents for NMR measurements. Chemical shifts (δ) are given in parts per million (ppm) downfield from the solvent signal (for ^1H NMR: CHCl_3 δ 7.26 ppm; 1,1,2,2-tetrachloroethane- d_2 δ 5.97 ppm; for ^{13}C NMR: CDCl_3 δ 77.2 ppm) as an internal standard with coupling constants (J) in hertz (Hz). The abbreviations s and d signify singlet and doublet, respectively. Melting points were determined on an Optimelt MPA100 automated melting point apparatus (Stanford Research Systems, Inc.) and expressed without correction. High-resolution mass spectra (HRMS) were measured on JEOL-JMS-700 MStation (FAB or EI). Infrared (IR) spectroscopy measurements were performed on a JASCO FT IR-4100 spectrometer by transmission mode using the KBr pellet method. Ultraviolet-visible (UV-vis) absorption spectroscopy was measured on a JASCO V-670 spectrophotometer by transmission method. The absorption bands were given in wavelength (nm). A quartz cell (optical path length; 10 mm) was used. Fluorescence spectra were recorded on a JASCO FP6500 spectrofluorometer and expressed after normalization. A quartz cell (optical path length; 10 mm) was used.

Unless otherwise noted, all reagents purchased from commercial suppliers were used without further purification.

n-Hexane, ethyl acetate (EtOAc), methanol (MeOH), chloroform (CHCl_3), acetone, dimethyl sulfoxide (DMSO), toluene, *o*-dichlorobenzene (*o*DCB), zirconium tetrachloride (ZrCl_4), hydroiodic acid (HI, 55.0~58.0% in water), silver acetate (AgOAc), and iron sulfate heptahydrate ($\text{FeSO}_4 \cdot 7\text{H}_2\text{O}$) were purchased from FUJIFILM Wako Pure Chemical Corporation.

Sodium iodide (NaI) was purchased from KISHIDA CHEMICAL Co., Ltd.

Potassium carbonate (K_2CO_3), trimethylsilyl chloride (TMSCl), and acetic acid (AcOH) were purchased from Nacalai Tesque, Inc.

Tetrahydrofuran (THF, dehydrated, stabilizer free, Super Plus) was purchased from Kanto Chemical Co., Inc. and purified by passing through a Glass Contour Ultimate Solvent System (Nikko Hansen & Co. Ltd.) under nitrogen atmosphere.

Thioacetic acid (AcSH) was purchased from Kanto Chemical Co., Inc.

1,3,5-Trioxane, hydrogen bromide (HBr, 30% in acetic acid), tetrabutylammonium chloride ((*n*-Bu)₄NCl), methoxymethyl chloride, sodium borohydride (NaBH₄), and acetonitrile (MeCN) were purchased from Tokyo Chemical Industry Co., Ltd.

2,3,5,6,8,9-Hexakis(bromomethyl)-4,7-dihydro-1H-tricyclopenta[*def,jkl,pqr*]-triphenylene (Hexakis(bromomethyl)sumanene) (8)

To a mixture of sumanene (1) (50.0 mg, 189 μmol) and 1,3,5-trioxane (205 mg, 2.28 mmol) was added HBr (30% in AcOH, 5.1 mol/L, 2.2 mL) at room temperature and the mixture was stirred for 16 h at 80 °C. After cooling to room temperature, to the mixture were added saturated aqueous NaHCO₃ solution and saturated aqueous Na₂SO₃ solution and extracted with CHCl₃. The organic extract was washed with brine and dried over Na₂SO₄. After filtration, the filtrate was concentrated under reduced pressure. The residue was purified by silica-gel column chromatography (*n*-hexane/CHCl₃ = 1:1) to give **8** (150 mg, 183 μmol, 97%).

Colorless solid; mp: 186 °C (dec); TLC: *R*_f = 0.46 (AcOEt/*n*-hexane = 1:5); ¹H NMR (400 MHz, CDCl₃) δ (ppm) 4.81 (d, *J* = 10.5 Hz, 6H, H³ or H⁴), 4.77 (d, *J* = 10.5 Hz, 6H, H³ or H⁴), 4.71 (d, *J* = 19.0 Hz, 3H, H²), 3.80 (d, *J* = 19.0 Hz, 3H, H¹); ¹³C NMR (100 MHz, CDCl₃) δ (ppm) 147.7 (6C, C⁵), 147.2 (6C, C⁴), 131.9 (6C, C³), 40.3 (3C, C²), 16.9 (6C, C¹); IR (KBr): 3445, 2969, 2885, 2781, 1740, 1399, 1209 cm⁻¹; HRMS(FAB): *m/z* calcd for C₂₇H₁₈Br₆ [M]⁺: 815.6509, found: 815.6498; elemental analysis calcd (%) for C₂₇H₁₈Br₆: C 39.46%, H, 2.21%. Found: C 39.54%; H 2.50%.

(4,7-Dihydro-1H-tricyclopenta[*def,jkl,pqr*]triphenylene-2,3,5,6,8,9-hexayl)hexakis-(methylene) hexaacetate (9)

To a mixture of **8** (50.0 mg, 61.3 μmol) and AgOAc (184 mg, 1.10 mmol) was added MeCN (5.0 mL), and the mixture was stirred for 20 min at 80 °C. After cooling to room temperature, to the reaction mixture was added H₂O and extracted with AcOEt. The organic extract was washed with brine and dried over Na₂SO₄. After filtration, the filtrate was concentrated under reduced pressure. The residue was purified by silica-gel column chromatography (AcOEt/CHCl₃ = 1:3) to give **9** (32.0 mg, 46.0 μmol, 75%).

Colorless solid; mp: 285 °C (dec); TLC: *R*_f = 0.41 (AcOEt/CHCl₃ = 1:3); ¹H NMR (400 MHz, CDCl₃) δ (ppm) 5.40 (d, *J* = 12.6 Hz, 6H, H⁴ or H⁵), 5.20 (d, *J* = 12.6 Hz, 6H, H⁴ or H⁵), 4.77 (d, *J* = 19.7 Hz, 3H, H³), 3.79 (d, *J* = 19.7 Hz, 3H, H²), 2.07 (s, 18H, H¹); ¹³C NMR (100 MHz, CDCl₃) δ (ppm) 170.82 (6C, C⁷), 150.15 (6C, C⁶), 148.34 (6C, C⁵), 130.98 (3C, C⁴), 61.97 (6C, C³), 41.14 (3C, C²), 21.11 (6C, C¹); IR (KBr):

3458, 2974, 2938, 2444, 2134, 2052, 1732, 1438, 1377, 1216, 1024, 966 cm^{-1} ; HRMS(EI): m/z calcd for $\text{C}_{39}\text{H}_{36}\text{O}_{12}$ $[\text{M}]^+$: 696.2207, found: 696.2213.

2,3,5,6,8,9-Hexamethyl-4,7-dihydro-1H-tricyclopenta[defjkl,pqr] triphenylene (10)

To a mixture of **8** (20.0 mg, 24.5 μmol) and NaBH_4 (33.4 mg, 882 μmol) was added DMSO (2.0 mL), and the mixture was stirred for 1 h at 80 $^\circ\text{C}$. After cooling to room temperature, to the reaction mixture was added H_2O and extracted with CHCl_3 . The organic extract was washed with brine and dried over Na_2SO_4 . After filtration, the filtrate was concentrated under reduced pressure. The residue was purified by silica-gel chromatography (CHCl_3) to give **10** (5.8 mg, 17 μmol , 67%).

Colorless solid; mp: 184 $^\circ\text{C}$ (dec); TLC: R_f = 0.66 ($\text{AcOEt}/n\text{-hexane}$ = 1:5); ^1H NMR (400 MHz, CDCl_3) δ (ppm) 4.52 (d, J = 19.0 Hz, 3H, H^3), 3.31 (d, J = 19.0 Hz, 3H, H^2), 2.25 (s, 18H, H^1); ^{13}C NMR (100 MHz, CDCl_3) δ (ppm) 147.68 (6C, C^5), 147.18 (6C, C^4), 131.87 (6C, C^3), 40.29 (3C, C^2), 16.89 (6C, C^1); IR (KBr): 3432, 2918, 2872, 1733, 1575, 1450, 1383, 1018 cm^{-1} ; HRMS(EI): m/z calcd for $\text{C}_{27}\text{H}_{24}$ $[\text{M}]^+$: 348.1878, found: 348.1870.

2,3,5,6,8,9-Hexakis(chloromethyl)-4,7-dihydro-1H-tricyclopenta [defjkl,pqr]-triphenylene (11)

To a mixture of **8** (20.0 mg, 24.5 μmol) and tetrabutylammonium chloride (122.6 mg, 441 μmol) was added MeCN (2.0 mL) and the mixture was stirred for 40 h at 80 $^\circ\text{C}$. After cooling to room temperature, to the reaction mixture were added H_2O and extracted with CHCl_3 . The organic extract was washed with brine and dried over Na_2SO_4 . After filtration, the filtrate was concentrated under reduced pressure. The residue was purified by PTLC (CHCl_3) to give **11** (10.4 mg, 18.9 μmol , 77%).

Colorless solid; mp: 250 $^\circ\text{C}$ (dec); TLC: R_f = 0.39 ($\text{AcOEt}/n\text{-hexane}$ = 1:5); ^1H NMR (400 MHz, CDCl_3) δ (ppm) 4.90 (d, J = 11.9 Hz, 6H, H^3 or H^4), 4.83 (d, J = 11.9 Hz, 6H, H^3 or H^4), 4.80 (d, J = 19.2 Hz, 3H, H^2), 3.80 (d, J = 19.2 Hz, 3H, H^1); ^{13}C NMR (100 MHz, CDCl_3) δ (ppm) 149.90 (6C, C^5), 148.50 (6C, C^4), 132.80 (6C, C^3), 40.94 (6C, C^2), 40.20 (3C, C^1); IR (KBr): 2919, 2850, 1739, 1394, 1210, 1146, 752 cm^{-1} ; HRMS(EI): m/z calcd for $\text{C}_{27}\text{H}_{18}\text{Cl}_6$ $[\text{M}]^+$: 551.9540, found: 551.9545.

2,3,5,6,8,9-Hexakis(iodomethyl)-4,7-dihydro-1H-tricyclopenta [defjkl,pqr]-triphenylene (12)

To a mixture of **8** (20.0 mg, 24.5 μmol) and NaI (66.0 mg, 441 μmol) was added acetone (2.0 mL). After stirring for 24 h at 27 $^\circ\text{C}$ under dark condition, the mixture was directly purified by silica-gel column chromatography (CHCl_3) to give **12** (26.2 mg, 23.7 μmol , 97%).

Yellow solid; mp: 205 $^\circ\text{C}$ (dec); TLC: R_f = 0.63 ($\text{AcOEt}/n\text{-hexane}$ = 1:5); ^1H NMR (400 MHz, CDCl_3) δ (ppm) 4.73 (d, J = 10.1 Hz, 6H, H^3 or H^4), 4.68 (d, J = 10.1 Hz, 6H, H^3 or H^4), 4.46 (d, J = 19.0 Hz, 3H, H^2), 3.70 (d, J = 19.0 Hz, 3H, H^1); ^{13}C NMR (100 MHz, CDCl_3) δ (ppm) 149.10 (6C, C^5), 147.81 (6C, C^4),

133.53 (6C, C³), 39.91 (3C, C²), 0.27 (6C, C¹); IR (KBr): 3475, 2993, 2919, 2850, 1739, 1394, 1146, 752 cm⁻¹; elemental analysis calcd (%) for C₂₇H₁₈I₆: C 29.38%, H, 1.64%. Found: C 29.22%; H 2.05%.

2,3,5,6,8,9-Hexakis(methoxymethyl)-4,7-dihydro-1H-tricyclopenta [*def,jkl,pqr*]-triphenylene (13)

To a mixture of **8** (20.0 mg, 24.5 μmol) and FeSO₄ · 7H₂O (40.9 mg, 147 μmol) was added MeOH (2.0 mL) and the mixture was stirred for 2 h at 80 °C. After cooling to room temperature, to the reaction mixture was added H₂O. The resulting mixture was extracted with CHCl₃. The organic extract was washed with brine and dried over Na₂SO₄. After filtration, the filtrate was concentrated under reduced pressure. The residue was purified by PTLC (CHCl₃/AcOEt = 3:1) to give **13** (9.7 mg, 18 μmol, 75%).

Colorless solid; mp: 209 °C (dec); TLC: R_f = 0.48 (AcOEt); ¹H NMR (400 MHz, CDCl₃) δ (ppm) 4.73 (d, *J* = 19.2 Hz, 3H, H⁵), 4.64 (d, *J* = 11.9 Hz, 6H, H³ or H⁴), 4.56 (d, *J* = 11.9 Hz, 6H, H³ or H⁴), 3.62 (d, *J* = 19.2 Hz, 3H, H²), 3.40 (s, 18H, H¹); ¹³C NMR (100 MHz, CDCl₃) δ (ppm) 149.55 (6C, C⁶), 148.24 (6C, C⁵), 132.67 (6C, C⁴), 70.43 (6C, C³), 58.31 (6C, C²), 41.19 (3C, C¹); IR (KBr): 3459, 2975, 2929, 2892, 2808, 1460, 1405, 1122 cm⁻¹; HRMS(EI): *m/z* calcd for C₃₃H₃₆O₆ [M]⁺: 528.2512, found: 528.2514.

S,S',S'',S''',S''''',S''''''-((4,7-Dihydro-1H-tricyclopenta[*def,jkl,pqr*] triphenylene-2,3,5,6,8,9-hexayl)hexakis(methylene)) hexaethanethioate (14)

To a mixture of **8** (20.0 mg, 24.5 μmol) and K₂CO₃ (61.2 mg, 440 μmol) were added THF (2.0 mL) and thioacetic Acid (31.3 μL, 88 μmol), and the mixture was stirred for 15 min at 60 °C. After cooling to room temperature, the mixture was concentrated under reduced pressure. The residue was dissolved with CHCl₃ and filtrated through cotton. After concentration under reduced pressure, the residue was purified by PTLC (*n*-hexane/CHCl₃/AcOEt = 2:10:1) followed by GPC (CHCl₃) to give **14** (5.8 mg, 7.4 μmol, 33%).

Colorless solid; mp: 319 °C (dec); TLC: R_f = 0.41 (AcOEt/CHCl₃ = 1:10); ¹H NMR (400 MHz, CDCl₃) δ (ppm) 4.67 (d, *J* = 19.2 Hz, 3H, H⁵), 4.31 (d, *J* = 13.5 Hz, 6H, H³ or H⁴), 4.22 (d, *J* = 13.5 Hz, 6H, H³ or H⁴), 3.54 (d, *J* = 19.2 Hz, 3H, H²), 2.38 (s, 18H, H¹); ¹³C NMR (100 MHz, CDCl₃) δ (ppm) 195.19 (6C, C⁷), 149.23 (6C, C⁶), 147.57 (6C, C⁵), 131.38 (6C, C⁴), 41.09 (3C, C³), 30.56 (6C, C²), 29.22 (6C, C¹); IR (KBr): 3439, 2979, 2925, 2809, 1689, 1436, 1354, 1129, 958 cm⁻¹; HRMS(EI): *m/z* calcd for C₃₉H₃₆O₆S₆ [M]⁺: 792.0836, found: 792.0824.

Variable-temperature NMR experiments

To an NMR tube equipped with a J. Young valve (Figure S1a) was added **8** and this was connected to a vacuum line as shown in Figure S1b. A Schlenk flask equipped with J. Young valve containing 1,1,2,2-tetrachloroethane- d_2 , which was dried over CaH_2 , was connected to the other end of the vacuum line (The valve was closed). Then, the pressure inside of the glassware was reduced using high vacuum system. After that, the solvent was solidified with liquid nitrogen, and the valve of the Schlenk flask was opened. The main valve of the high vacuum system was then closed, and the liquid nitrogen bath was removed from the Schlenk flask. Then, the NMR tube was cooled with liquid nitrogen to transfer 1,1,2,2-tetrachloroethane- d_2 . After the appropriate amount of solvent was reached, the valve of the NMR tube was closed, and the liquid nitrogen bath was removed from the NMR tube. Variable-temperature NMR (VT-NMR) measurements (400 MHz) were performed at 25, 50, 75, 100, and 120 °C, respectively.

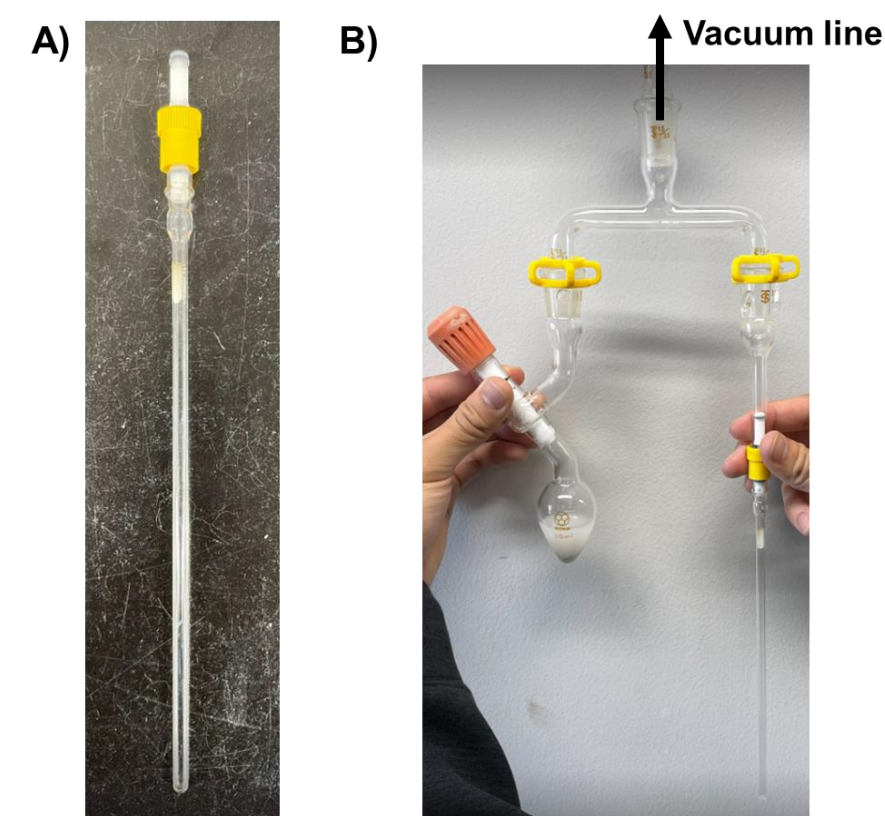


Figure 28. A) An NMR tube bearing J. Young valve. B) The setup of vacuum transfer equipment.

Solubility experiments

Bromomethylsumanene (**8**) (10.0 mg, 12.3 μmol) or hexabromosumanene (**7**) (9.1 mg, 12.3 μmol) was charged in a sample bottle and each solvent is added to it with a syringe while stirring until the compound is completely dissolved.

Computational study

All theoretical calculations using the density functional theory (DFT) method were conducted using Gaussian 09 (revision E.01) program package.¹⁸ Geometry optimization calculations were performed at the B3LYP level of theory with 6-31+G(d,p)¹⁹ as a basis set. Effective core potential (ECP) basis set of LanL2DZ²⁰ was for I. The self-consistent field energies (298.15 K, 1 atm) for the optimized geometry were calculated at the same level of theory.

Theoretical investigation of the packing structure of **8** with dimer model

The coordinates of **8-dimer** were obtained from the result of single crystal X-ray diffraction analysis (CCDC: 2204443), and those of H were optimized at the $\omega\text{B97X-D}^{21}$ level of theory with def2-SVP²² as a basis set in gas phase. Self-consistent field (SCF) calculation for the optimized coordinates was conducted at the $\omega\text{B97X-D}$ level of theory with def2-TZVP²² as a basis set in gas phase. The wavefunction files in a formatted gaussian checkpoint (fchk) format were generated using Gaussian 09 package. Complexation energies were calculated at the $\omega\text{B97X-D}$ level of theory with def2-TZVP as a basis set in gas phase using the counterpoise method to correct the Basis Set Superposition Error (BSSE).²³ The simulation of ^{13}C NMR was performed using GIAO²⁴ method at the B3LYP level of theory with 6-311+G(2d,p)²⁵ as a basis set. The solvent effect was considered using solvation model based on density (SMD) model (chloroform).²⁶

Qualitative noncovalent interactions (NCIs) of **8-dimer** were visualized with the noncovalent interaction index in a calculation box dimensions of $2.65 \times 2.65 \times 2.65 \text{ \AA}^3$ centered on a Br atom using Multiwfn program.²⁷ The grid points were set to $100 \times 100 \times 100$. The following thresholds were applied to generate the NCI isosurface; $\text{sign}(\lambda_2)\rho$ ranging from -0.50 to 0.50 a.u. and reduced density gradient (RDG) = 0.40 a.u. The surfaces were colored on a blue-green-red (BGR) scale using VMD program²⁸ according to values of $\text{sign}(\lambda_2)\rho$ ranging from -0.035 to 0.02 a.u. The blue and green regions indicate strong and weak attractive interactions, respectively.

The quantum theory atoms-in-molecules (QTAIM)¹³ analyses was performed using Multiwfn program. The obtained bond paths and the bond critical points (BCPs) were visualized using VMD program.

Theoretical investigation of pK_a ' value of bromomethylsumanene (**8**) at benzyl positions

The pK_a values using the first thermodynamic cycle (Figure 29) are determined by eq.¹⁶ ΔG_{gas} and ΔG_{THF} were calculated at cbs-4m//B3LYP/6-31G(d) and SMD(THF)/hf/6-311+G(2d,p)//B3LYP/ 6-31G(d), respectively.

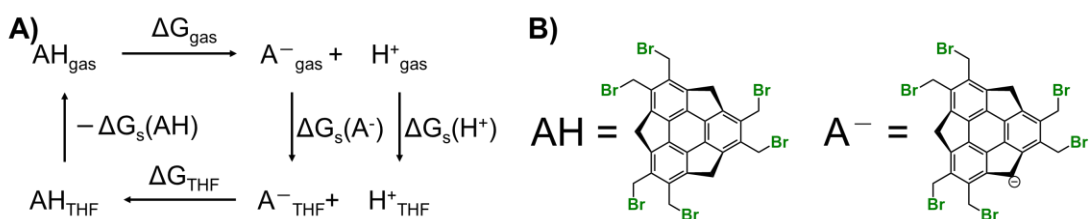
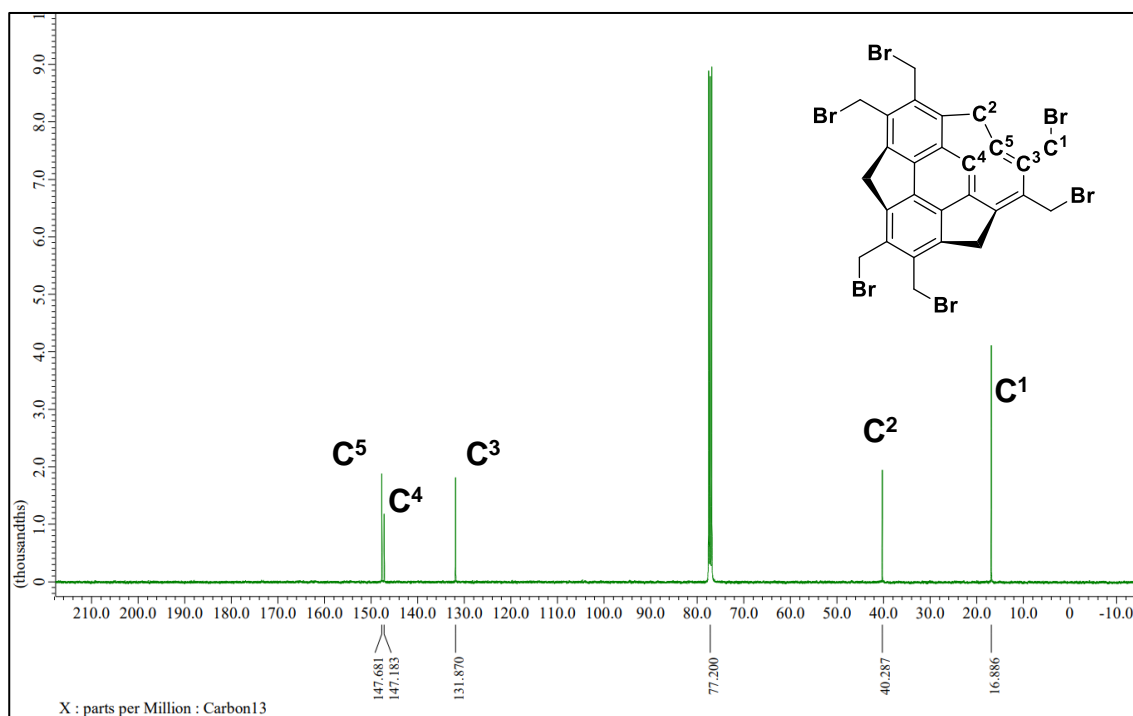
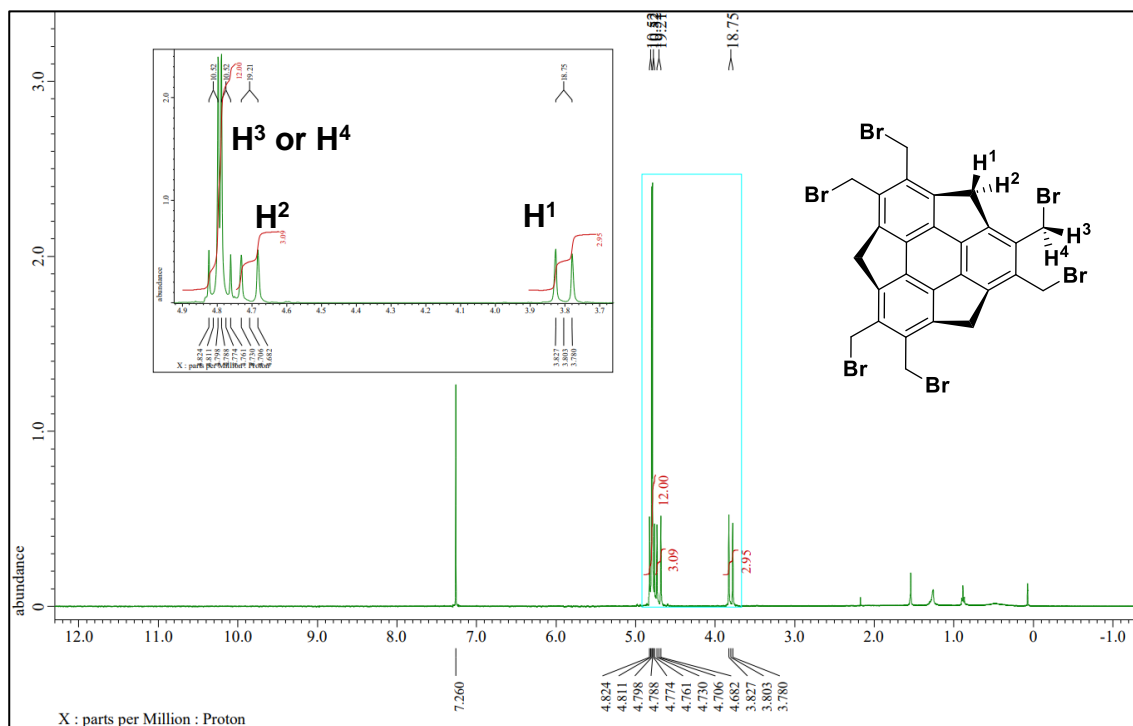


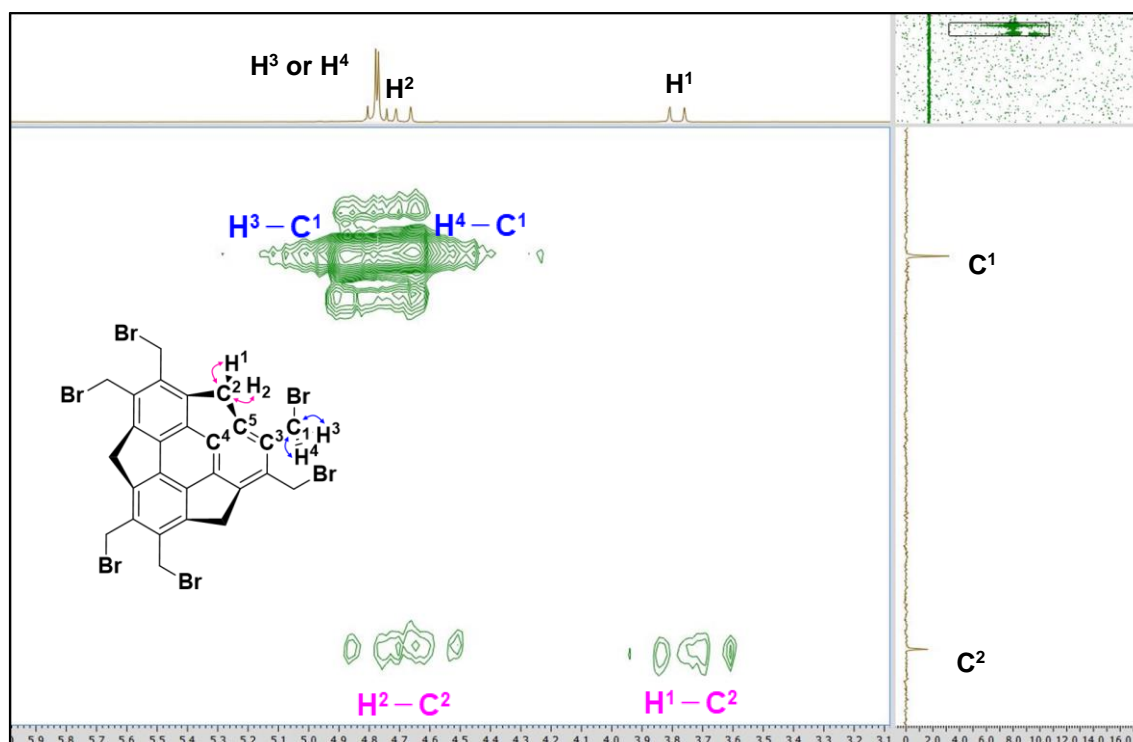
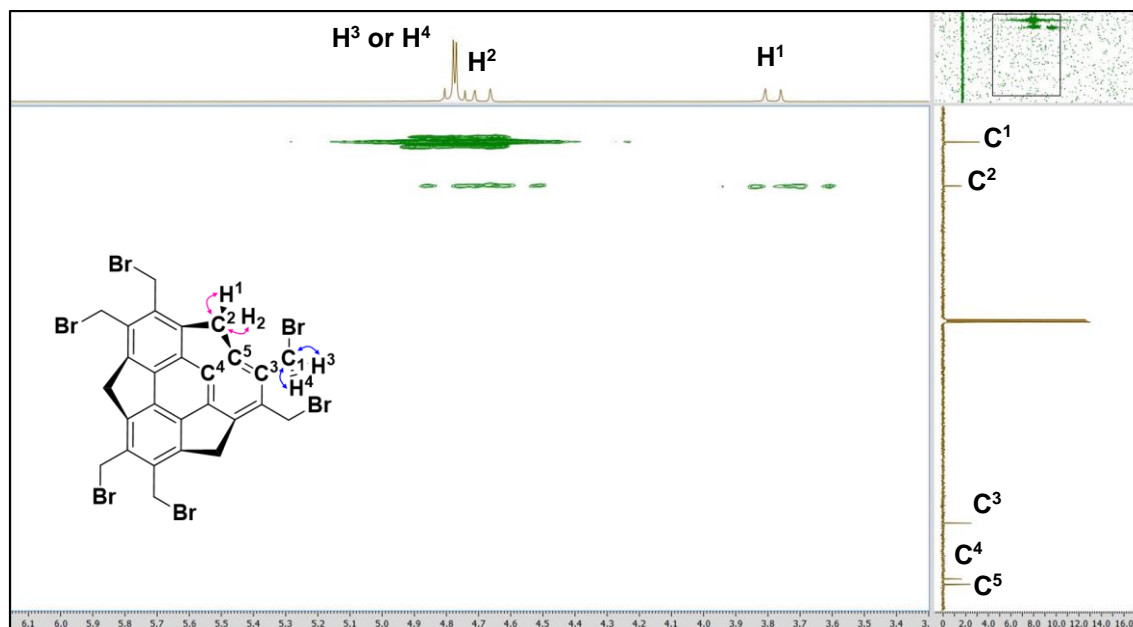
Figure 29. A) The first thermodynamic cycle and B) the definition of AH and A^{-} .

^1H and ^{13}C NMR spectra

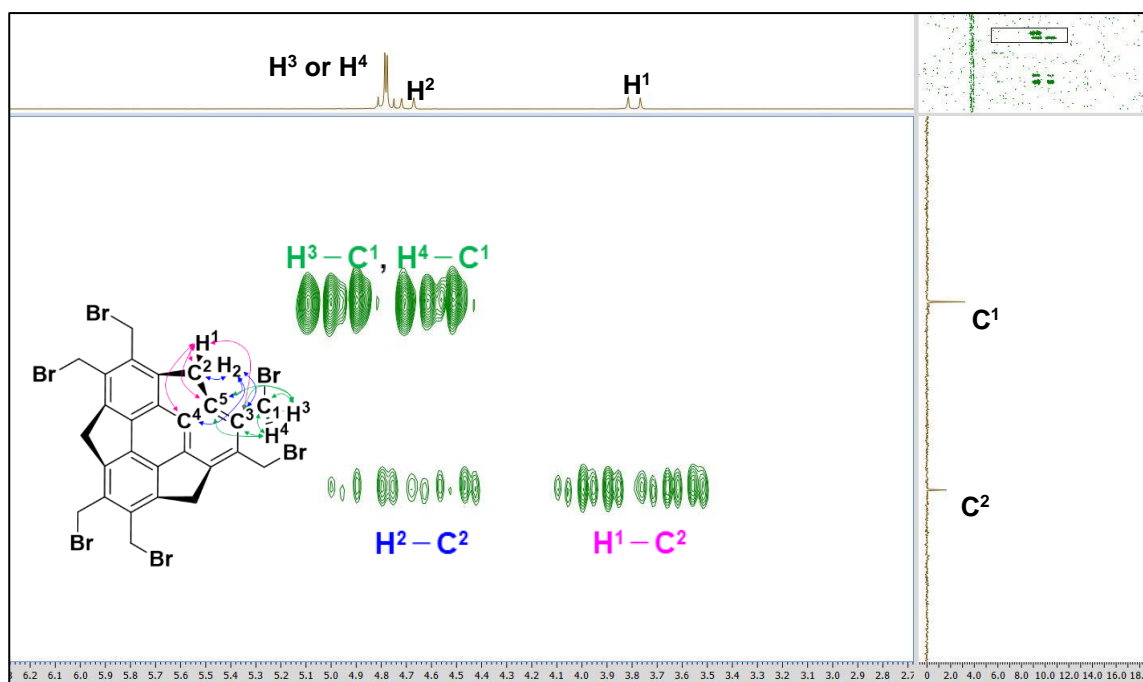
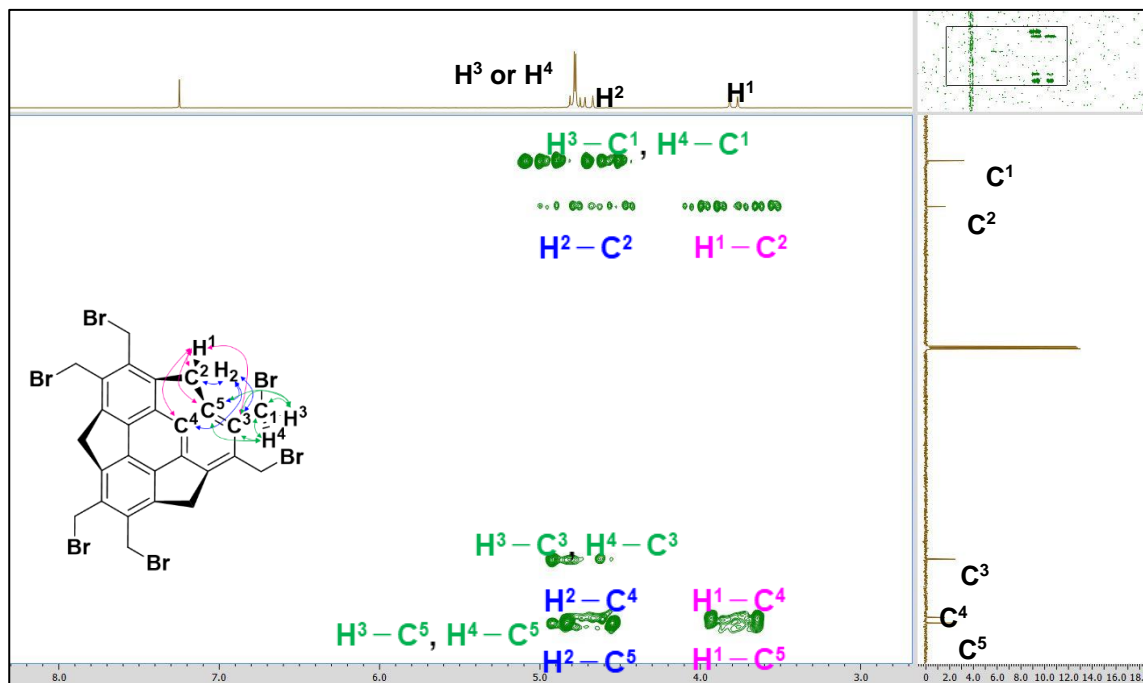
^1H NMR (400 MHz) and ^{13}C NMR (100 MHz) spectra of **8** (CDCl_3)

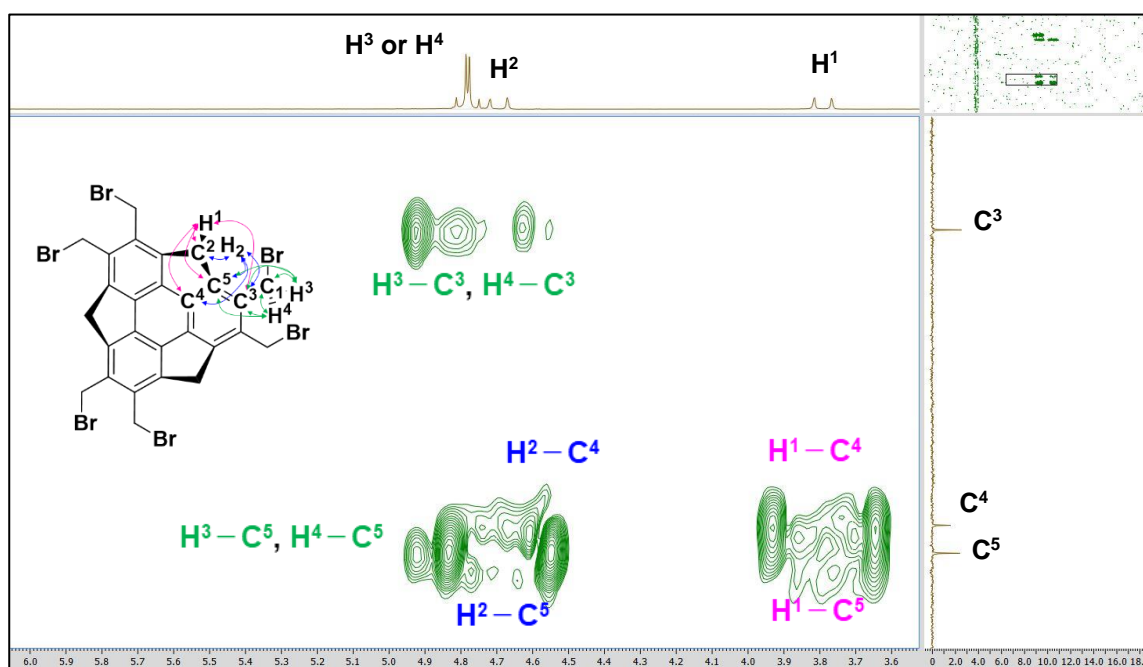


^1H - ^{13}C HMQC NMR spectra of **8** (CDCl_3)

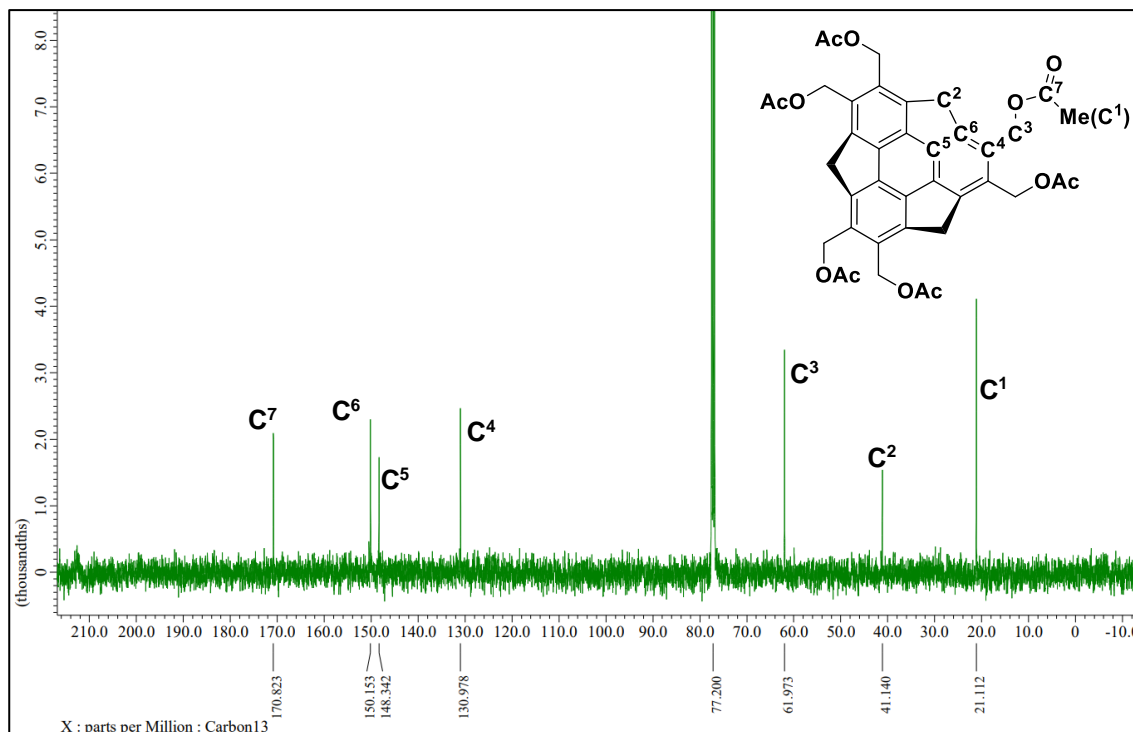
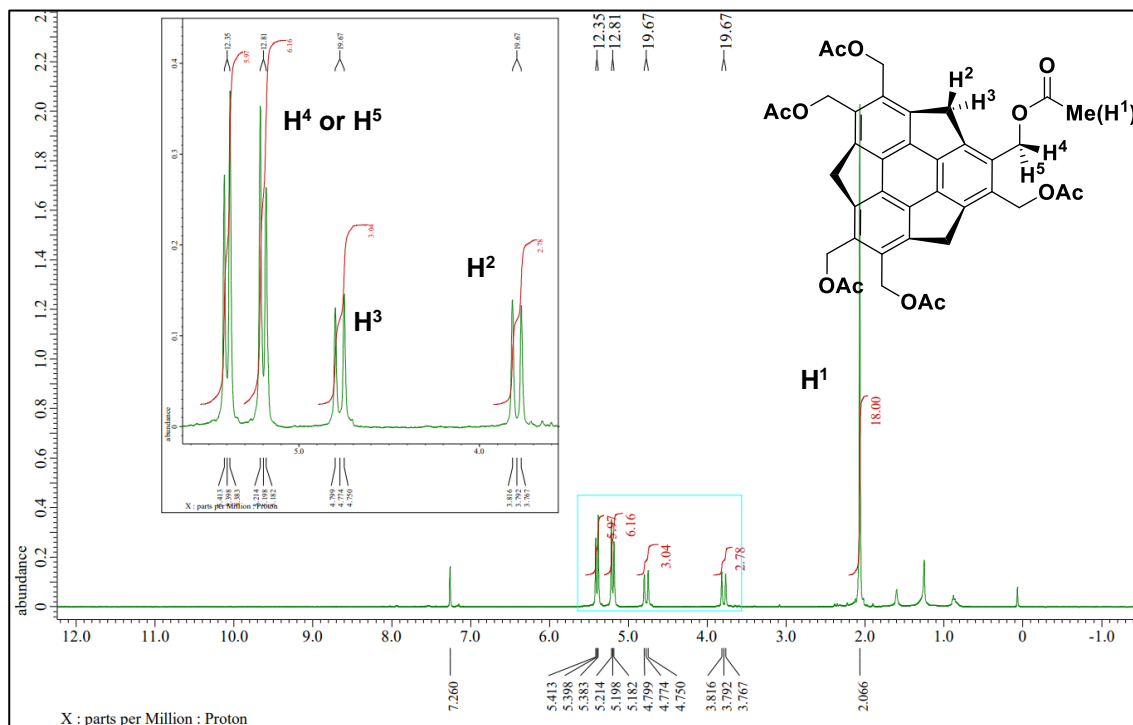


^1H - ^{13}C HMBC NMR spectra of **8** (CDCl_3)

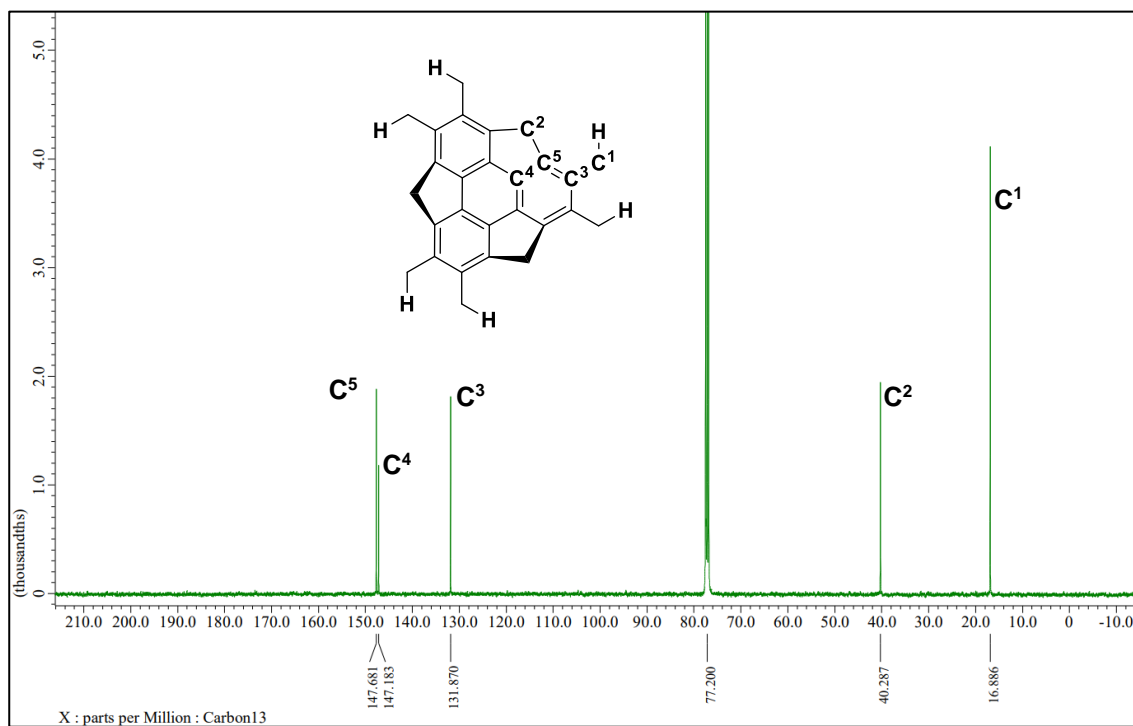
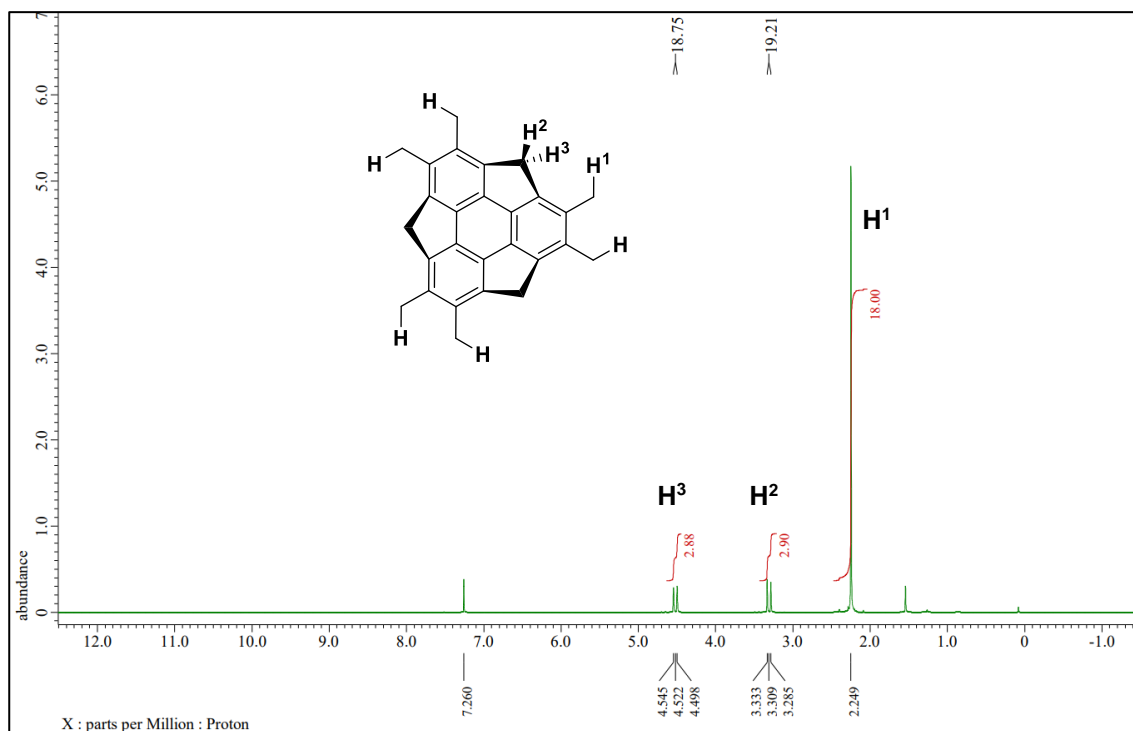




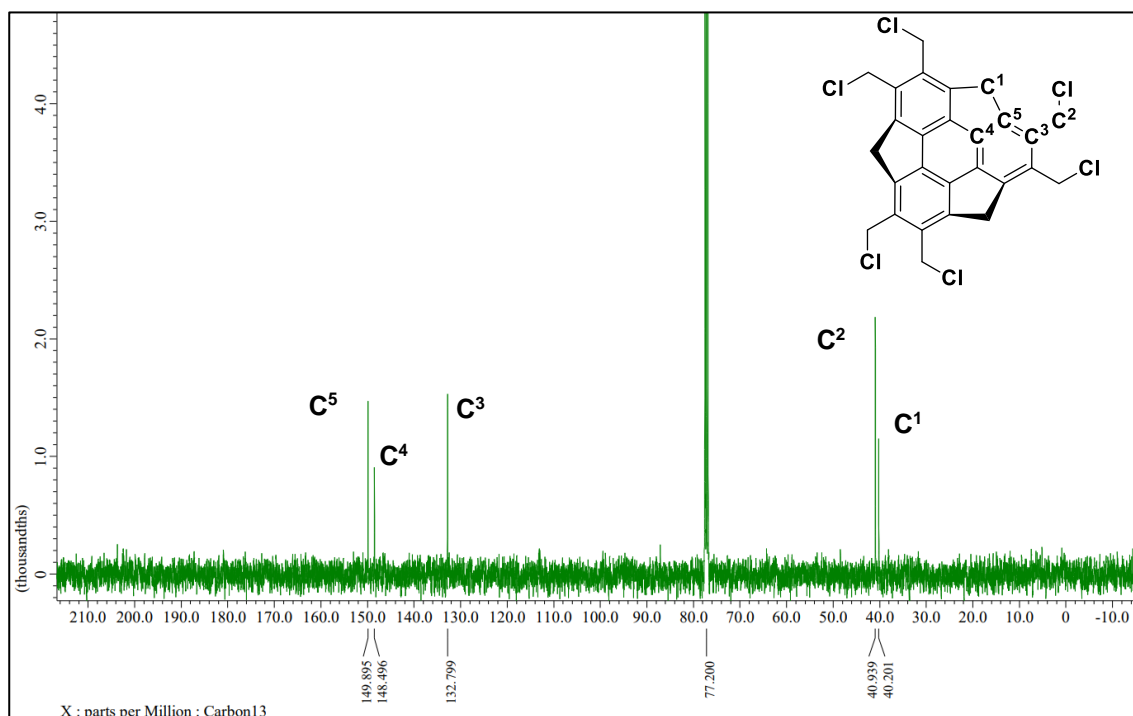
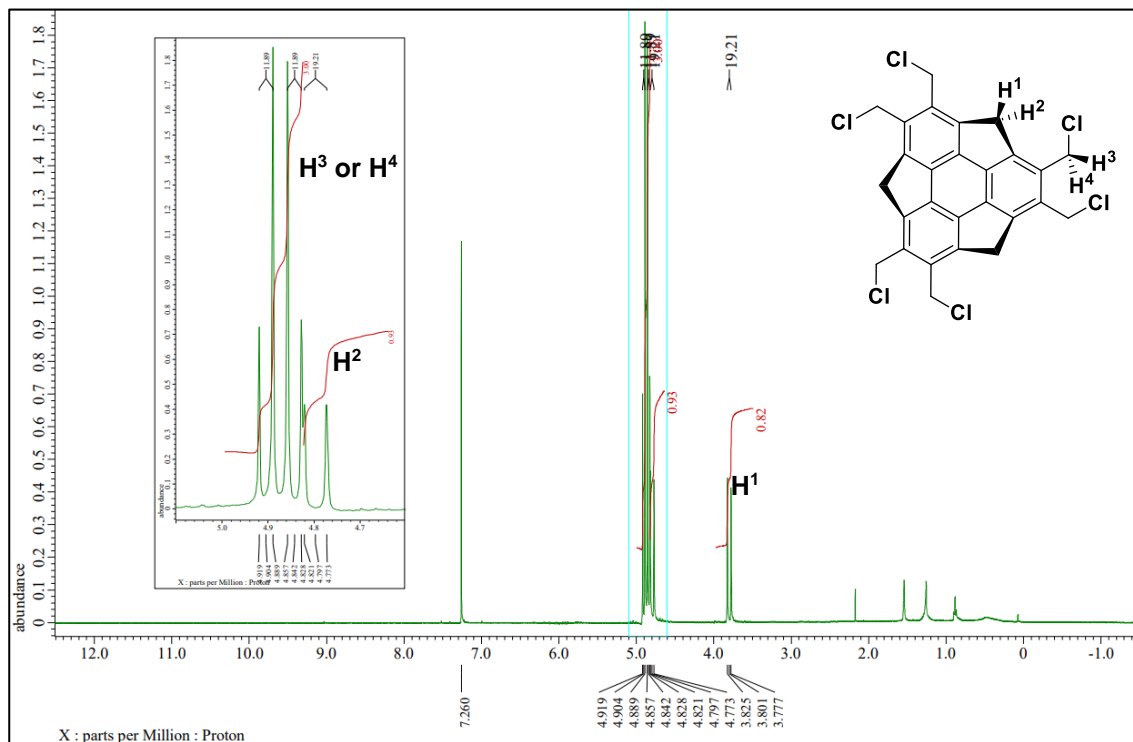
^1H NMR (400 MHz) and ^{13}C NMR (100 MHz) spectra of **9** (CDCl_3)



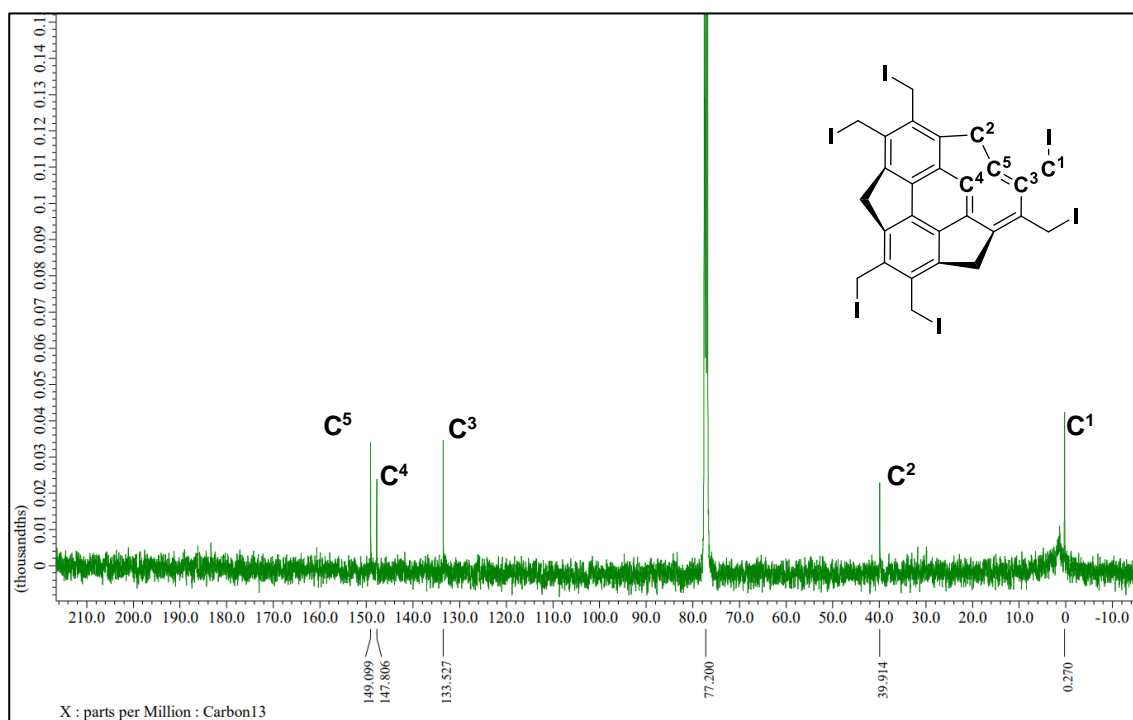
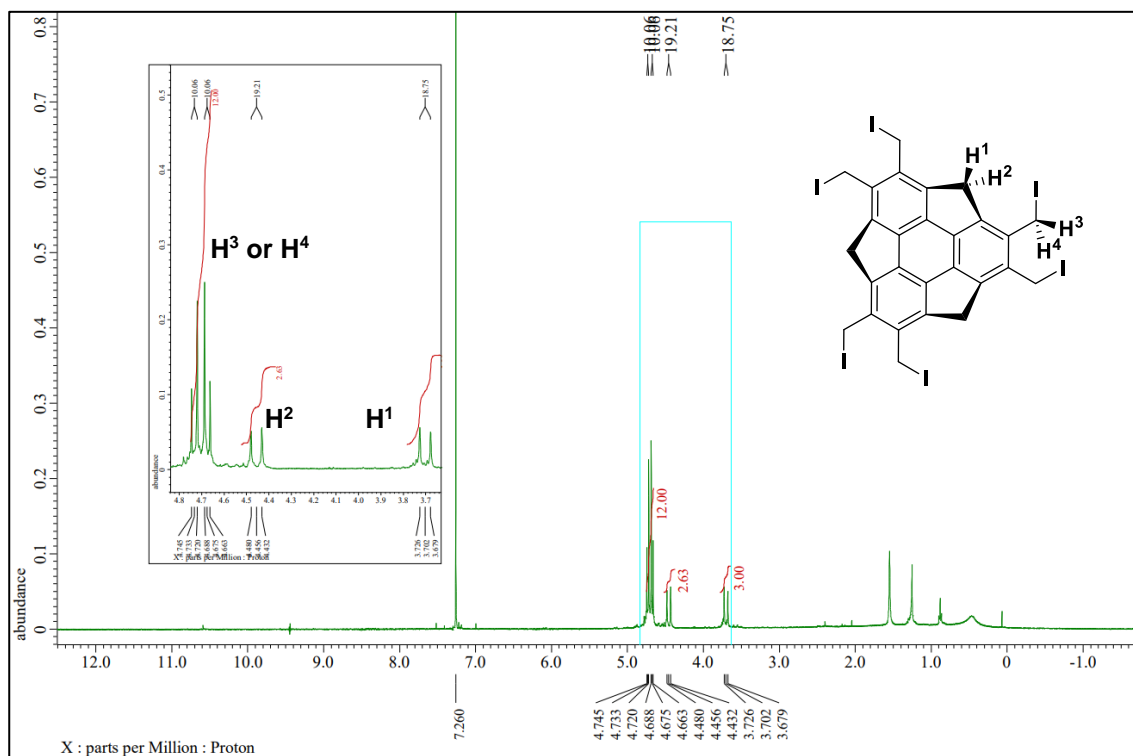
^1H NMR (400 MHz) and ^{13}C NMR (100 MHz) spectra of **10** (CDCl_3)



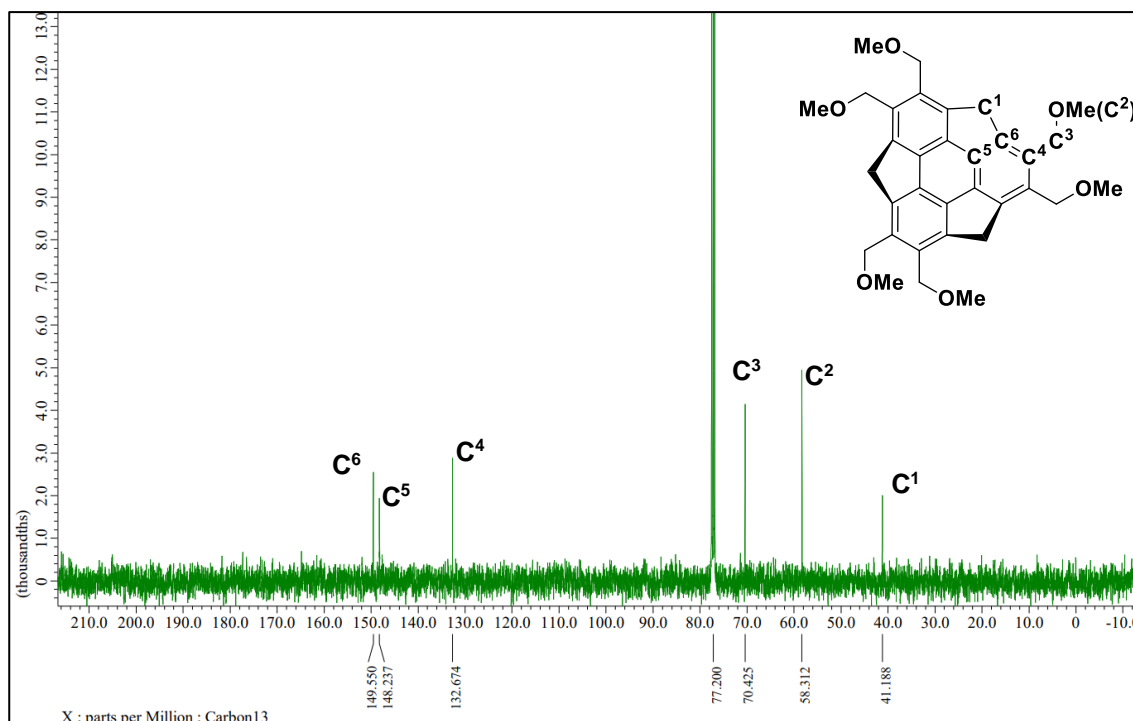
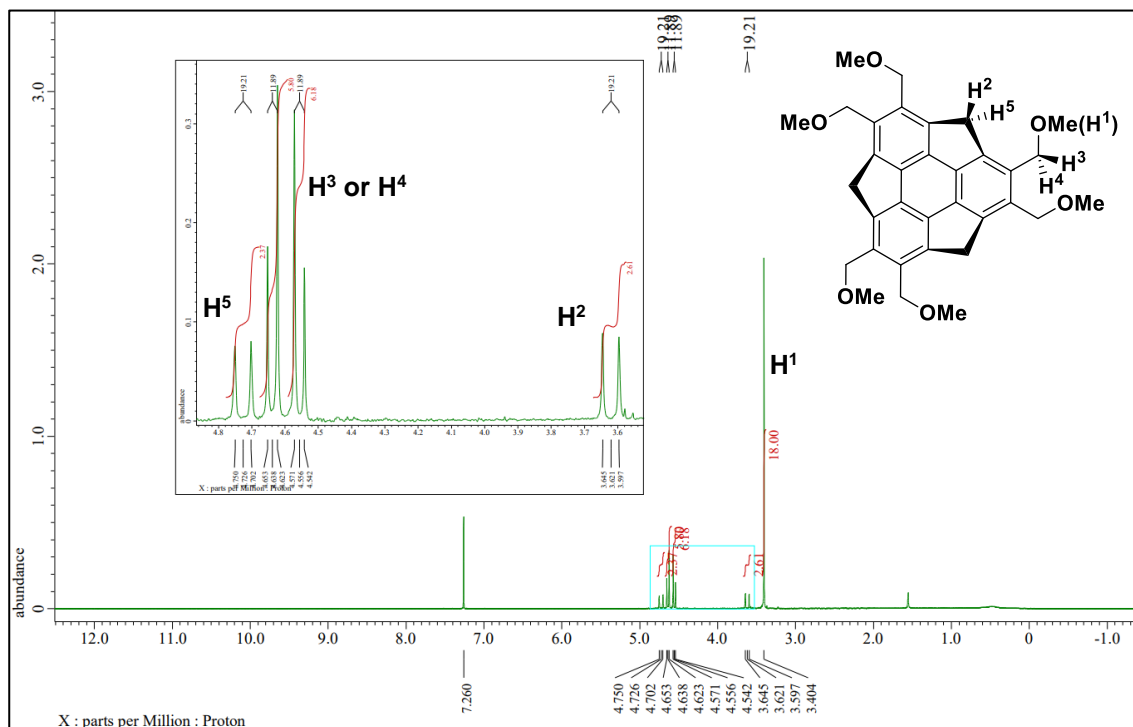
^1H NMR (400 MHz) and ^{13}C NMR (100 MHz) spectra of **11** (CDCl_3)



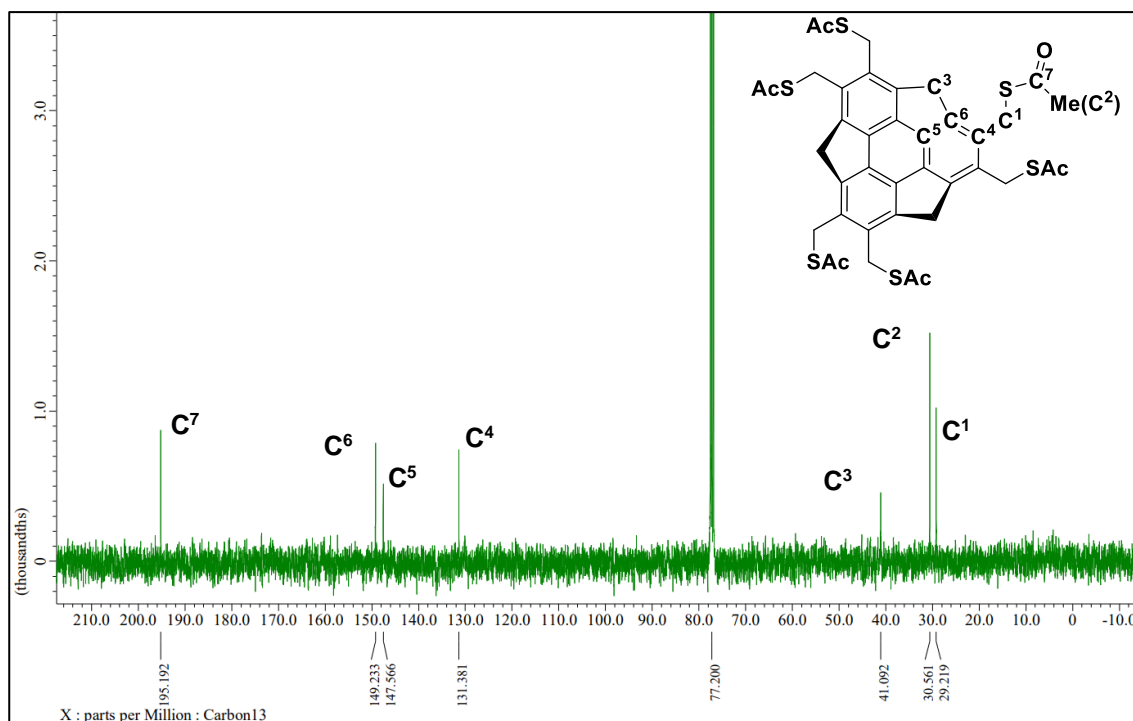
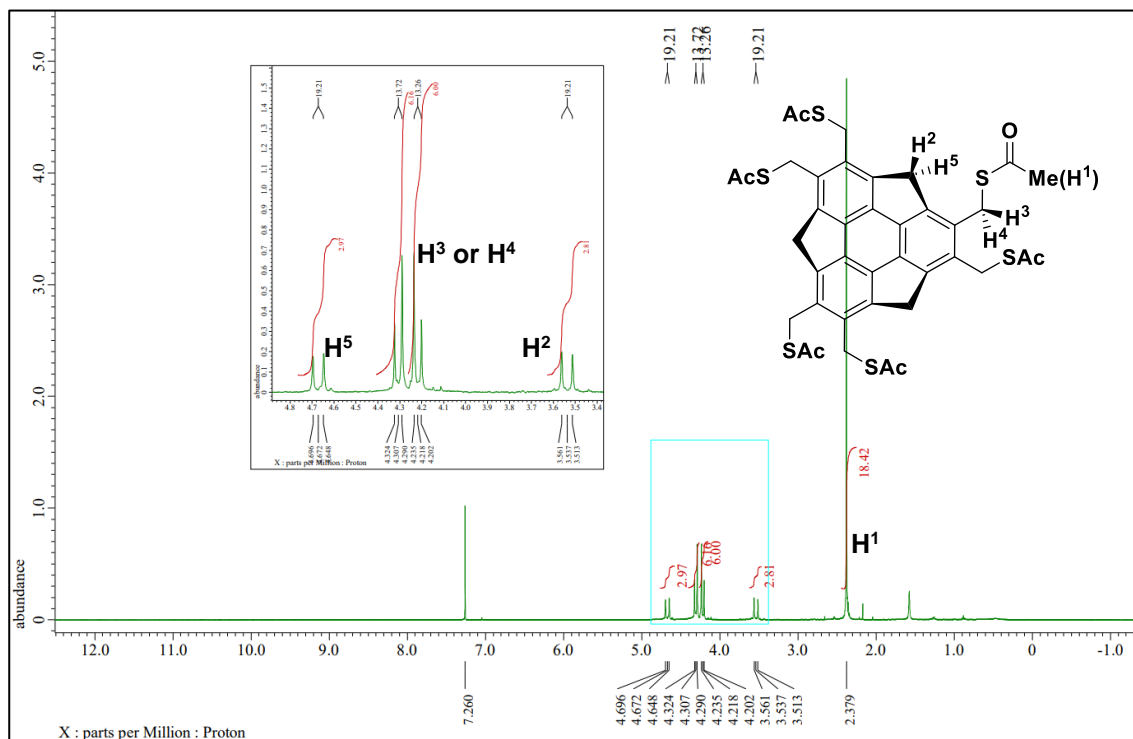
^1H NMR (400 MHz) and ^{13}C NMR (100 MHz) spectra of **12** (CDCl_3)



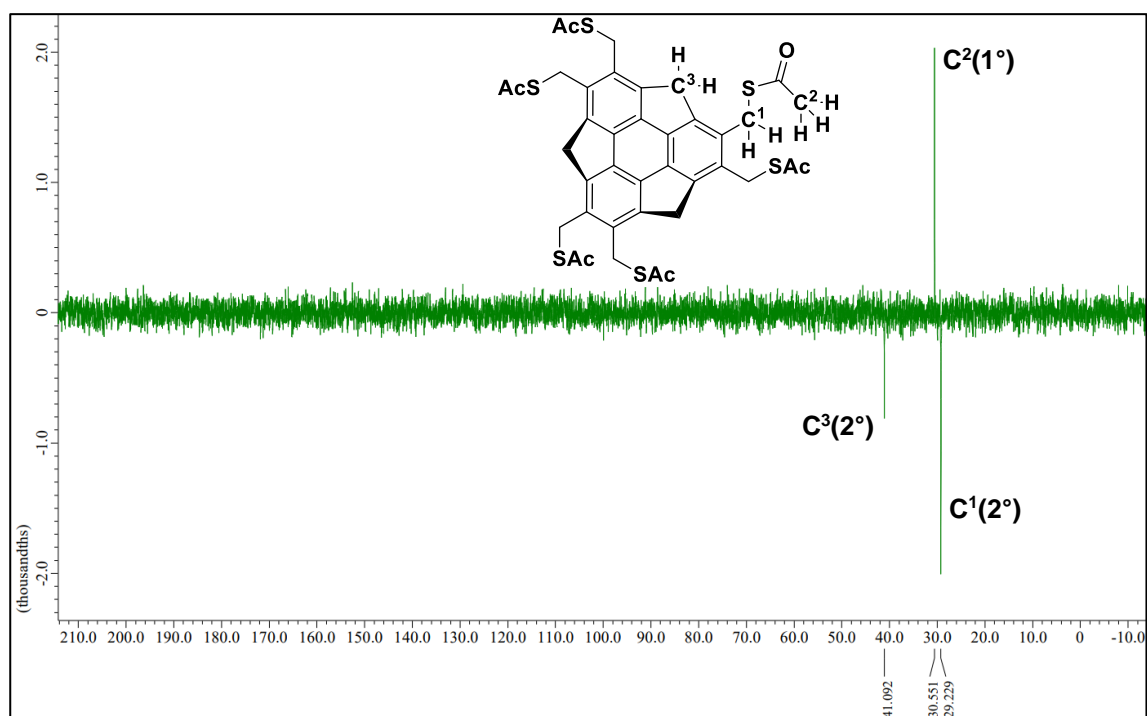
^1H NMR (400 MHz) and ^{13}C NMR (100 MHz) spectra of **13** (CDCl_3)



^1H NMR (400 MHz) and ^{13}C NMR (100 MHz) spectra of **14** (CDCl_3)



^{13}C NMR (DEPT135) spectrum of **14** (CDCl_3)



References

- 1 a) H. Higashibayashi, H. Sakurai, *Chem. Lett.* **2011**, 40, 122. b) M. Saito, H. Shinokubo, H. Sakurai, *Mater. Chem. Front.* **2018**, 2, 635. c) H. Sakurai, *Bull. Chem. Soc. Jpn.* **2021**, 94, 1579.
- 2 P. C. Cheng, Ph.D. Dissertation, Boston College, Boston, MA, **1996**. L. T. Scott, *Pure Appl. Chem.* **1996**, 68, 291.
- 3 Y. Y. Xu, H. R. Tian, S. H. Li, Z. C. Chen, Y. R. Yao, S. S. Wang, X. Zhang, Z. Z. Zhu, S. L. Deng, Q. Zhang, S. Yang, S. Y. Xie, R. B. Huang, L. S. Zheng, *Nat. Commun.* **2019**, 10, 485.
- 4 H. Toda, Y. Yakiyama, Y. Shoji, F. Ishiwari, T. Fukushima, H. Sakurai, *Chem. Lett.* **2017**, 46, 1368.
- 5 a) Y. Shoji, T. Kajitani, F. Ishiwari, Q. Ding, H. Sato, H. Anetai, T. Akutagawa, H. Sakurai, T. Fukushima, *Chem. Sci.* **2017**, 8, 8405. b) I. Hisaki, H. Toda, H. Sato, N. Tohnai, H. Sakurai, *Angew. Chem. Int. Ed.* **2017**, 56, 15294. c) H. Toda, Y. Uetake, Y. Yakiyama, H. Nakazawa, T. Kajitani, T. Fukushima, H. Sakurai, *Synthesis* **2019**, 51, 4576. d) Y. Yakiyama, T. Hasegawa, H. Sakurai, *J. Am. Chem. Soc.* **2019**, 141, 18099.
- 6 a) P. Walden, *Ber. Dtsch. Chem. Ges.* **1893**, 26, 210. b) F. A. Carey, R. J. Sundberg, *Adv. Org. Chem.*, Plenum Press, New York, USA, **1984**. c) M. B. Smith, *March's Advanced Organic Chemistry: Reactions, Mechanisms and Structure*; 7th ed. Wiley: New York, **2013**. d) S. Shaik, H. B. Schlegel, S. Wolfe, *Theoretical Aspects of Physical Organic Chemistry: The S_N2 Reaction*, Wiley, New York, **1992**. e) J. M. Riveros, S. M. JosØ, K. Takashima, *Adv. Phys. Org. Chem.* **1985**, 21, 197. f) A. de Cozar, E. Ortega-Carrasco, E. San Sebastian, O. Larranaga, J.-D. Marechal, F. M. Bick-elhaupt, F. P. Cossío, *ChemPhysChem* **2016**, 17, 3932.
- 7 K. Mizoguchi, T. Higashihara, M. Ueda, *Macromolecules* **2010**, 43, 2832.
- 8 T. Amaya, S. Katoha, T. Hirao, *Synlett* **2016**, 27, 2128.
- 9 Y. Segawa, T. Watanabe, K. Yamanoue, *Nat. Synth.* **2022** 1, 535.
- 10 H. Sakurai, T. Daiko, T. Hirao, *Science* **2003**, 301, 1878.
- 11 H. Sakurai, T. Daiko, H. Sakane, T. Amaya, T. Hirao, *J. Am. Chem. Soc.* **2005**, 127, 11580.
- 12 E. R. Johnson, S. Keinan, P. Mori-Sánchez, J. Contreras-García, A. J. Cohen, W. Yang, *J. Am. Chem. Soc.* **2010**, 132, 6498.
- 13 W. B. Richard, *Chem. Rev.* **1991**, 91, 893.
- 14 M. A. A. Ibrahim, N. A. M. Moussa, *ACS Omega* **2020**, 5, 21824.
- 15 a) W. Williamson, *Liebigs Ann. Chem.* **1851**, 77, 37. b) O. C. Dermer, *Chem. Rev.* **1934**, 14, 385.
- 16 M. D. Liptak, G. C. Shields, *J. Am. Chem. Soc.* **2001**, 123, 7314.
- 17 G. Joshi, S. Adimurthy, *Synth. Commun.* **2011**, 41, 720.
- 18 Gaussian 09, revision E.01, M. J. Frisch, G. W. Trucks, H. B. Schlegel, G. E. Scuseria, M.A. Robb, J. R. Cheeseman, G. Scalmani, V. Barone, G. A. Petersson, H. Nakatsuji, X. Li, M.

- Caricato, A. Marenich, J. Bloino, B. G. Janesko, R. Gomperts, B. Mennucci, H. P. Hratchian, J. V. Ortiz, A. F. Izmaylov, J. L. Sonnenberg, D. Williams-Young, F. Ding, F. Lipparini, F. Egidi, J. Goings, B. Peng, A. Petrone, T. Henderson, D. Ranasinghe, V. G. Zakrzewski, J. Gao, N. Rega, G. Zheng, W. Liang, M. Hada, M. Ehara, K. Toyota, R. Fukuda, J. Hasegawa, M. Ishida, T. Nakajima, Y. Honda, O. Kitao, H. Nakai, T. Vreven, K. Throssell, J. A. Montgomery, Jr., J. E. Peralta, F. Ogliaro, M. Bearpark, J. J. Heyd, E. Brothers, K. N. Kudin, V. N. Staroverov, T. Keith, R. Kobayashi, J. Normand, K. Raghavachari, A. Rendell, J. C. Burant, S. S. Iyengar, J. Tomasi, M. Cossi, J. M. Millam, M. Klene, C. Adamo, R. Cammi, J. W. Ochterski, R. L. Martin, K. Morokuma, O. Farkas, J. B. Foresman, D. J. Fox, Gaussian, Inc., Wallingford CT, 2016.
- 19 a) R. Ditchfield, W. J. Hehre, J. A. Pople, *J. Chem. Phys.* **1971**, *54*, 724. b) P. C. Hariharan, J. A. Pople, *Theor. Chim. Acta* **1973**, *28*, 213. c) W. J. Hehre, R. Ditchfield, J. A. Pople, *J. Chem. Phys.* **1972**, *56*, 2257. d) V. A. Rassolov, M. A. Ratner, J. A. Pople, John A., P. C. Redfern, L. A. Curtiss, *J. Comput. Chem.* **2001**, *22*, 976.
- 20 W. R. Wadt, P. J. Hay, *J. Chem. Phys.* **1985**, *82*, 284.
- 21 J.-D. Chai, M. Head-Gordon, *Phys. Chem. Chem. Phys.* **2008**, *10*, 6615.
- 22 a) K. A. Peterson, D. G. Figgen, S. T. Erich, M. Dolg, *J. Chem. Phys.* **2003**, *119*, 11113. b) F. Weigend, R. Ahlrichs, *Phys. Chem. Chem. Phys.* **2005**, *7*, 3297.
- 23 S. F. Boys, F. Bernardi, *Mol. Phys.* **1970**, *19*, 553.
- 24 a) P. v. R. Schleyer, C. Maerker, A. Dransfeld, H. Jiao, N. J. R. v. E. Hommes, *J. Am. Chem. Soc.* **1996**, *118*, 6317. b) P. v. R. Schleyer, *Chem. Rev.* **2001**, *101*, 1115. c) A. D. Allen, T. T. Tidwell, *Chem. Rev.* **2001**, *101*, 1333.
- 25 a) C. Timothy, C. Jayaraman, W. S. Günther, P. V. R. Ragué, *J. Comput. Chem.* **1983**, *4*, 294, 301. b) R. Krishnan, J. S. Binkley, R. Seeger, J. A. Pople, *J. Chem. Phys.* **1980**, *72*, 650.
- 26 A. V. Marenich, J. C. Christopher, G. T. Donald, *Phys. Chem. B* **2009**, *113*, 6378.
- 27 T. Lu, F. Chen, *J. Comput. Chem.* **2012**, *33*, 580.
- 28 W. Humphrey, A. Dalke, K. Schulten, *J. Mol. Graph.* **1996**, *14*, 33.

Chapter 4. Pentagon-fused sumanenes on the aromatic peripheries en route to the bottom-up synthesis of fullerenes

Section 1. Introduction of C₆₀ synthesis

The existence of fullerene C₆₀ was predicted by Osawa et al. in 1970,¹ and its formation was first confirmed by Kroto, Smalley, and Curl in 1985.² Since then, efficient synthesis of C₆₀ has been sought for several decades. In the modern era, the development of methods such as the arc discharge treatment of graphite and the combustion method using organic materials as starting materials has established a method for the bulk synthesis of C₆₀. And C₆₀, now commercially available from reagent companies, has become the subject of research by many chemists.³

On the other hand, the chemical synthesis of fullerenes from small organic molecules (bottom-up synthesis) is suitable for manipulating the elements that make up fullerenes at the single atomic level. This approach also has the advantage of minimizing the formation of isomers, which are difficult to separate and simplifying the purification process. For example, Rubin and Tobe et al. independently observed C₆₀⁺ by treating carbon cages with laser irradiation in MALDI-TOF MS (Figure 30A).⁴ Scott et al. also synthesized C₆₀ by flash vacuum pyrolysis (FVP) using a planar truxene derivative with chlorine atoms as the starting material (Figure 30B).⁵ Furthermore, Otero and Biddau have found that C₆₀ can be obtained by heating on platinum surfaces even from planar molecules consisting only of carbon and hydrogen atoms (Figure 30C).⁶ In this way, forming the C₆₀ skeleton is possible by using a densely designed organic molecule with 60 carbons as a starting material. However, these methods require large amounts of energy, such as laser irradiation and heating, and the products obtained are tiny amounts, and bulk-scale synthesis using only liquid-phase reactions in flasks has yet to be achieved.

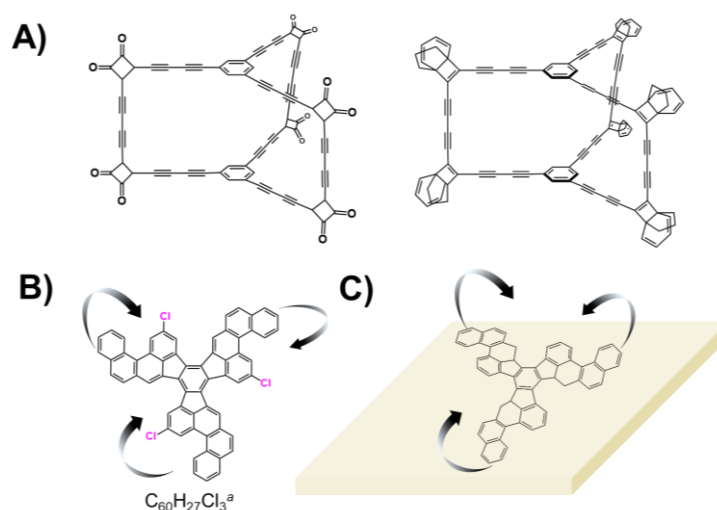


Figure 30. Synthesis of fullerenes by synthetic organic method.

A different approach is to synthesize fullerenes by dimerization of organic molecules with hemispherical structures such as C_{30} . The biggest drawback of bottom-up synthesis of C_{60} is its highly distorted structure, which makes it challenging to synthesize C_{60} from planar π -conjugated molecules. On the other hand, by using pre-curved π -conjugated molecules such as buckybowls, the energy required for sphere formation can be lower than when using planar molecules. Previously, the synthesis of $C_{30}H_{12}$ (**15**, Figure 31), a hemispherical molecule with 30 carbons, was reported by Sygula and Scott et al. independently.⁷ However, the synthesis of C_{60} by dimerization from it has not yet been achieved. The main possible reasons for this are that the peripheral moiety of **15** is composed of aromatic carbons and does not have a suitable functional group for dimerization. Another possible reason is that for **15** to dimerize with each other to obtain C_{60} , forming a five-membered ring and a six-membered ring simultaneously complicates the reaction. Therefore, the ideal hemispherical structure to form C_{60} should have functional groups suitable for dimerization and satisfy the isolated pentagon rule (IPR), with each five-membered ring arranged so that they are not next to each other. In addition, it is considered that the precursor has 30 carbons and forms C_{60} by dimerization involving only the formation of a six-membered ring structure.⁸ Previously, a hemispherical molecule (**16**) with a corannulene skeleton has been proposed as a molecule that meets above requirement, but the synthesis of **16** has yet to be achieved (Scheme 15).⁹

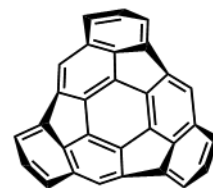
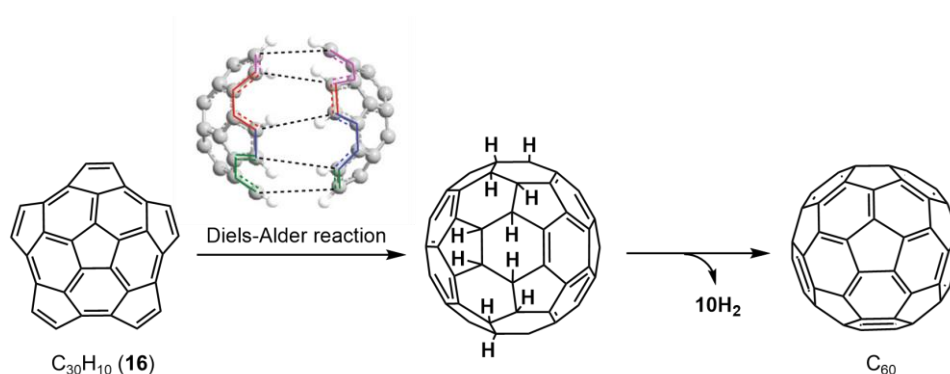


Figure 31. $C_{30}H_{12}$ (**15**)



Scheme 15. Proposed synthesis of C_{60} using corannulene-based hemisphere (**16**).

In this study, the author aimed at the synthesis of fullerene C_{60} and considered the synthesis of a hemispherical molecule based on sumanene (**1**) instead of corannulene (Figure 32). The hemispherical molecule the author has in mind here already has 30 carbons (C_{30}), a benzyl position for easy chemical modification, and six independent five-membered rings. Therefore, it can be converted to C_{60} by dimerization involving only the formation of a six-membered ring structure, which is the ideal precursor structure for a hemispherical molecule.

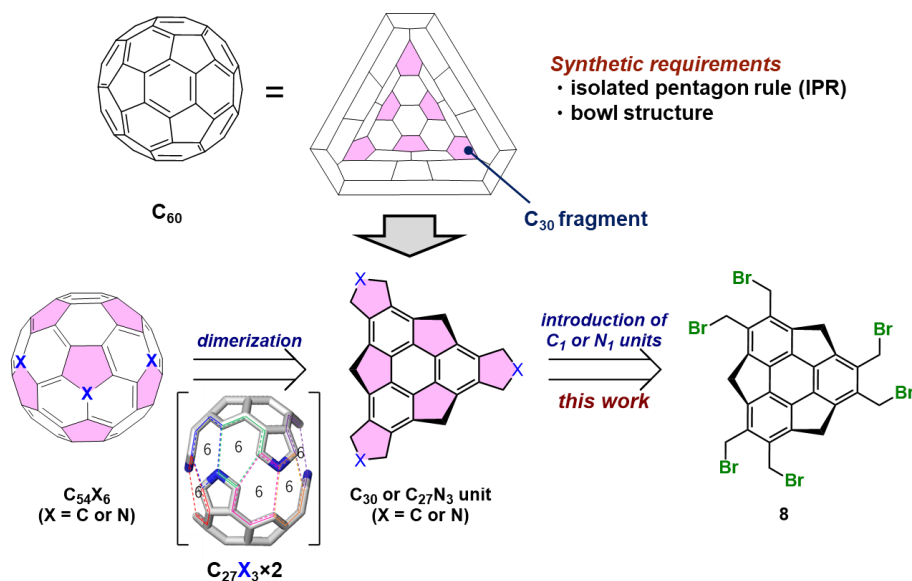


Figure 32. A strategy for the bottom-up synthesis of fullerenes via sumanene-based hemisphere.

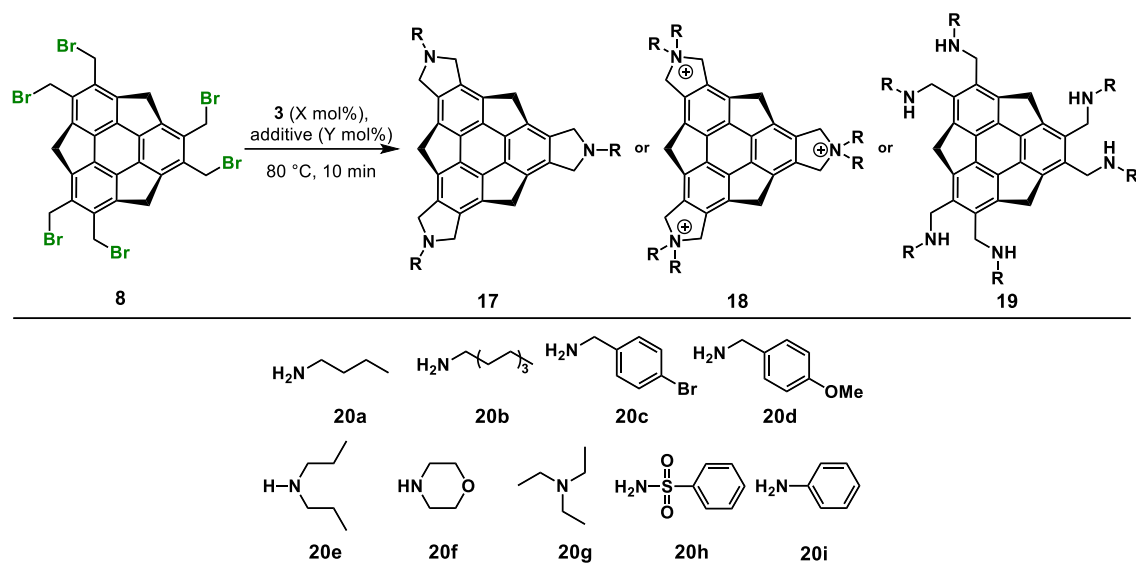
The author has already achieved the synthesis of bromomethylsumanene (**8**) with 27 carbons in one step from sumanene (**1**) in Chapter 3. Therefore, the author thought that the hemispherical molecule (C_{30}) could be synthesized if sequential alkylation could be achieved using the methylene equivalent as the C_1 unit. Furthermore, it is possible to synthesize triaminosumanene ($C_{27}N_3$) with a hemispherical skeleton of azafullerene $C_{54}N_6$ by changing the nucleophile used to amines. Therefore, the author first investigated the synthesis of triaminosumanene, which is considered to have high nucleophilicity and can be easily synthesized as a hemispherical molecule.

Section 2. Synthesis of azafullerene $C_{54}N_6$ and fullerene C_{60} fragments

Based on the results of Chapter 3, It is expected that the decomposition of **8** would occur under strongly basic conditions, so the investigation began with finding the conditions for the reaction to proceed in a weakly basic state. (Table 8). First, **8** was reacted with *n*-butylamine (300 mol%) and sodium hydrogen carbonate (600 mol%) as an additive to trap HBr produced in situ at 27, 40, and 80 °C, respectively (entries 1-3). However, the decomposition of **8** proceeded, probably due to the strong basicity of the RHN^- formed in situ. Similarly, when the reaction was carried out using a Proton-sponge, a base with low nucleophilicity, the target product (**17a**) was not obtained (entries 4-6). Therefore, the addition of an excess amount of *n*-butylamine (900 mol%) without an external base was considered. As a result, triaminosumanene **17a** was obtained in 37% yield (entry 7). On the other hand, no **17a** was not obtained with acetonitrile and *N,N*-dimethylformamide (entries 8 and 9). Furthermore, similar reactions were found to be applicable to primary amines such as *n*-octylamine with long alkyl chains, *p*-bromobenzylamine, which is expected to give excellent crystalline products, and *p*-methoxybenzylamine,¹⁰ which is easily deprotected (entries 10 -12). On

the other hand, when secondary or tertiary amines were used instead of primary amines, no ammonium salts (**18**) or hexa-amines (**19**) were formed, and decomposition of the starting materials was observed (entries 13-15). Nucleophilic substitution reactions were also examined using sulfonamide and aniline, but no products were obtained (entries 16-21). These results suggested that the introduction of amines into **8** requires high nucleophilicity.

Table 8. Optimization of amination conditions



entry	20 (X mol%)	additive (Y mol%)	solvent	yield ^a
1	20a (300)	NaHCO ₃ (600)	THF	0
2 ^b	20a (300)	NaHCO ₃ (600)	THF	0
3 ^c	20a (300)	NaHCO ₃ (600)	THF	0
4	20a (300)	Proton sponge (600)	THF	0
5 ^b	20a (300)	Proton sponge (600)	THF	0
6 ^c	20a (300)	Proton sponge (600)	THF	0
7	20a (900)	-	THF	37% (17a)
8	20a (900)	-	MeCN	0
9	20a (900)	-	DMF	0
10	20b (900)	-	THF	28 (17b)
11	20c (900)	-	THF	25 (17c)
12	20d (900)	-	THF	24 (17d)

13	20e (900)	-	THF	0
14	20f (900)	-	THF	0
15	20g (900)	-	THF	0
16	20h (900)	-	THF	0
17	20h (900)	Proton sponge (600)	THF	0
18	20h (900)	NaHCO ₃ (600)	THF	0
19	20i (900)	-	THF	0
20	20i (900)	Proton sponge (600)	THF	0
21	20i (900)	NaHCO ₃ (600)	THF	0

^aIsolated yield. ^b27 °C, 48 h. ^c40 °C, 48 h.

Single crystals of **17c** were obtained as yellow blocks by vapor diffusion using CHCl₃/*n*-hexane, and single crystal X-ray structure analysis was performed (Figure 33A). First, to evaluate the degree of curvature of the bowl structure, the bowl depth of each molecule was compared (Figure 33B and Table 9). The results showed that the bowl depth of **17c** was in the range of 1.27-1.28 Å in the crystalline state. While this value indicated a shallower bowl structure than azafullerenes such as C₅₄N₆ (1.68 Å) and [C₅₄N₆]⁶⁺ (1.67 Å), it also indicated a deeper bowl structure when compared to **1**.¹¹ Comparing the POAV angle, which indicated the curvature of the bowl molecules, **17c** had a value of 9.61°, much larger than the 8.80° of **1**. Next, to clarify whether the deep bowl structure of **17c** is due to packing requirements in the crystal or the structure itself, structural optimization of the unimolecular state at the B3LYP/6-31+G(d,p) level in a vacuum was performed, and evaluated the curvature. The coordinates of the initial structure of **17c** used in the calculations were obtained from the single crystal X-ray structure analysis results. The results showed that the bowl depth of the optimized structure of **17c** (1.11 Å) was shallower than that observed in the crystal, and the POAV angle (8.62°) was similar. Therefore, the large bowl depth observed in the crystal was due to intermolecular packing requirements. Next, focusing on the packing structure, **17c** formed a 1D columnar structure along the *c*-axis, trapping the disordered chloroform in the free space created between the convex and concave surfaces of the sumanene skeleton (Figure 33C). This chloroform incorporation is unique to **17c**, given that sumanene derivatives form dense columnar structures due to relatively strong intermolecular CH···π interactions between the benzyl position σ(C-H) and the surrounding π* orbitals.

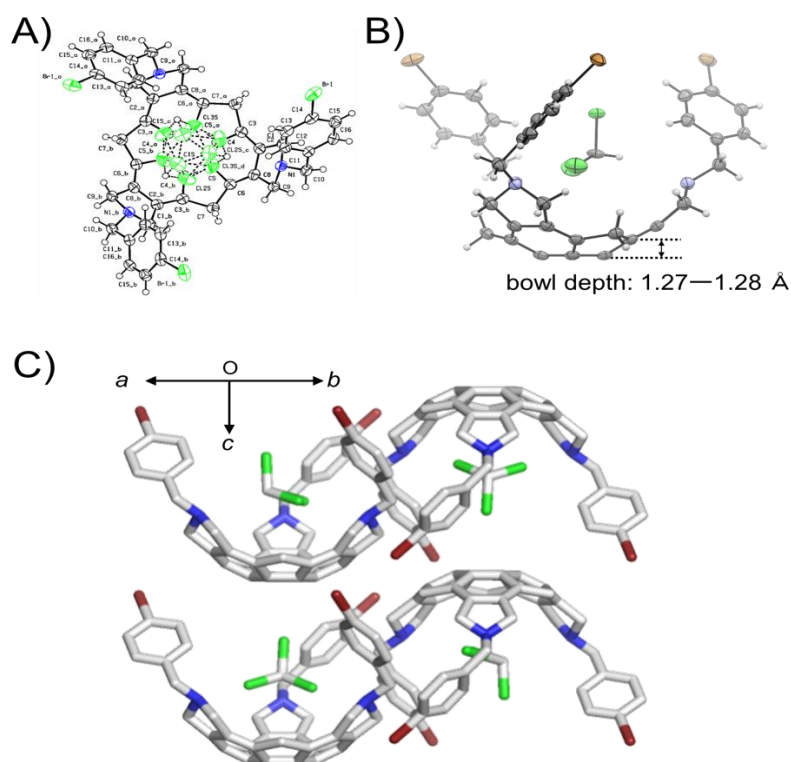


Figure 33. The crystallographic structure of **17c**. A) Displacement ellipsoid plot at 50% probability. B) Bowl depth of the sumanene skeleton. C) The packing structures.

Table 9. The experimental and theoretical values of bowl depth and POAV angles.

Figure 33 consists of three panels. Panel A shows a displacement ellipsoid plot of the crystallographic structure of **17c** at 50% probability, with atoms labeled C1 through C18 and N1 through N6. Panel B shows the bowl depth of the sumanene skeleton, with a measurement of 1.27–1.28 Å. Panel C shows the packing structures of **17c** in the crystal, with axes a, b, and c indicated.

	Bowl depth (Å)		POAV ¹² (deg.)	
	single crystal XRD	calculation	single crystal XRD	calculation
sumanene (1)	1.11	1.14	8.80	8.79
17c	1.27–1.28	1.11	9.61	8.62
$C_{54}N_6$	-	1.68	-	11.8
$[C_{54}N_6]^{6+}$	-	1.67	-	11.9

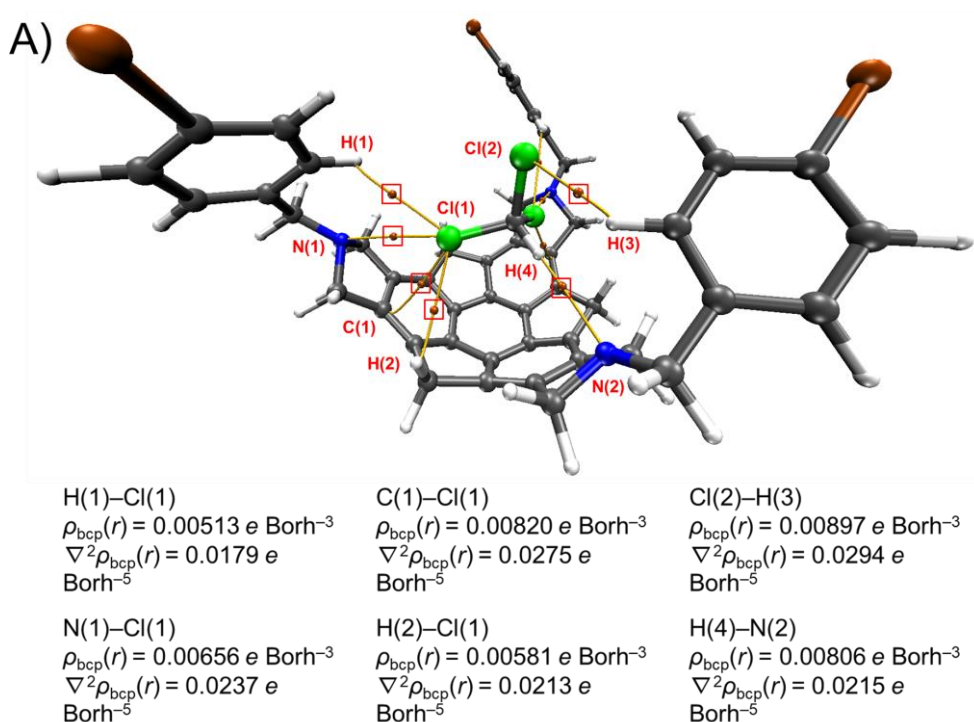
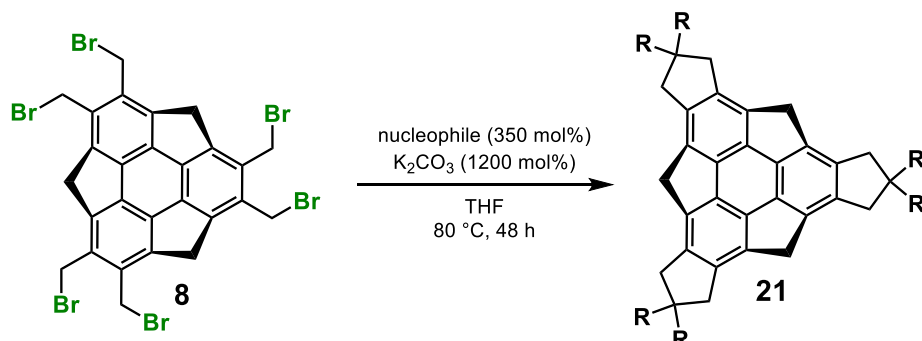
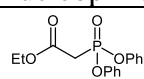
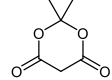
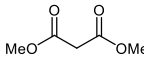


Figure 34. QTAIM analysis of **17c**. The interactions between the concave face of **17c** and CHCl_3 and within columnar structure are shown. The bond paths (yellow line), bond critical points (orange), and electron density at the bond critical points [$\rho_{\text{BCP}}(r)$ ($e \text{ bohr}^{-3}$)] are shown.

The chloroform incorporation of the synthesized triaminosumanene **17c** into a 1D column was further analyzed by the QTAIM method (quantum theory of atoms in molecules)¹³ (Figure 34). The coordinates of C, N, and Br used in this calculation were obtained from the results of single crystal X-ray structure analysis, and the coordinates of H were those obtained by optimization of the $\omega\text{B97X-D/def2-SVP}$ level calculation with the coordinates of the other elements fixed. The electron density calculated at the $\omega\text{B97X-D/def2-TZVP}$ level was used for the optimized coordinates to account for long-range corrections. As a result, a total of six bond critical points (BCPs) were observed between chloroform and **17c**, along with six bond paths. In particular, the electron densities [$\rho_{\text{BCP}}(r)$] between C(1)–Cl(1), Cl(2)–H(2), and H(4)–N(2) were large, with values of 8.20, 8.97, and 8.06 ($10^{-3} \text{ e bohr}^{-3}$), indicating that $\text{C}\cdots\text{Cl}$, $\text{CH}\cdots\text{Cl}$ and $\text{CH}\cdots\text{N}$ interactions, respectively. The Laplacian of the electron density in BCP ($\nabla^2 \rho_{\text{BCP}}(r)$) was all positive.

Table 10. Screening of carbon nucleophile

		
entry	nucleophile	Yield (%)
1		0
2		0
3		34 21a

Next, Introducing a C1 unit into **8** for synthesizing the C₃₀ skeleton was attempted (Table 10). The reaction did not proceed when phosphate or Meldrum's acid was used as the carbon nucleophile (entries 1 and 2), but when dimethyl malonate was used, **21a** was obtained in 34% yield (entry 3).

Section 3. Properties of azafullerene C₅₄N₆ and fullerene C₆₀ fragments

The UV-vis absorption and emission spectra of the resulting triaminosumanene (**17a-d**) and **21a** were then examined (Figure 35). The UV-vis absorption spectra of **17a-d** showed a strong absorption band at 280-300 nm with a broadening shoulder peak at 360 nm and a bathochromic shift compared to **1** ($\lambda = 278$ nm, 308 nm) (Figure 35A), possibly due to the expansion of the orbital to the introduced nitrogen atom by the through-bond interaction.¹⁴ On the other hand, two peaks were observed in the emission spectra, one around 360-420 nm and the other around 500-620 nm (Figure 35B). This is probably due to the conformational change in the excited state of triaminosumanene (**17**). In the case of the C₃₀ framework, **21a**, UV-vis absorption and emission peaks were also observed at slightly longer wavelengths than those of sumanene due to the through-bond interaction (Figure 36).

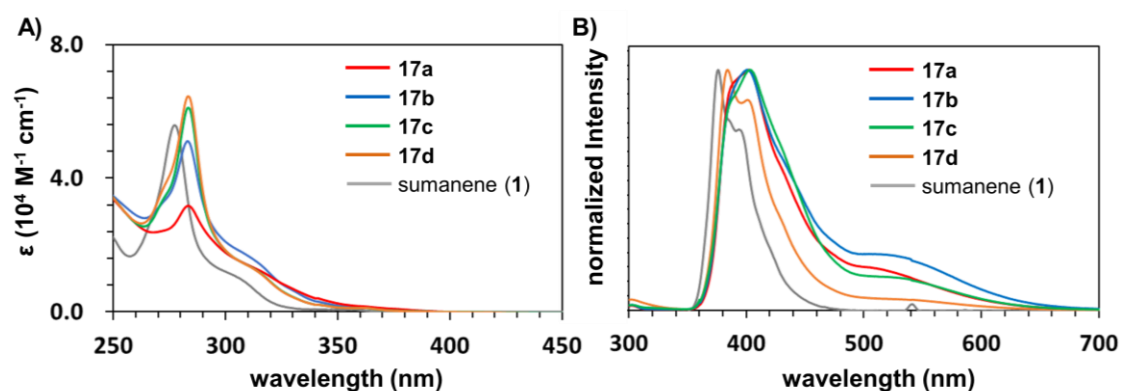


Figure 35. A) UV-vis absorption and B) emission spectra of amines (**17**) in THF (1.0×10^{-5} mol/L). Excitation wavelength: 278 nm.

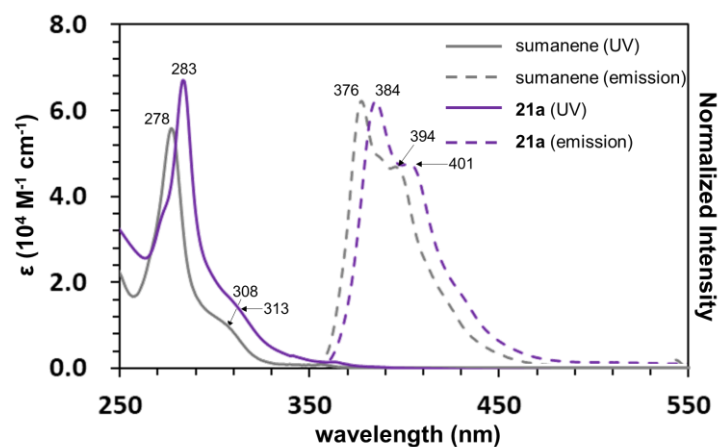


Figure 36. UV-vis absorption and emission spectra of C_{60} fragment (**21a**) in THF (1.0×10^{-5} mol/L). Excitation wavelength: 278 nm.

Section 4. Summary

In conclusion, a two-step synthesis of azafullerenes $C_{54}N_6$ and fullerene C_{60} fragment molecules was synthesized from commercially available sumanene. The obtained molecular structures have six independent five-membered rings and retain the reactive benzyl carbons of the sumanene skeleton, fulfilling 50% of the conformations of $C_{54}N_6$ and C_{60} , respectively. In the future, triaminosumanene will play an important role in the bottom-up synthesis of various azabuckybowls and azafullerene ($C_{54}N_6$).

Experimental section

Instrumentations and chemicals

All manipulations of moisture or air-sensitive compounds were performed by standard Schlenk techniques in anhydrous solvents under a nitrogen atmosphere using flame-dried glassware. Unless otherwise noted, chemical reactions were conducted in a 4 mL (15 × 45 mm) screw-thread clear vial (Thermo Scientific, Cat. No. C4015-1) with a cap assembled with a septum (Thermo Scientific, Cat. No. C4015-75A) using KOIKE PRECISION INSTRUMENTS HHE · 19G · US THERMO-MIGHTY STIRRER, or in a test-tube using EYELA PPS-2511 personal organic synthesizer. analytical thin-layer chromatography (TLC) was performed on precoated silica-gel aluminium sheets (Merck silica gel 60 F254, catalog no.1.05554.0001). Preparative thin-layer chromatography (PTLC) was prepared using Wako Wakogel B-5F. ¹H NMR (400 MHz) and ¹³C NMR (100 MHz) spectra were measured on a JEOL JNM-ECZS400 spectrometer at room temperature. Chloroform-*d*₁ (CDCl₃) was used as a solvent for NMR measurements. Chemical shifts (δ) are given in parts per million (ppm) downfield from the solvent signal (for ¹H NMR: CHCl₃ δ 7.26 ppm; for ¹³C NMR: CDCl₃ δ 77.2 ppm) as an internal standard with coupling constants (*J*) in hertz (Hz). The abbreviations s, d, t, q, and m signify singlet, doublet, triplet, quartet and multiplet, respectively. Melting points were determined on an Optimelt MPA100 automated melting point apparatus (Stanford Research Systems, Inc.), and expressed without correction. High-resolution mass spectra (HRMS) were measured on JEOL-JMS-T100LP (ESI⁺). Infrared (IR) spectroscopy measurements were performed on a JASCO FT IR-4100 spectrometer by transmission mode using KBr pellet method or attenuated total reflection (ATR) method. The absorption bands were given in wavenumber (cm⁻¹). Ultraviolet-visible (UV-vis) absorption spectroscopy was measured on a JASCO V-670 spectrophotometer by transmission method. The absorption bands were given in wavelength (nm). A quartz cell (optical path length; 10 mm) was used. Fluorescence spectra were recorded on a JASCO FP6500 spectrofluorometer and expressed after normalization. A quartz cell (optical path length; 10 mm) was used.

Unless otherwise noted, all reagents purchased from commercial suppliers were used without further purification.

n-Butylamine, morpholine, benzenesulfonamide, *n*-hexane, ethyl acetate (EtOAc), methanol (MeOH) and chloroform (CHCl₃) were purchased from FUJIFILM Wako Pure Chemical Corporation.

n-Octylamine was purchased from KISHIDA CHEMICAL Co., Ltd.

Triethylamine (NEt₃), diisopropylamine, aniline, dimethyl malonate, acetonitrile (MeCN), *N,N*-dimethylformamide (DMF), and potassium carbonate (K₂CO₃) were purchased from Nacalai Tesque, Inc.

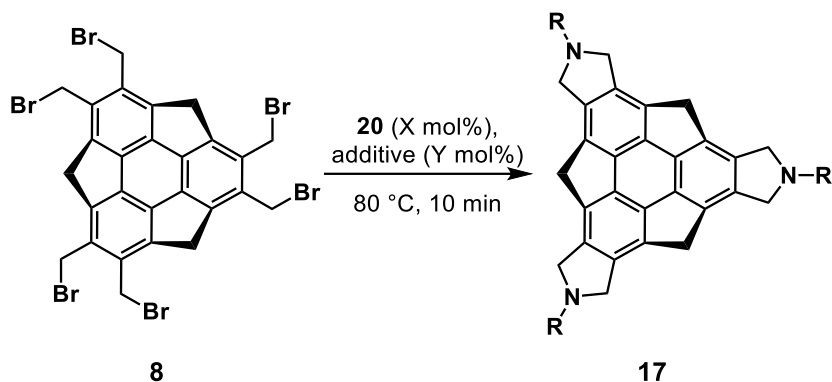
Tetrahydrofuran (THF, dehydrated, stabilizer free, Super Plus) was purchased from Kanto Chemical Co., Inc. and purified by passing through a Glass Contour Ultimate Solvent System (Nikko Hansen & Co. Ltd.)

under nitrogen atmosphere.

Sodium hydrogen carbonate (NaHCO₃) was purchased from Kanto Chemical Co., Inc.

α,α' -Dibromo-*o*-xylene, *p*-methoxybenzylamine, *p*-bromobenzylamine, and 1,8-bis(dimethylamino)-naphthalene (Proton sponge) were purchased from Tokyo Chemical Industry Co., Ltd.

General procedure for the synthesis of sumanenlytriamine **17**



To a reaction vial equipped with a magnetic stir bar were added **8** (40.0 mg, 49.1 μmol , 100 mol%) and solvent (4.0 mL). To this were added amine **20** (X mol%) and additive (Y mol%), and the mixture was stirred at 80 $^{\circ}\text{C}$ for 10 min. After cooling to room temperature, to the mixture was added H₂O and extracted with AcOEt. The combined organic extract was washed with brine and dried over Na₂SO₄. After filtration, the filtrate was concentrated under reduced pressure. The residue was purified by silica-gel column chromatography to give sumanenlytriamines **17**.

2,6,10-Tributyl-3,4,5,7,8,9,11,12-octahydro-1H-tricyclopenta[4,5:8,9:12,1]triphenyleno [2,3-*c*:6,7-*c'*:10,11-*c''*]tripyrrole (**17a**)

The crude product was purified by silica-gel column chromatography (MeOH/CHCl₃ = 1:10) to give **17a** (10.2 mg, 18.3 μmol , 37%);

Brownish solid; mp: 198 $^{\circ}\text{C}$ (dec); TLC: R_f = 0.52 (MeOH/CHCl₃ = 1:10); ¹H NMR (400 MHz, CDCl₃) δ (ppm) 4.45 (d, *J* = 19.2 Hz, 3H), 3.98 (d, *J* = 11.9 Hz, 6H), 3.70 (d, *J* = 11.9 Hz, 6H), 3.28 (d, *J* = 19.2 Hz, 3H), 2.69 (t, *J* = 7.3 Hz, 6H), 1.55 (tt, *J* = 7.3, 6.6 Hz, 6H), 1.38 (tq, *J* = 7.3, 6.6 Hz, 6H), 0.93 (t, *J* = 7.3 Hz, 9H); ¹³C NMR (100 MHz, CDCl₃) δ (ppm) 147.77 (6C), 142.15 (6C), 136.22 (6C), 57.80 (6C), 56.33 (3C), 38.84 (3C), 31.18 (3C), 20.76 (3C), 14.26 (3C); IR (KBr): 2955, 2927, 2871, 2789, 2743, 1682, 1458, 1330, 1152 cm⁻¹; HRMS(ESI⁺): *m/z* calcd for C₃₉H₄₅N₃ [M+H]⁺: 556.3686, found: 556.3667.

2,6,10-Trioctyl-3,4,5,7,8,9,11,12-octahydro-1H-tricyclopenta[4,5:8,9:12,1]triphenyleno [2,3-*c*:6,7-*c'*:10,11-*c''*]tripyrrole (**17b**)

The crude product was purified by silica-gel column chromatography (MeOH/CHCl₃ = 1:10) to give **17b** (9.9 mg, 46.0 μmol, 28%);

Brownish liquid; TLC: R_f = 0.51 (MeOH/CHCl₃ = 1:10); ¹H NMR (400 MHz, CDCl₃) δ (ppm) 4.46 (d, J = 19.2 Hz, 3H), 4.06 (d, J = 13.0 Hz, 6H), 3.76 (d, J = 13.0 Hz, 6H), 3.29 (d, J = 19.2 Hz, 3H), 2.72 (t, J = 7.6 Hz, 6H), 1.60 (m, 6H), 1.40–1.20 (m, 30H), 0.88 (t, J = 7.3 Hz, 6H); ¹³C NMR (100 MHz, CDCl₃) δ (ppm) 147.80 (6C), 142.27 (6C), 135.41 (6C), 57.65 (6C), 56.62 (3C), 38.92 (3C), 32.02 (3C), 29.69 (3C), 29.43 (3C), 28.60 (3C), 27.53 (3C), 22.84 (3C), 14.28 (3C);

IR (ATR): 2922, 2853, 2789, 2746, 1671, 1466, 1356, 1331, 1151 cm⁻¹; HRMS(ESI⁺): m/z calcd for C₅₁H₆₉N₃ [M+H]⁺: 724.5564, found: 724.5563.

2,6,10-Tri(4-bromobenzyl)-3,4,5,7,8,9,11,12-octahydro-1H-tricyclopenta[4,5:8,9:12,1] triphenyleno[2,3-c:6,7-c':10,11-c'']tripyrrole (17c)

The crude product was purified by silica-gel column chromatography (AcOEt/*n*-hexane = 10:1) to give **17c** (10.9 mg, 12.2 μmol, 25%);

Colorless solid; mp: 161 °C (dec); TLC: R_f = 0.64 (AcOEt/*n*-hexane = 5:1); ¹H NMR (400 MHz, CDCl₃) δ (ppm) 7.44 (d, J = 8.5 Hz, 6H), 7.23 (d, J = 8.5 Hz, 6H), 4.40 (d, J = 19.4 Hz, 3H), 3.94 (d, J = 12.1 Hz, 6H), 3.82 (s, 6H), 3.69 (d, J = 12.1 Hz, 6H), 3.22 (d, J = 19.4 Hz, 3H); ¹³C NMR (100 MHz, CDCl₃) δ (ppm) 147.82 (6C), 142.32 (6C), 138.28 (6C), 136.02 (3C), 131.68 (6C), 130.54 (6C), 121.09 (3C), 59.85 (3C), 57.56 (6C), 38.88 (3C); IR (KBr): 2925, 2880, 2762, 1684, 1487, 1329, 1144, 1012 cm⁻¹; HRMS(ESI⁺): m/z calcd for C₄₈H₃₆N₃Br₃ [M+H]⁺: 892.0532, found: 892.0498.

2,6,10-Tri(4-methoxybenzyl)-3,4,5,7,8,9,11,12-octahydro-1H-tricyclopenta[4,5:8,9:12,1] triphenyleno[2,3-c:6,7-c':10,11-c'']tripyrrole (17d)

The crude product was purified by silica-gel column chromatography (AcOEt/*n*-hexane = 10:1) to give **17d** (8.8 mg, 11.8 μmol, 24%);

Colorless solid; mp: 152 °C (dec); TLC: R_f = 0.28 (AcOEt/*n*-hexane = 5:1); ¹H NMR (400 MHz, CDCl₃) δ (ppm) 7.29 (d, J = 8.7 Hz, 6H), 6.87 (d, J = 8.7 Hz, 6H), 4.38 (d, J = 19.2 Hz, 3H), 3.97 (d, J = 12.4 Hz, 6H), 3.69 (d, J = 12.4 Hz, 6H), 3.23 (d, J = 19.2 Hz, 3H); ¹³C NMR (100 MHz, CDCl₃) δ (ppm) 159.01 (3C), 147.79 (6C), 142.32 (6C), 135.89 (3C), 130.83 (6C), 130.12 (6C), 113.95 (6C), 59.82 (3C), 57.38 (6C), 55.44 (3C), 38.86 (3C); IR (KBr): 2929, 2834, 2776, 1611, 1513, 1250, 1178, 1033 cm⁻¹; HRMS(ESI⁺): m/z calcd for C₅₁H₄₅N₃O₃ [M+H]⁺: 748.3534, found: 748.3526.

Hexamethyl 3,4,5,7,8,9,11,12-octahydrohexacyclopenta[*b,def,h,jkl,n,pqr*]triphenylene-2,2,6,6,10,10(1H)-hexacarboxylate (21a)

To a test tube equipped with a magnetic stir bar were added **8** (10.0 mg, 12.3 μmol , 100 mol%), K_2CO_3 (20.3 mg, 147 μmol , 1200 mol%), and THF (1.5 mL). To this was added dimethyl malonate (4.9 μL , 36.8 μmol , 350 mol%) and the mixture was stirred at 80 $^\circ\text{C}$ for 48 h. After cooling to room temperature, to the reaction mixture was added H_2O and extracted with AcOEt. The combined organic extract was washed with brine and dried over Na_2SO_4 . After filtration, the filtrate was concentrated under reduced pressure. The residue was purified by silica-gel column chromatography (AcOEt/ CHCl_3 /*n*-hexane = 10:5:7) followed by GPC (CHCl_3) to give **21a** (3.1 mg, 4.2 μmol , 34%);

Colorless solid; mp: 246 $^\circ\text{C}$ (dec); TLC: R_f = 0.61 (AcOEt/ CHCl_3 /*n*-hexane = 10:5:7); ^1H NMR (400 MHz, CDCl_3) δ (ppm) 4.48 (d, J = 19.4 Hz, 3H), 3.82 (s, 9H), 3.73 (d, J = 16.7 Hz, 6H), 3.62 (s, 9H), 3.38 (d, J = 16.7 Hz, 6H), 3.29 (d, J = 19.4 Hz, 3H); ^{13}C NMR (100 MHz, CDCl_3) δ (ppm) 172.41 (3C), 172.04 (3C), 147.43 (6C), 143.57 (6C), 135.82 (6C), 60.36 (3C), 53.31 (3C), 53.13 (3C), 39.20 (3C), 39.04 (6C); IR (KBr): 3461, 3001, 2953, 2845, 1736, 1434, 1282, 1242, 1201, 1161, 1070 cm^{-1} ; HRMS(ESI $^+$): m/z calcd for $\text{C}_{42}\text{H}_{36}\text{O}_{12}$ $[\text{M}+\text{Na}]^+$: 755.2099. found: 755.2092.

X-ray crystallographic data for 17c

The diffraction data for **17c** was recorded on a DECTRIS PILATUS3 X CdTM 1M Detector System ($\lambda = 0.4194 \text{ \AA}$) at 100 K at SPring-8 BL02B1. The diffraction images were processed by using RIGAKU RAPID AUTO.¹⁵ The structure was solved by direct methods (SHELXT-2015, 2018/2)¹⁶ and refined by full-matrix least squares calculations on F^2 (SHELXL-2018/3)¹⁷ using the Olex2¹⁸ program package.

17c: $\text{C}_{48}\text{H}_{36}\text{Br}_3\text{N}_3\text{O}_{0.33}(\text{C}_3\text{Cl}_9)$, trigonal, space group $P\bar{3}$ (No. 147), $a = 16.097(3) \text{ \AA}$, $b = 16.097(3) \text{ \AA}$, $c = 9.513(2) \text{ \AA}$, $\alpha = 90^\circ$, $\beta = 90^\circ$, $\gamma = 120^\circ$, $V = 2134.6(10) \text{ \AA}^3$, $\rho_{\text{calcd}} = 1.577 \text{ g/cm}^3$, $Z = 2$, 2862 unique reflections out of 3270 with $I > 2\sigma(I)$, 199 parameters, $0.996^\circ < \theta < 15.788^\circ$, $R_1 = 0.0379$, $wR_2 = 0.1008$, GOF = 1.040, CCDC 2214511.

Computational study

All theoretical calculations using the density functional theory (DFT) method were conducted using Gaussian 16 (revision C.01) program package.¹⁹ Geometry optimization calculations were performed at the B3LYP²⁰ level of theory with 6-31+G(d,p)²¹ as a basis set in gas phase for all atoms.

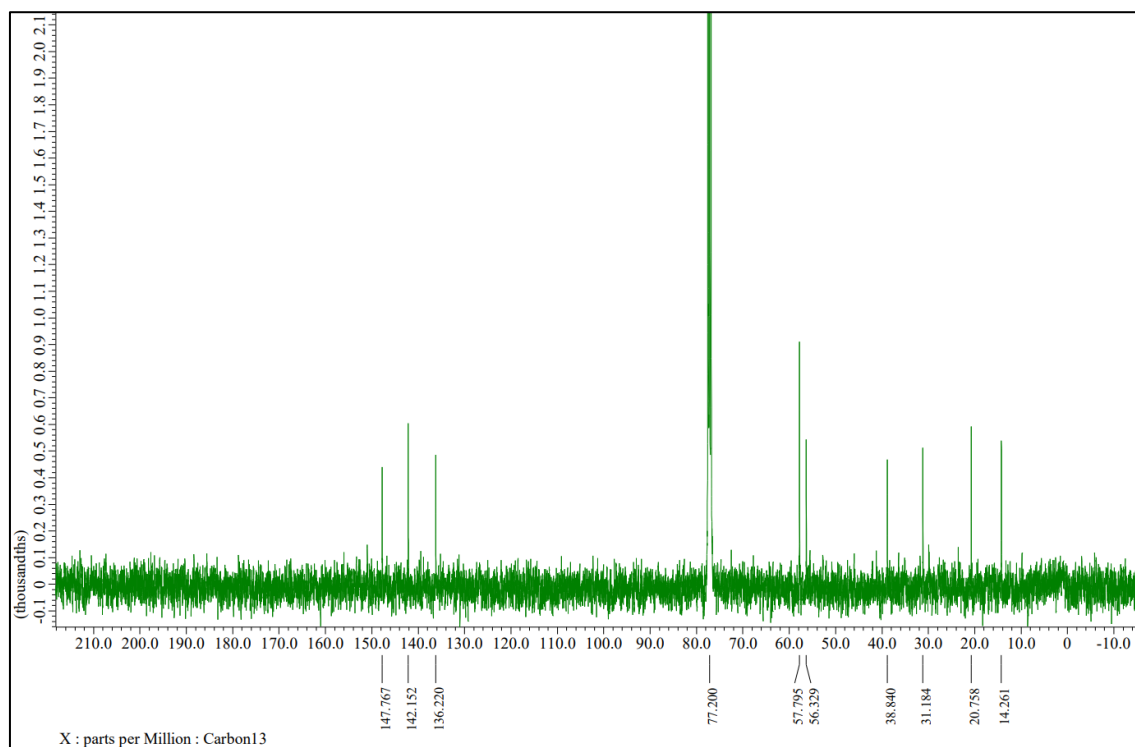
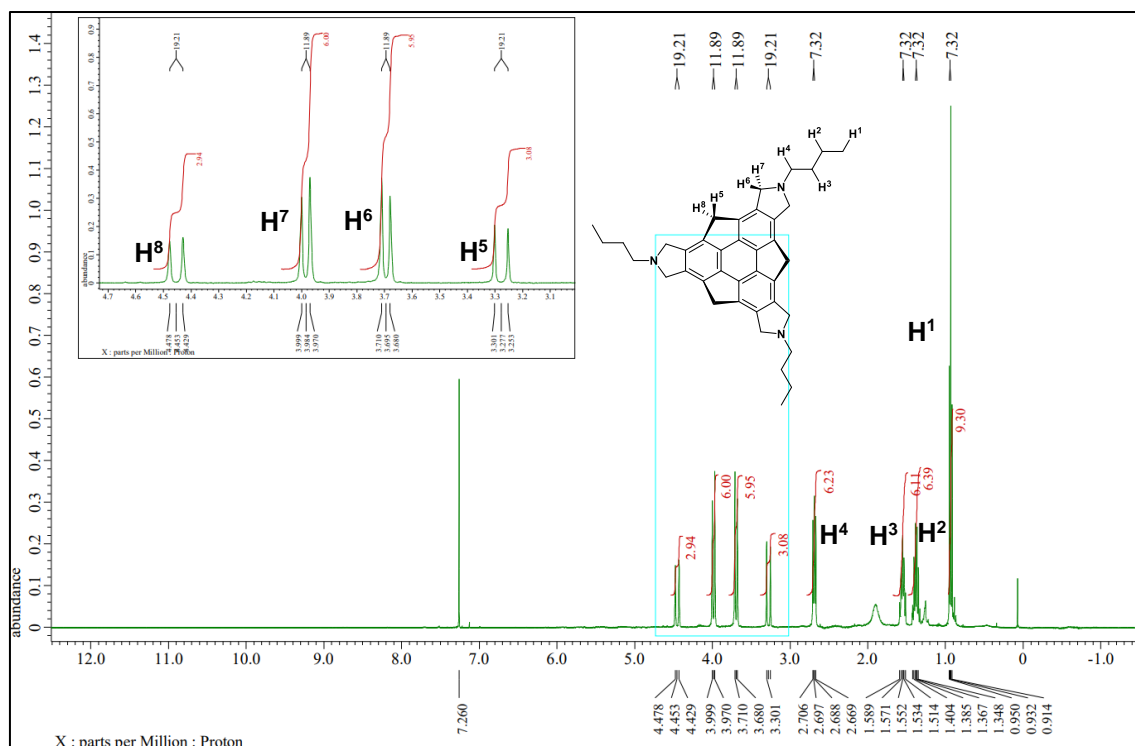
Theoretical investigation of the packing structure of 17c with dimer model

The coordinates of **17c** were obtained from the result of single crystal X-ray diffraction analysis (CCDC: 2214511), and those of hydrogen atoms were optimized at the ω B97X-D²² level of theory with def2-SVP²³ as a basis set in gas phase. Self-consistent field (SCF) calculation for the optimized coordinates was conducted at the ω B97X-D level of theory with def2-TZVP²³ as a basis set in gas phase. The wavefunction files in a formatted gaussian checkpoint (fchk) file format were generated using Gaussian 09 package. Complexation energies were calculated at the ω B97X-D level of theory with Def2-TZVP as a basis set in gas phase using the counterpoise method to correct the Basis Set Superposition Error (BSSE).²⁴

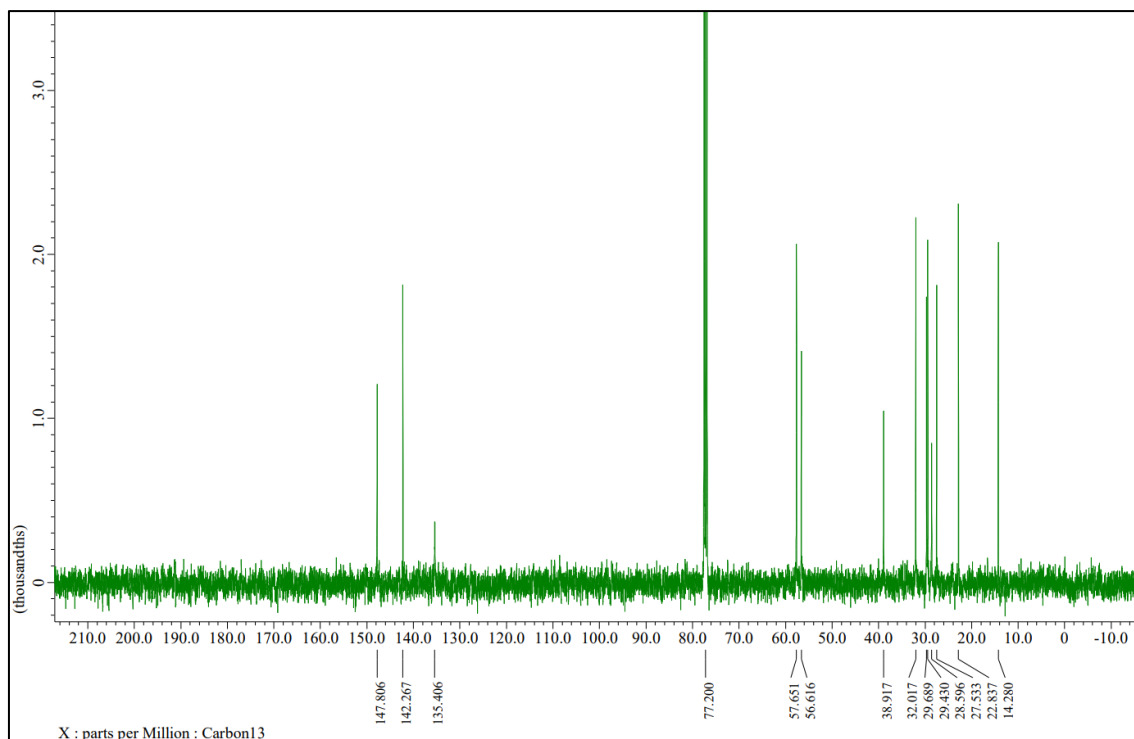
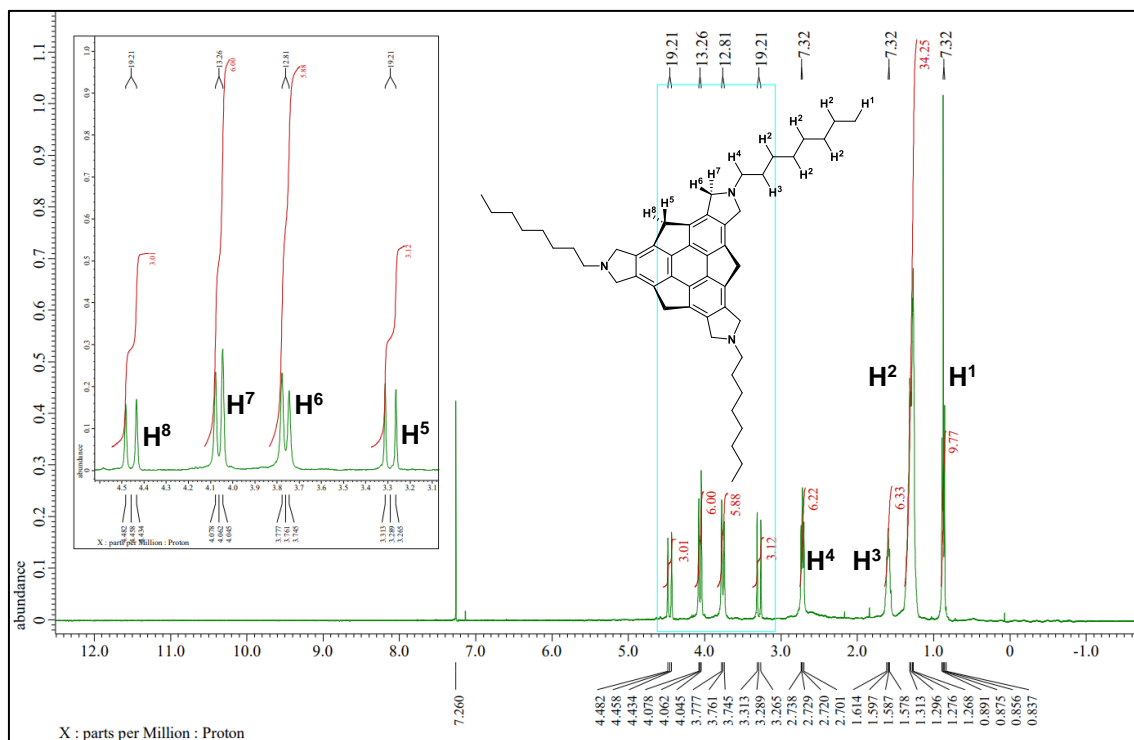
The quantum theory atoms-in-molecules (QTAIM)¹³ analyses was performed using Multiwfn program.²⁵ The obtained bond paths and the bond critical points (BCPs) were visualized using VMD program.²⁶

^1H and ^{13}C NMR spectra

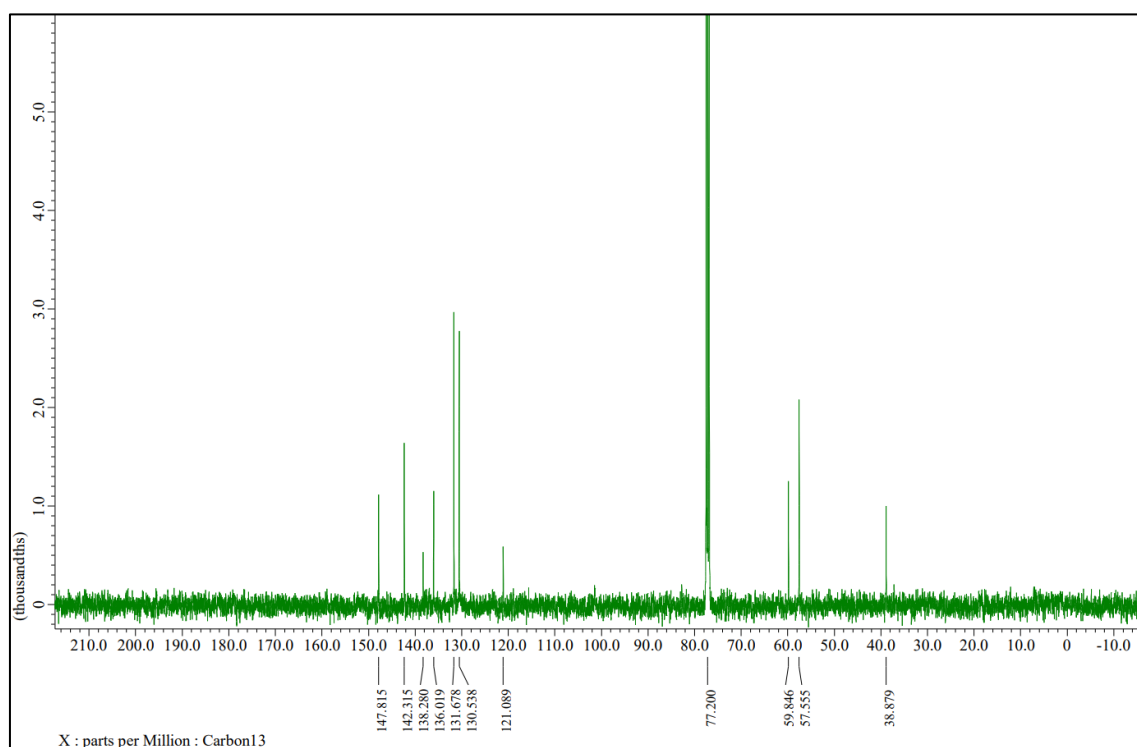
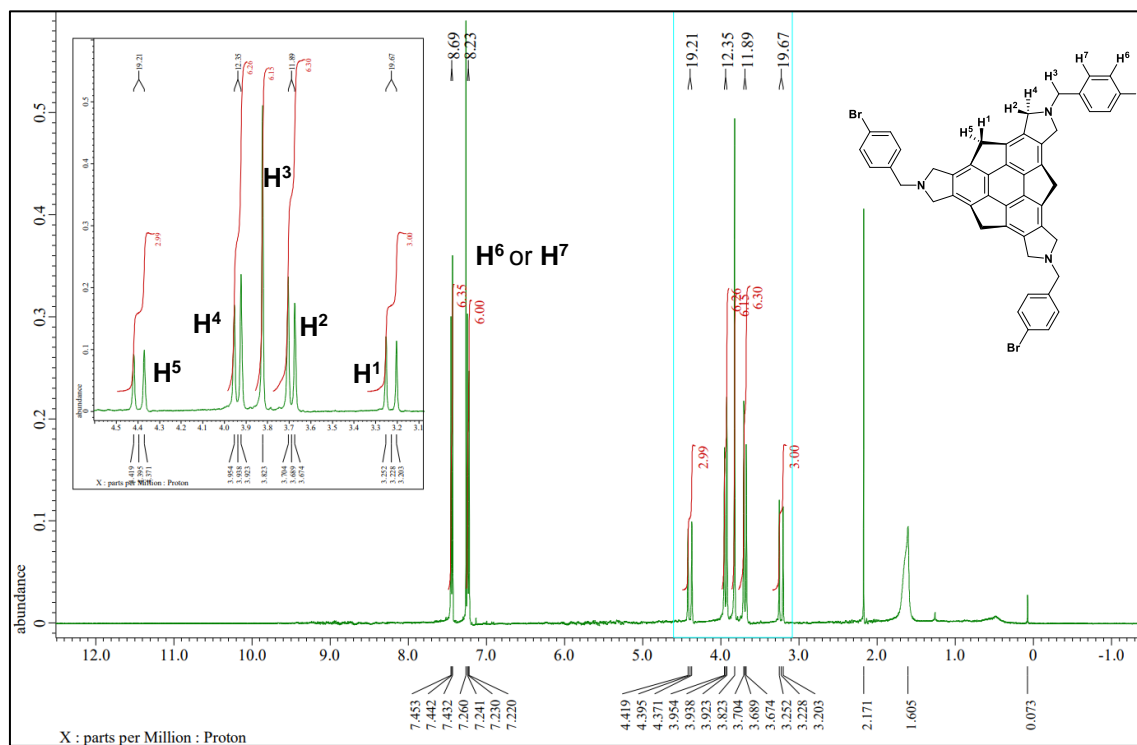
^1H NMR (400 MHz) and ^{13}C NMR (100 MHz) spectra of **17a** (CDCl_3)



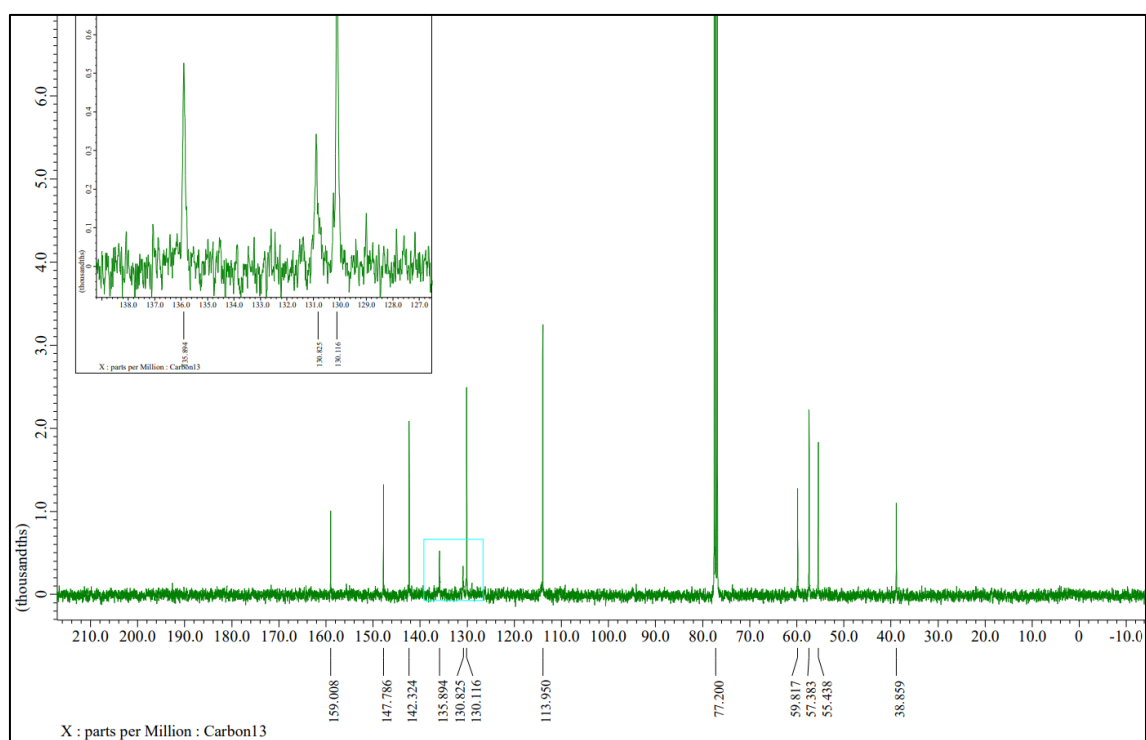
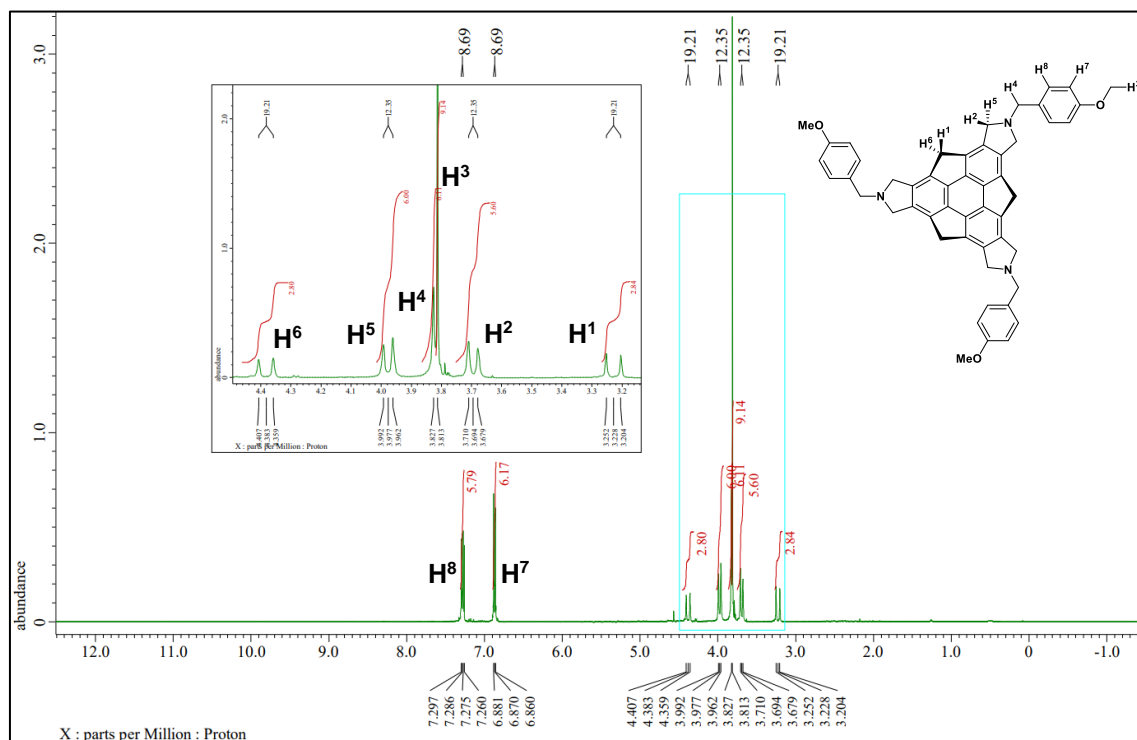
^1H NMR (400 MHz) and ^{13}C NMR (100 MHz) spectra of **17b** (CDCl_3)



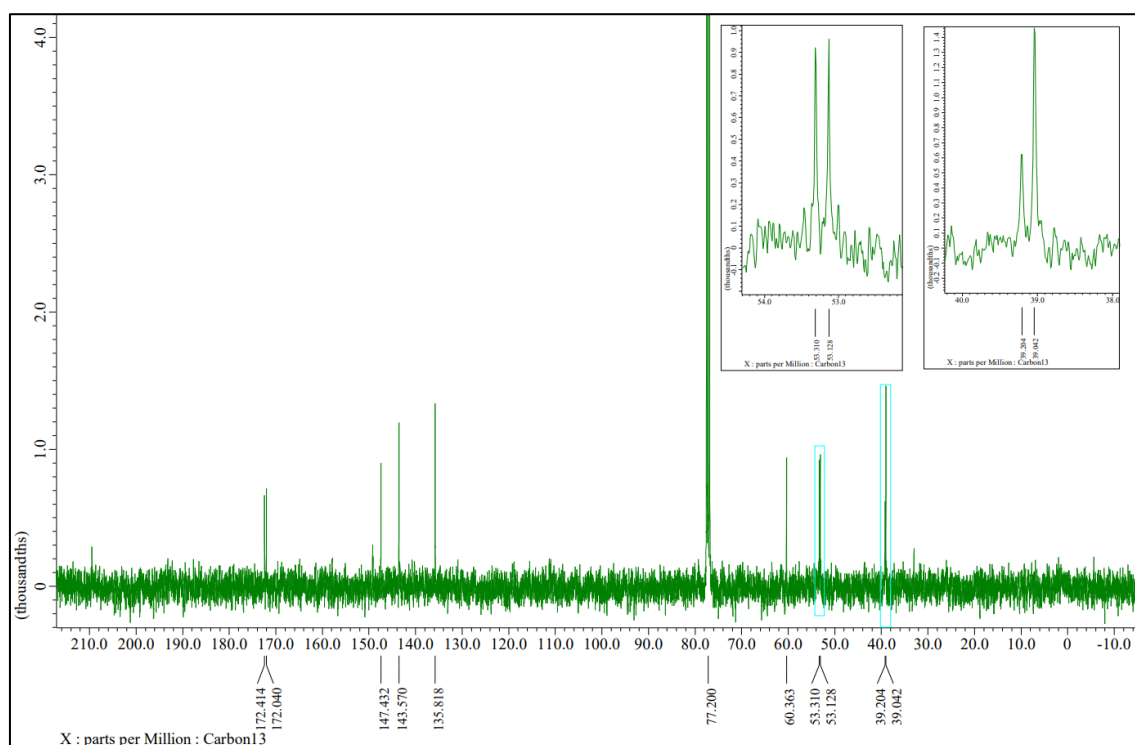
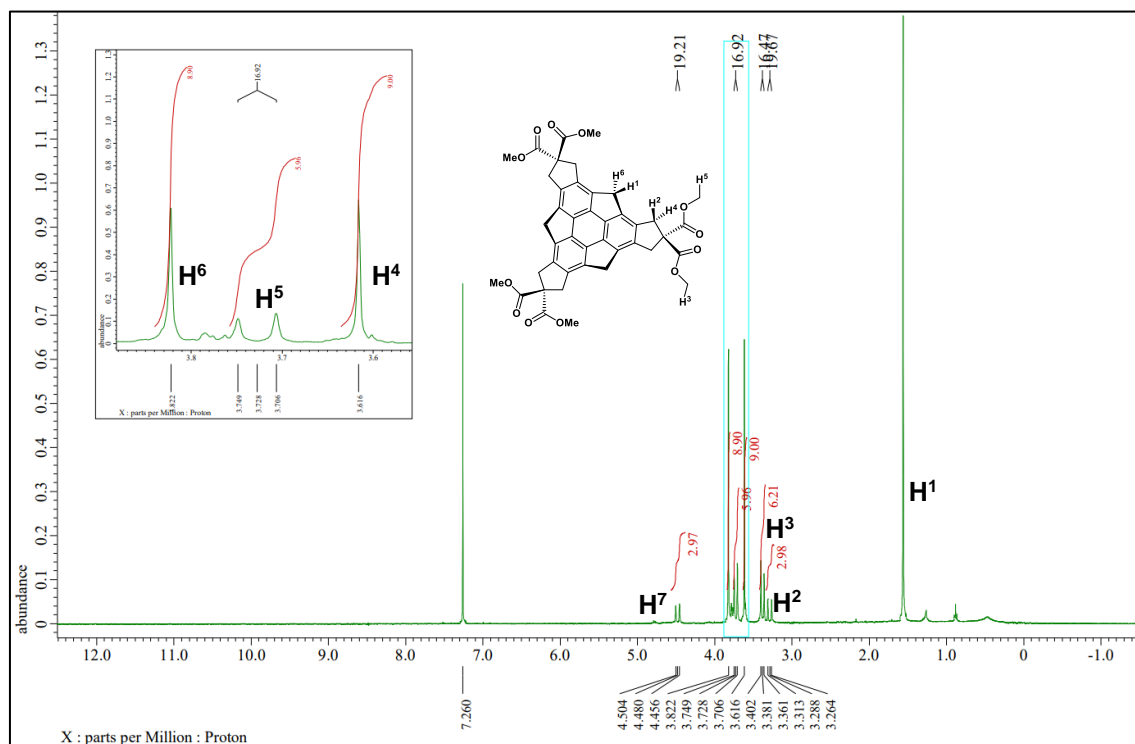
^1H NMR (400 MHz) and ^{13}C NMR (100 MHz) spectra of **17c** (CDCl_3)



^1H NMR (400 MHz) and ^{13}C NMR (100 MHz) spectra of **17d** (CDCl_3)



^1H NMR (400 MHz) and ^{13}C NMR (100 MHz) spectra of **21a** (CDCl_3)



References

- 1 E, Osawa, *Hyperaromaticity Kagaku*, **1970**, 25, 854.
- 2 a) H. W. Kroto, J. R. Heath, S. C. O'Brien, R. F. Curl, R. E. Smalley, *Nature* **1985**, 318, 162. b) H. W. Kroto, A. W. Allaf, S. P. Balm, *Chem. Rev.* **1991**, 91, 1213.
- 3 a) T. Pradeep, V. Vijayakrishnan, A. K. Santra, C. N. R. Rao, *J. Phys. Chem.* **1991**, 95, 10564. b) R. Yu, M. Zhan, D. Cheng, S. Yang, Z. Liu, L. -S. Zheng, *J. Phys. Chem.* **1995**, 99, 1818. c) Z. C. Ying, R. L. Hettich, R. N. Compton, R. E. Haufler, *J. Phys. B: At. Mol. Opt. Phys.* **1996**, 29, 4935. d) A. Rockenbauer, G. Csúnyi, F. Fülöp, S. Garaj, L. Korecz, R. Lukács, F. Simon, L. Forró, S. Pekker, A. Jönossy, *Phys. Rev. Lett.* **2005**, 94, 066603.
- 4 a) Y. Rubin, T. C. Parker, S. J. Pastor, S. Jalisatgi, C. Boule, C. L. Wilkins, *Angew. Chem., Int. Ed.* **1998**, 37, 1226. b) Y. Tobe, N. Nakagawa, K. Naemura, T. Wakabayashi, T. Shida, Y. Achiba, *J. Am. Chem. Soc.* **1998**, 120, 4544.
- 5 L. T. Scott, M. M. Boorum, B. J. McMahon, S. Hagen, J. Mack, J. Blank, H. Wegner, A. de Meijere, *Science* **2002**, 295, 1500.
- 6 G. Otero, G. Biddau, C. Sánchez-Sánchez, R. Caillard, M. F. López, C. Rogero, F. J. Palomares, N. Cabello, M. A. Basanta, J. Ortega, J. Méndez, A. M. Echavarren, R. Pérez, B. Gómez-Lor, J. A. Martín-Gago, *Nature* **2008**, 454, 865.
- 7 a) A. H. Abdourazak, Z. Marcinow, A. Sygula, R. Sygula, P. W. Rabideau, *J. Am. Chem. Soc.* **1994**, 117, 6410. b) S. Hagen, M.S. Bratcher, M.S. Erickson, G. Zimmermann, L. T. Scott, *Angew. Chem. Int. Ed.* **1997**, 36, 406.
- 8 a) H. W. Kroto, *Nature* **1987**, 329, 529. b) T. G. Schmalz, W. A. D. Seitz, J. Klein, G. E. Hite, *J. Am. Chem. Soc.* **1988**, 110, 1113.
- 9 A. Richaud, M. J. López, M. Mojica, J. A. Alonso, F. Méndez, *Org. Chem. Front.* **2022**, 9, 4981.
- 10 I. T. Forbes, C. N. Johnson, M. Thompson, *J. Chem. Soc. Perkin. Trans.* **1992**, 1, 275.
- 11 H. Sakurai, T. Daiko, H. Sakane, T. Amaya, T. Hirao, *J. Am. Chem. Soc.* **2005**, 127, 11580.
- 12 R. C. Haddon, *J. Am. Chem. Soc.* **1987**, 109, 1676.
- 13 W. B. Richard, *Chem. Rev.* **1991**, 91, 893.
- 14 a) R. Hoffmann, *Acc. Chem. Res.* **1971**, 4, 1. b) R. Gleiter, *Angew. Chem., Int. Ed.* **1974**, 13, 696.
- 15 RAPID-AUTO. Rigaku Corporation, Tokyo, Japan (**2001**).
- 16 G. M. Sheldrick, *Acta Cryst. A*, **2015**, 71, 3.
- 17 G. M. Sheldrick, *Acta Cryst. C*, **2015**, 71, 3.
- 18 Olex2: a complete structure solution, refinement and analysis program; O. V. Dolomanov, L.J. Bourhis, R. J. Gildea, J. A. K. Howard, H. J. Puschmann, *Appl. Cryst.* **2009**, 42, 339.

- 19 Gaussian 16, Revision C.01, M. J. Frisch, G. W. Trucks, H. B. Schlegel, G. E. Scuseria, M. A. Robb, J. R. Cheeseman, G. Scalmani, V. Barone, G. A. Petersson, H. Nakatsuji, X. Li, M. Caricato, A. V. Marenich, J. Bloino, B. G. Janesko, R. Gomperts, B. Mennucci, H. P. Hratchian, J. V. Ortiz, A. F. Izmaylov, J. L. Sonnenberg, D. Williams-Young, F. Ding, F. Lipparini, F. Egidi, J. Goings, B. Peng, A. Petrone, T. Henderson, D. Ranasinghe, V. G. Zakrzewski, J. Gao, N. Rega, G. Zheng, W. Liang, M. Hada, M. Ehara, K. Toyota, R. Fukuda, J. Hasegawa, M. Ishida, T. Nakajima, Y. Honda, O. Kitao, H. Nakai, T. Vreven, K. Throssell, J. A. Montgomery, Jr., J. E. Peralta, F. Ogliaro, M. J. Bearpark, J. J. Heyd, E. N. Brothers, K. N. Kudin, V. N. Staroverov, T. A. Keith, R. Kobayashi, J. Normand, K. Raghavachari, A. P. Rendell, J. C. Burant, S. S. Iyengar, J. Tomasi, M. Cossi, J. M. Millam, M. Klene, C. Adamo, R. Cammi, J. W. Ochterski, R. L. Martin, K. Morokuma, O. Farkas, J. B. Foresman, and D. J. Fox, Gaussian, Inc., Wallingford CT, **2016**.
- 20 a) A.D. Becke, *J. Chem. Phys.* **1993**, *98*, 5648. b) C. Lee, W. Yang, R.G. Parr, *Phys. Rev. B* **1988**, *37*, 785. c) P.J. Stephens, F.J. Devlin, C.F. Chabalowski, M.J. Frisch, *J. Phys. Chem.* **1994**, *98*, 11623.
- 21 a) R. Ditchfield, W. J. Hehre, J. A. Pople, *J. Chem. Phys.* **1971**, *54*, 724. b) P. C. Hariharan, J. A. Pople, *Theor. Chim. Acta* **1973**, *28*, 213. c) W. J. Hehre, R. Ditchfield, J. A. Pople, *J. Chem. Phys.* **1972**, *56*, 2257. d) V. A. Rassolov, M. A. Ratner, J. A. Pople, John A., P. C. Redfern, L. A. Curtiss, *J. Comput. Chem.* **2001**, *22*, 976.
- 22 J.-D. Chai, M. Head-Gordon, *Phys. Chem. Chem. Phys.* **2008**, *10*, 6615.
- 23 a) K. A. Peterson, D. G. Figgen, S. T. Erich, M. Dolg, *J. Chem. Phys.* **2003**, *119*, 11113. b) F. Weigend, R. Ahlrichs, *Phys. Chem. Chem. Phys.* **2005**, *7*, 3297.
- 24 S. F. Boys, F. Bernardi, *Mol. Phys.* **1970**, *19*, 553.
- 25 T. Lu, F. Chen, *J. Comput. Chem.* **2012**, *33*, 580.
- 26 W. Humphrey, A. Dalke, K. Schulten, *J. Mol. Graph.* **1996**, *14*, 33.

Conclusions

In this doctoral dissertation, the author aimed at the synthesis of functional molecules and achieved the synthesis of various ortho-disubstituted and hexa-substituted sumanene derivatives by aromatic electrophilic substitution reactions.

In Chapter 2, the synthesis of acene molecules with the introduction of bowl structure was carried out, oriented toward the application of sumanene-fused acenes to singlet fission (SF). Specifically, sumanene-fused quinones were synthesized by double acylation of sumanene, followed by reductive aromatization to sumanene-fused acenes. The obtained sumanene-fused quinone and acenes were found to form 1D columnar structures commonly observed in sumanene derivatives, respectively, by single-crystal X-ray structure analysis. This feature of the preferential formation of 1D columnar structure by the introduction of the sumanene skeleton could be one of the excellent molecular design strategies for the arrangement of the acene moiety. In the future, it is expected to be applied to phenomena such as SF, where the arrangement of molecules is the key to the expression of their functions and high efficiency.

In Chapter 3, the synthesis and transformation of bromomethylsumanenes were achieved. It was found that bromomethyl sumanene exhibits higher solubility in organic solvents than hexabromosumanene, and various substituents can be introduced using nucleophiles. The author believes that bromomethylsumanene, which can be easily substituted by nucleophilic substitution, will be the first milestone in the project on nonplanar conjugated systems including network structures such as liquid crystals and covalent bonds.

In Chapter 4, the first application of the bromomethylsumanene synthesized in Chapter 3 is the synthesis of hemispherical molecules (C_{30} and $C_{27}N_3$) directed toward the bottom-up synthesis of fullerenes C_{60} and $C_{54}N_6$. These molecules can be synthesized in one step by reacting with the corresponding C1 or N1 units from bromomethylsumanene. The obtained molecules are expected to be developed into new (aza)buckybowls as well as the synthesis of fullerenes in the future.

In this study, the author synthesized bowl-shaped acenes, hexa-substituted sumanenes, and fragment molecules of (aza)fullerenes from sumanenes by aromatic electrophilic substitution reactions and investigated their properties. The knowledge of chemical modification methods and properties of sumanene derivatives obtained in this study is expected to lead to the creation of curved π -conjugated molecules with new functions.

List of Publications

The content of this thesis has been published in the following papers.

- 1) Synthesis of Sumanene-fused Acenes

Hironobu Nakazawa, A. Ohya, Y. Morimoto, Y. Uetake, N. Ikuma, K. Okada, M. Nakano, Y. Yakiyama, H. Sakurai

Asian J. Org. Chem. **2022**, *11*, e202200471.

- 2) Synthesis of fully substituted sumanenes at the aromatic periphery through hexabromomethylation

Hironobu Nakazawa, Y. Uetake, Y. Yakiyama, H. Sakurai

Asian J. Org. Chem. **2023**, *12*, e202200585.

- 3) Pentagon-fused sumanenes on the aromatic peripheries en route to the bottom-up synthesis of fullerenes

Hironobu Nakazawa, Y. Uetake, Y. Yakiyama, H. Sakurai

Synlett **2023**, *34*, ST-2022-11-0499-L.

Copyright

The author has obtained permission to reuse contents. The author wishes to express his thanks to Copyright Clearance Center, Creative Commons, Wiley-VCH Verlag GmbH, Weinheim, and Thieme E-Books & E-Journals.

Credits

Reprinted with permission from Hironobu Nakazawa, A. Ohya, Y. Morimoto, Y. Uetake, N. Ikuma, K. Okada, M. Nakano, Y. Yakiyama, H. Sakurai, *Asian J. Org. Chem.* **2022**, *11*, e202200471. Copyright 2022 Wiley-VCH Verlag GmbH, Weinheim.

Reprinted with permission from Hironobu Nakazawa, Y. Uetake, Y. Yakiyama, H. Sakurai, *Asian J. Org. Chem.* **2023**, *12*, e202200585. Copyright 2023 Wiley-VCH Verlag GmbH, Weinheim.

Reprinted with permission from Hironobu Nakazawa, Y. Uetake, Y. Yakiyama, H. Sakurai, *Synlett* **2023**, *34*, ST-2022-11-0499-L, Copyright 2023 Thieme E-Books & E-Journals.

Acknowledgments

I would like to express my sincere gratitude to professor Hidehiro Sakurai of the division of applied chemistry, graduate school of engineering Osaka university for his direct guidance in the course of this research. I would also like to thank associate professor Yumi Yakiyama and assistant professor Yuta Uetake of the division of applied chemistry, graduate school of engineering Osaka university for their guidance and encouragement throughout the course of this research.

I would like to express my sincere gratitude to professor Satoshi Minakata and professor Norimitsu Tohnai for reviewing my doctoral dissertation and for their suggestions and advice.

I thank professor Masayoshi Nakano, associate professor Ryohei Kishi, and Mr. Kenji Okada of the division of chemical engineering, department of materials engineering science, graduate school of engineering science, Osaka university for their helpful advice and guidance on the quantum chemical calculations of singlet fission of sumanene-fused acenes. I thank associate professor Yohei Takeda, department of applied chemistry, graduate school of engineering, Osaka university, for his help in measuring the fluorescence lifetime and quantum yield of sumanene-fused acenes. I thank Mr. Hiroaki Tanaka of the analytical center, graduate school of engineering, Osaka university, for his cooperation in the mass measurement of various organic compounds.

I would like to express my deepest gratitude to Mr. Yufeng Wang for providing me with a fruitful deal of knowledge and experience, including how to conduct research and experimental techniques. I am deeply grateful to Dr. Mikey Nishimoto, with whom I had a friendly competition in the same year, and who helped me in my research and personal life. I am deeply grateful to Ms. Michiko Ebukuro, Ms. Yuki Matsuo, Ms. Karin Fujino, and Ms. Marika Moriyasu for their support in various administrative tasks and research activities. I would like to express my deepest gratitude to all the students in Sakurai Laboratory who worked with me day and night and also had fun with me outside of research.

Single crystal X-ray structure analyses were performed at SPring-8 BL40XU (project numbers: 2019B1654, 2022B1690) and Pohang Accelerator Laboratory (PAL) 2D beamline (project number: 2016-3rd-2D-021). Quantum chemical calculations were performed at the Institute for Molecular Science, Center for Computational Science (Project: 22-IMS-C068). This work was also supported by a Grant-in-Aid for Young Scientists (JP21J10937).

March 2023

Hironobu Nakazawa